



1N-34  
381732

# TECHNICAL NOTE

D-338

EFFECTS OF SWEEP ANGLE ON THE BOUNDARY-LAYER STABILITY

CHARACTERISTICS OF AN UNTAPERED WING AT LOW SPEEDS

By Frederick W. Boltz, George C. Kenyon,  
and Clyde Q. Allen

Ames Research Center  
Moffett Field, Calif.

NATIONAL AERONAUTICS AND SPACE ADMINISTRATION  
WASHINGTON

October 1960

1  
2  
3

4  
5  
6

7

8

9

10

## NATIONAL AERONAUTICS AND SPACE ADMINISTRATION

## TECHNICAL NOTE D-338

## EFFECTS OF SWEEP ANGLE ON THE BOUNDARY-LAYER STABILITY

## CHARACTERISTICS OF AN UNTAPERED WING AT LOW SPEEDS

By Frederick W. Boltz, George C. Kenyon,  
and Clyde Q. Allen

## SUMMARY

An investigation was conducted in the Ames 12-Foot Low-Turbulence Pressure Tunnel to determine the effects of sweep on the boundary-layer stability characteristics of an untapered variable-sweep wing having an NACA 64<sub>2</sub>A015 section normal to the leading edge. Pressure distribution and transition were measured on the wing at low speeds at sweep angles of 0°, 10°, 20°, 30°, 40°, and 50° and at angles of attack from -3° to 3°. The investigation also included flow-visualization studies on the surface at sweep angles from 0° to 50° and total pressure surveys in the boundary layer at a sweep angle of 30° for angles of attack from -12° to 0°.

It was found that sweep caused premature transition on the wing under certain conditions. This effect resulted from the formation of vortices in the boundary layer when a critical combination of sweep angle, pressure gradient, and stream Reynolds number was attained. A useful parameter in indicating the combined effect of these flow variables on vortex formation and on beginning transition is the crossflow Reynolds number. The critical values of crossflow Reynolds number for vortex formation found in this investigation range from about 135 to 190 and are in good agreement with those reported in previous investigations. The values of crossflow Reynolds number for beginning transitions were found to be between 190 and 260. For each condition (i.e., development of vortices and initiation of transition at a given location) the lower values in the specified ranges were obtained with a light coating of flow-visualization material on the surface.

A method is presented for the rapid computation of crossflow Reynolds number on any swept surface for which the pressure distribution is known. From calculations based on this method, it was found that the maximum values of crossflow Reynolds number are attained under conditions of a strong pressure gradient and at a sweep angle of about 50°. Due to the primary dependence on pressure gradient, effects of sweep in causing premature transition are generally first encountered on the lower surfaces of wings operating at positive angles of attack.

## INTRODUCTION

In general, there are three distinct types of laminar boundary-layer instability which may be encountered in real viscous flows. These have been classified by several authors according to their predominant characteristics. The following convention will be adopted in this report.

- (1) Dynamic (Taylor-Görtler) instability.
- (2) Viscous (Tollmien-Schlichting) instability.
- (3) Inflectional instability.

Dynamic instability is the type in which energy is transferred from the mean flow to the disturbance motion in the boundary layer through the action of forces other than viscous; it is found in the flow over concave surfaces where the velocity increases in the direction toward the center of curvature. Viscous instability is the type in which energy is transferred from the mean flow to the disturbance motion in the boundary layer through the action of viscosity; it is found in the flow over flat or convex surfaces where the potential flow is nearly two-dimensional and the stream turbulence level is low. Inflectional instability exists when the boundary-layer velocity profile contains an inflection point. (Such velocity profiles are found in regions of positive pressure gradient on unswept wings.) This type of instability is more powerful than the viscous type and, when present, generally governs the behavior of the boundary layer.

Through experimental and theoretical work reported in references 1 to 3, it has been established that another manifestation of inflectional instability is to be found in the boundary-layer flow on swept wings. This instability arises from the secondary (spanwise) flow in the boundary layer and is operative in regions of negative as well as positive pressure gradients. The result of this type of instability is that discrete vortices form in the boundary layer when critical flow conditions are attained. It has been suggested in reference 1 that a significant parameter in indicating the onset of these critical conditions is the crossflow Reynolds number.

Although the results of references 1 to 3 provide considerable evidence that the instability limiting the length of laminar boundary-layer flow on a swept wing is of the inflectional type, the extent of available knowledge concerning the conditions required for this instability to develop is rather limited. Furthermore, there is at present no definitive information as to the effect of wing sweep on the location of beginning transition. The purpose of the present report is to supply such information as well as to provide further experimental data concerning the effects of wing sweep on boundary-layer stability for a wide range of sweep angles and angles of attack. The experimental data are analyzed in conjunction with theoretical boundary-layer calculations in order to determine whether or not there are critical values of crossflow Reynolds number for vortex formation and for the beginning of transition.

## NOTATION

The following symbols are used throughout the report:

$C_p$	pressure coefficient, $\frac{p-p_\infty}{q_\infty}$
$F(\eta)$	boundary-layer velocity-profile parameter, $2\eta - 2\eta^3 + \eta^4$
$G(\eta)$	boundary-layer velocity-profile parameter, $\frac{\eta}{6} (1-\eta)^3$
$M$	free-stream Mach number
$R$	chord Reynolds number based on flow in streamwise direction
$R_{trans}$	transition Reynolds number based on flow in streamwise direction
$R_x$	crossflow Reynolds number, $\frac{w_{n,max} \delta_x}{\nu}$
$U$	component of potential-flow velocity normal to leading edge of wing
$U_\infty$	component of free-stream velocity normal to leading edge of wing
$V$	component of potential-flow velocity parallel to leading edge of wing
$V_\infty$	component of free-stream velocity parallel to leading edge of wing
$W$	resultant potential-flow velocity
$W_\infty$	free-stream velocity
$a$	speed of sound
$c$	wing chord in streamwise direction
$c_l$	section lift coefficient, $\frac{\text{section lift}}{cq_\infty}$
$c_1$	wing chord in direction normal to leading edge
$f(C_{p\Lambda=0}, \Lambda)$	function of $C_{p\Lambda=0}$ and $\Lambda$
$p$	local static pressure
$p_\infty$	free-stream static pressure

$q_{\infty}$	free-stream dynamic pressure	
$s$	surface distance normal to leading edge from forward stagnation point	
$u$	boundary-layer velocity component normal to leading edge of wing	
$v$	boundary-layer velocity component parallel to leading edge of wing	
$w$	resultant boundary-layer velocity	A
$w_n$	boundary-layer velocity component normal to potential-flow streamline	2 2 2
$w_t$	boundary-layer velocity component parallel to potential-flow streamline	
$x$	chord distance normal to leading edge of wing	
$x'$	chord distance in streamwise direction from leading edge of wing	
$y$	distance parallel to leading edge of wing	
$z$	distance from surface of wing	
$\Lambda$	angle of sweep of leading edge	
$\alpha$	angle of attack in streamwise plane	
$\delta_x$	boundary-layer thickness for flow in $x$ direction	
$\delta_y$	boundary-layer thickness for flow in $y$ direction	
$\eta_x$	dimensionless distance normal to surface, $\frac{z}{\delta_x}$	
$\eta_x'$	dimensionless distance normal to surface at which $w_n$ is a maximum value	
$\eta_y$	dimensionless distance normal to surface, $\frac{z}{\delta_y}$	
$\lambda$	Pohlhausen boundary-layer parameter, $\frac{\delta_x^2}{\nu} \frac{dU}{ds}$	
$\nu$	kinematic viscosity	
$\theta$	$\tan^{-1} \frac{V}{U}$	

## Subscript

$\Lambda = 0$  conditions which would exist if the component of stream flow normal to the leading edge of the wing were the resultant stream flow

## MODEL AND INSTRUMENTATION

A  
2  
2  
2  
The model used in this investigation was a constant-chord, variable-sweep wing with an NACA 64<sub>2</sub>A015 section normal to the leading edge. Coordinates of the airfoil section were obtained in reference 4, and are listed in table I. The wing, which had a 4-foot chord, was of all steel construction and was mounted in semispan manner on the turntable in the test section of the Ames 12-Foot Pressure Tunnel, as shown in figures 1 and 2. In the unswept position, the wing had a nominal aspect ratio of 2.5, based on its actual dimensions, and an effective aspect ratio of 5.0 considering it as a semispan model.

Sweep angles of 0°, 10°, 20°, 30°, 40°, and 50° were attainable with replacement of aluminum leading- and trailing-edge fairings at the root of the wing. For sweep angles of 0°, 10°, and 20° a half body of molded Fiberglas and resin, with radii corresponding to the airfoil ordinates, was used to form the wing tip. For sweep angles of 30°, 40°, and 50°, a tip extension was fastened to the wing. This extension also had a molded Fiberglas half body at its tip which made an angle of 40° with respect to the leading edge. The wing at 0° and 40° of sweep is shown in figure 2 installed in the test section.

The surface of the wing was formed from 3/8-inch-thick steel plates which were rolled to the approximate contour, welded to three channel beam spars, and machined to the airfoil shape. The final metal finish was obtained by sanding with number 400 sandpaper. The surface waviness was found to be less than 0.0005 inch per inch as measured with a 2-1/2-inch-span surface gage. In order to obtain a dark surface suitable for flow-visualization studies, the wing was sprayed with a primer and several coats of flat black lacquer. White stripes were added at intervals of approximately 10 percent of the chord to provide a frame of reference in these tests. The surface was then hand rubbed to a smooth finish with number 600 sandpaper.

The model was equipped with two rows of static-pressure orifices, 0.030 inch in diameter, on both the upper and lower surfaces as indicated in figure 1 and listed in table II. Pressure distributions were measured on multiple-tube manometers and were recorded photographically. Transition detection was accomplished through the use of small microphones located in the model and closely coupled to the static-pressure orifices (see table II). These microphones were magnetic-type receivers used in

headsets (U. S. Signal Corps Headset HS-30-U). The output signal from each microphone was amplified and passed through a band-pass filter to a headset receiver and an oscilloscope, permitting the signal to be interpreted both audibly and visually.

A small surface probe was used in observing the distribution of total pressure in the boundary layer at several distances from the model surface. The probe consisted of a battery of 30 hypodermic needles, 0.016 inch O.D. and 0.004-inch wall thickness, laid side by side and soldered together.

### TESTS

The tests of the wing at sweep angles of  $0^\circ$  to  $50^\circ$ , inclusive, were conducted in the Ames 12-Foot Pressure Tunnel. This is a low-turbulence facility in which the level of true turbulence or turbulent velocity fluctuations  $\Delta U/U$  is believed to be less than about 0.02 percent for the entire range of operation. However, as is true in any wind tunnel, there is a large increase in the noise level in the test section with increasing Mach number. A detailed study of the noise level has been made, and the results are to be found in reference 5. From an analysis of these results, it has been determined that the lowest noise level in the test section, for a given value of unit Reynolds number (Reynolds number per foot), is obtained by operating the tunnel at maximum pressure. Thus, in order to reduce the disturbing effect of noise, most of the transition measurements of the present investigation were made at or near the maximum allowable stagnation pressure of the tunnel, 60 pounds per square inch gage.

Both pressure-distribution and transition data on the wing were obtained, for all sweep angles, at angles of attack from  $-3^\circ$  to  $3^\circ$ . In the case of  $0^\circ$  of sweep, transition measurements were made also at an angle of attack of  $4^\circ$ . Pressure-distributions were measured in all cases at atmospheric pressure and at a Mach number of 0.27. Because of several small leaks which developed in the internal tubing to the orifices on the upper surface, where the microphones were connected, the pressure distributions presented in the report are those which were measured on the lower surface. These leaks did not have any significant effect on the transition data obtained for sweep angles greater than  $10^\circ$ . The data for sweep angles of  $20^\circ$ ,  $30^\circ$ ,  $40^\circ$ , and  $50^\circ$  were obtained by increasing the tunnel speed until the onset of transition occurred at successive detection (orifice) stations, beginning at the rear and moving forward. At sweep angles of  $0^\circ$  and  $10^\circ$ , however, it was necessary to isolate individual orifices from contamination, when making transition measurements, by plugging the orifices ahead of the one being considered.

A  
2  
2  
2

Since there was found to be close agreement between the transition data obtained at the inboard and outboard orifice stations, only those data for the outboard station are presented in the report. The outboard station was selected because the inboard row of orifices was close to the tunnel wall at the higher sweep angles.

A  
2  
2  
2  
2

Flow-visualization studies were conducted on the upper surface of the wing at atmospheric stagnation pressure along with total-pressure surveys through the boundary layer. During these tests the model was set at angles of attack from  $-12^{\circ}$  to  $4^{\circ}$ . All sweep angles were included in the visual-flow studies whereas only  $30^{\circ}$  of sweep was employed in the total-pressure boundary-layer surveys. In order to visualize the paths of the vortices and the regions of transition, the model was sprayed with a solution of about one part (by volume) biphenyl crystals dissolved in eight parts of petroleum ether. This left a fine residue of biphenyl crystals on the surface which slowly sublimed, differentiating regions of high and low surface shear.

All of the wing data presented have been corrected for blockage effects by the method of reference 6. There is believed to be a small rotation of the flow in the test section resulting in a maximum helix angle of the order of  $0.25^{\circ}$ , but no correction for this has been applied to the data.

## RESULTS AND DISCUSSION

In general, there are two rather different types of destabilizing mechanisms operating in the boundary-layer flow on a swept wing. One of these is the usual viscous instability which, in combination with disturbances introduced into the boundary layer, governs the extent of laminar flow according to Tollmien-Schlichting two-dimensional theory or a modification of this theory to account for three-dimensional effects. The other is an inflectional instability which can produce greatly increased amplification of disturbance waves in regions of positive pressure gradient, or can result in the development of stationary waves or fixed vortices in regions of negative pressure gradient. The primary factors that determine which type of instability prevails, in a given case, are the intensity levels and frequency spectra of disturbances present in the stream, the angle of sweep, the Reynolds number, and the pressure distribution on the surface. The combined effects of the angle of sweep, the Reynolds number, and the pressure distribution on boundary-layer stability are the subject of the present report.

It has been shown for the case of viscous instability (see refs. 5 and 7) that the effects of Reynolds number and pressure distributions on transition are intimately related to the intensity and frequency spectra of disturbances present in the stream. In order to minimize the effects

of these disturbances, most of the boundary-layer transition data presented in this report were obtained for test conditions which would provide the least possible noise and turbulence in the test section of the wind tunnel.

In the case of swept wings, results presented in reference 1 indicate that there is a critical value of crossflow Reynolds number above which vortices develop. These vortices in turn generally cause reductions in the length of "laminar" flow.<sup>1</sup> Both types of instability are greatly influenced by the local static-pressure gradient, and the pressure distribution which existed on the wing at various sweep angles will be presented prior to the presentation and discussion of the boundary-layer transition results.

A  
2  
2  
2

### Pressure-Distribution Characteristics

The chordwise distributions of static-pressure coefficient on the upper surface of the wing in a direction normal to the leading edge are presented for two spanwise stations in figures 3 and 4. Data are presented for angles of attack from  $-3^\circ$  to  $3^\circ$  at sweep angles of  $0^\circ$ ,  $10^\circ$ ,  $20^\circ$ ,  $30^\circ$ ,  $40^\circ$ , and  $50^\circ$ . Since the wing was uncambered, the pressure distributions for the lower surface of the wing at a given angle of attack are found by simply changing the signs of the angles of attack indicated in the figures.

The pressure distributions for the unswept wing have been compared in figure 5 with theoretical pressure distributions for the NACA 64<sub>2</sub>A015 section. The theoretical curves were obtained by using an experimentally obtained value of section lift-curve slope in conjunction with the basic theoretical data for the NACA 64<sub>2</sub>A015 section given in reference 4. Comparisons of the swept-wing pressure distributions at the outboard station with those calculated according to simple-sweep theory are shown in figure 6.

From an inspection of the data presented in figures 3 and 4, it is seen that small but significant differences existed in the pressure distributions measured at the inboard and outboard stations of the wing, particularly at the lower angles of sweep and at zero sweep. Thus, the boundary-layer flow over the wing only approximated infinite-span conditions. Since the differences in the pressure distributions over the forward portions were greatest in the case of the unswept wing and occurred even at zero lift, it is believed that they resulted from the combination of a small residual rotation of the flow entering the test section and a three-dimensional finite-span effect.

---

<sup>1</sup>The word "laminar", as used here, includes the type of ordered vortex motion resulting from the existence of chordwise vortices in the boundary layer.

A  
2  
2  
2

From the data presented in figure 5, it appears that better agreement was obtained between the experimental and theoretical pressure distributions at the inboard station of the unswept wing than at the outboard station. However, this result is partly due to the use of the same value of lift-curve slope, 0.092 per degree, in the theoretical calculations of the pressure distributions for the two stations. As indicated in reference 8, the experimental value of lift-curve slope for two-dimensional NACA 64-series airfoils having a thickness-chord ratio of 0.15 is very close to the theoretical value for thin airfoils of  $2\pi$  per radian or 0.110 per degree. From an integration of the experimental pressure distributions, it was found that the values of section lift-curve slope at the inboard and outboard stations of the wing were approximately 0.092 and 0.073, respectively. The reduction in section lift-curve slope outboard is a reflection of the variation in additional loading occurring along the span of finite straight wings.

Although good agreement between experiment and theory (based on experimental values of lift-curve slope) was obtained for the pressure distributions at the inboard station, such was not the case at the outboard station. In this case it was found that the use of a higher value of lift-curve slope than that determined from the experimental data provided better agreement between the experimental and calculated pressure distributions insofar as the shapes of the curves were concerned. Since the pressure or velocity gradients are primary factors in boundary-layer calculations, the value of 0.092 for section lift-curve slope has been considered applicable to the wing as a whole for the purpose of calculating crossflow Reynolds numbers.

According to simple-sweep theory, the relationship between the static-pressure coefficients based on the flow in the streamwise direction over a swept wing and those based on the flow in the direction normal to the leading edge (i.e., unswept wing) is given by the expression

$$C_p = C_{p_{\Lambda=0}} \cos^2\Lambda$$

In figure 6 the agreement of the swept-wing pressure distributions with those derived by the application of simple-sweep theory to the unswept-wing pressure-distribution data is shown to be generally very good. All of the data used in these comparisons were obtained at the outboard station of the wing. It should be noted that better agreement is obtained for the higher angles of sweep ( $\Lambda \geq 30^\circ$ ) if the unswept data obtained at the inboard station are used. The reason why this change in station gives better correlation for these conditions appears to be that the effective spanwise locations of the outboard station is reduced with increasing angles of sweep.

## Transition Reynolds Number Characteristics

The transition Reynolds numbers on the upper surface of the wing at sweep angles from  $0^\circ$  to  $50^\circ$  are presented in figures 7, 8, and 9. Transition data are shown for angles of attack from  $-3^\circ$  to  $4^\circ$ . As noted in the discussion of the pressure distributions, the data corresponding to the lower surface of the wing at a given angle of attack are obtained by changing the signs of the angles of attack indicated in the figures.

In figure 7 the variation of transition Reynolds number with angle of attack is presented for the various sweep angles with transition occurring at successive chordwise locations on the surface. The data for the unswept wing in this figure indicate a consistent trend of increasing transition Reynolds number with decreasing angle of attack for transition locations from 0.21c to 0.45c. This result is as would be expected in consideration of the increasingly favorable pressure gradients developing on the upper surface with reductions in the angle of attack. In the case of finite angles of sweep, however, a different result is obtained. Although a similar trend to that found for the unswept wing exists at the higher (positive) angles of attack, a lower limit is attained below which a completely different trend is observed. The value of this lower limit in angle of attack appears to be a function of sweep angle and increases with increasing sweep angle. It is believed that this latter trend is the result of vortex formation and that the angle of attack where one trend changes over into the other defines the condition where vortices (of considerable strength) first appear in the boundary layer. Thus, the peak of the curves shown in figure 7 divides conditions for which the extent of laminar flow in the boundary layer on a swept wing is governed by inflectional instability from conditions for which it is governed by viscous instability.

The transition data of figure 7 have been presented in a different manner in figure 8 wherein the variation of transition Reynolds number with sweep angle is shown for several angles of attack. This figure illustrates the powerful effect that sweep has in lowering the transition Reynolds numbers on the upper surface at the lower (negative) angles of attack. The slight reductions in transition Reynolds number with sweep angle at the higher angles of attack are explained by the reductions in the favorable pressure gradients with increasing sweep at a given angle of attack.

A final form of the transition data for the upper surface of the wing is presented in figure 9. The transition Reynolds numbers at various angles of sweep are plotted as functions of the chord Reynolds number on logarithmic scales for several angles of attack. In this type of plot, the lines of constant percent chord appear as a series of parallel lines as indicated in the figure. In order to extend the range of chordwise

A  
2  
2  
2

stations covered at the higher sweep angles, the basic data of figure 7 have been augmented with data obtained at a lower tunnel pressure. These lower pressure data are not always in close agreement with corresponding (i.e., equal Reynolds number) high-pressure data. In fact, in certain instances transition data obtained at different tunnel pressures have exhibited rather large (10 to 20 percent) quantitative differences, possibly due to different sound spectra present in the free stream. However, the trends which appear in low-speed data obtained at different pressures are nearly always similar.

A  
2  
4  
0

In figure 9 the individual curves for the different sweep angles show how the location of beginning transition on the wing and the value of transition Reynolds number vary as the chord Reynolds number increases. It is to be noted that, for a given value of chord Reynolds number, the stream unit Reynolds number (or Reynolds number per foot) decreases with increasing sweep angle. Thus, if the data were plotted in terms of unit Reynolds number, an even greater spread between the various sweep angles would appear. It is seen that, for most of the swept wing data, the curves indicate an abrupt forward movement of transition and a corresponding reduction in transition Reynolds number as the chord or unit Reynolds number is increased. In some cases the trend is seen to be more abrupt than in others, with transition moving suddenly from behind  $0.40c$  to ahead of  $0.20c$ . A certain amount of scatter is present in the data, due to the fact that the detection stations were not aligned in the streamwise direction for finite angles of sweep. The lateral displacement of the detection stations (in the direction normal to the free stream) increased with sweep angle, thereby increasing the possibility of having three-dimensional flow effects appear in the data. In all cases, however, it is believed that the formation of vortices was responsible for the sharp reductions in transition Reynolds number.

#### Experimental Evidence of Vortex Formation

The transition results of the preceding section strongly suggest that there was a sudden development of vortices in the boundary layer on the wing and it was considered advisable to attempt to obtain additional evidence of their existence. This was done in two different ways: (1) by means of flow-visualization tests, and (2) by means of total-pressure surveys through the boundary layer. It was also hoped that these tests would establish whether or not the vortex pattern remained fixed with respect to the wing surface and if there existed a double set of vortices in the boundary layer as was found theoretically in reference 3 for the case of the rotating disk in inviscid flow.

Although flow-visualization studies on the wing were conducted at various angles of attack for sweep angles from  $0^\circ$  to  $50^\circ$ , no evidence of vortices was ever found at sweep angles of  $0^\circ$  and  $10^\circ$ . However, ample

evidence of their existence was obtained at sweep angles of  $20^\circ$ ,  $30^\circ$ ,  $40^\circ$ , and  $50^\circ$ . The explanation of why vortex evidence was not found at  $10^\circ$  of sweep is that all of these flow-visualization tests were conducted at atmospheric stagnation pressure in the wind tunnel, and it was not possible to obtain the necessary stream Reynolds number for vortex formation as indicated in the transition Reynolds number results. In general, it was found that the initial appearance of vortices, with increasing Reynolds number, immediately preceded the forward movement of the point of beginning transition.

A few representative photographs of the type of results obtained at  $30^\circ$  of sweep are presented in figure 10. From the evidence of vortex activity shown here and observed in many close visual inspections of the sprayed wing surface, a few salient features may be noted. First, it would appear that, at least with the coating of biphenyl crystals on the wing surface, the vortex pattern remains fixed in position. Second, the spacing of the vortex cores is not always uniform, although the average distance between adjacent cores was found to be roughly proportional to the boundary-layer thickness. Third, the vortices appear to originate at various distances from the stagnation line, depending on the angle of attack, angle of sweep, and stream Reynolds number, and to follow the paths of the potential-flow streamlines. Fourth, the spread of turbulence in the transition region appears to be consistently asymmetrical a certain way, suggesting that the direction of rotation is the same for all vortices. This result is that which would be expected if a double set of vortices existed as pictured in reference 3.

From observations made using the 30-tube total-pressure probe parallel to the wing surface at  $x/c = 0.30$  for a sweep angle of  $30^\circ$ , it was found that a marked waviness in the total-pressure distribution existed under certain flow conditions. It appears that this type of periodic pressure pattern was probably due to the presence of vortices in the boundary layer. In an attempt to determine whether or not a second set of vortices farther from the surface existed in combination with the set near the surface, traverses of the total-pressure rake through the boundary layer were made at several different flow conditions. If a double set of vortices did exist, it was expected that there would be two distinct periodic patterns in total pressure at different heights from the surface and laterally displaced. However, in no case was this result obtained; only a single vortex pattern was found and the spacing was consistent with that in the sublimation photographs. The flow conditions at which the waviness initially appeared in the total-pressure distributions have been used in calculating the critical values of crossflow Reynolds number for the onset of vortex development.

A  
2  
2  
2

## Critical Values of Crossflow Reynolds Number

A  
2  
2  
2  
2

In order to establish whether or not there are certain values of crossflow Reynolds number associated with the onset of vortex development and beginning transition, the results of the flow-visualization studies and the experimental transition data of figure 9 have been analyzed in conjunction with the theoretical boundary-layer calculations described in the appendix. The results of the analysis are summarized in figure 11 which shows the variation with angle of attack of the critical bands of crossflow Reynolds number for several angles of sweep and at various chordwise locations on the wing. The critical values of crossflow Reynolds number for the onset of vortex development and for beginning transition are seen to remain essentially constant for angles of attack below about  $-0.5^\circ$ . The explanation for the reduction in the critical values of crossflow Reynolds number at higher angles of attack ( $\alpha > -0.5^\circ$ ) is that viscous instability probably causes transition to occur before vortices are sufficiently strong to do so. It is to be noted that somewhat lower critical values of crossflow Reynolds number were obtained by using the results of the flow-visualization studies than were obtained by using the results of the total-pressure surveys (for an indication of vortex initiation) and the microphone-detection measurements of beginning transition. In the case of initial vortex development at a given location, critical crossflow Reynolds numbers of about 135-160 compared to about 180-190 were obtained, and, in the case of beginning transition, critical crossflow Reynolds numbers of 190-210 compared to about 210-260 were obtained. Thus, it would appear that the light coating of biphenyl crystals on the wing during the flow-visualization tests may have caused premature vortex development (i.e., at a lower Reynolds number) and premature beginning transition at a given location. It should be noted that the critical values of crossflow Reynolds number obtained from the results of the sublimation studies in the present test are in good agreement with those values reported in other investigations using flow-visualization techniques (e.g., see ref. 1).

In order to arrive at a possible explanation for the difference in the rates at which transition moves toward the leading edge with increasing chord Reynolds number, reference is made to the calculations of crossflow Reynolds number given in the appendix. It is shown that, in addition to attaining considerably greater values, the crossflow Reynolds numbers for negative section lift coefficients and angles of attack have a chordwise variation different from those for positive section lift coefficients and angles of attack. Moreover, this effect is magnified with increasing sweep angle where larger differences in values exist. (It may be noted that chordwise distributions of crossflow Reynolds number are similar in their shape to distributions of pressure coefficient or potential-flow velocity along the surface, although the similarity does not extend to the relative values attained for various angles of attack.)

Assuming a constant critical value of crossflow Reynolds number for the onset of instability and vortex development, it is apparent that, for large angles of sweep and negative angles of attack, vortices should first appear near the end of the laminar run and progress forward gradually with further increase in chord Reynolds number. At small positive angles of attack ( $0^\circ < \alpha < 1.5^\circ$ ) it is to be expected that vortices would progress forward rapidly with a small increase in Reynolds number after their initial appearance. Thus, in one case a gradual forward movement of transition with increasing chord Reynolds number might be expected compared to a more abrupt movement in the other case.

When suitable conditions for vortex formation are not present, as was apparently the case for the wing at  $0^\circ$  sweep and on the upper surface of the wing at  $10^\circ$  and  $20^\circ$  sweep for certain angles of attack, transition results from viscous instability or inflectional instability associated with an adverse gradient. The slight reductions in transition Reynolds number under these conditions, as the stream Reynolds number was increased and the location of beginning transition moved forward on the wing, are believed to have been due to changes in the intensity and frequency spectrum of tunnel sound (e.g., see ref. 5). This trend of a reduction in transition Reynolds number with increasing stream Reynolds number was generally reversed as the location of transition moved further forward into regions of more favorable pressure gradients.

A  
2  
2  
2

#### Airfoil Section Characteristics at Maximum Transition Reynolds Number

As has been indicated in the foregoing discussion, the boundary layer on a swept wing is governed by both viscous and inflectional instability. It has been found that, in the general case, one or the other of these two types of instability is responsible for the breakdown of laminar flow. In the special case where conditions are such that both types of instability occur simultaneously on an airfoil and promote transition, the greatest possible value of transition Reynolds number is attained for the particular surface. The optimum condition then, from the standpoint of maximum laminar boundary-layer flow, is one where this particular situation exists on both surfaces at the design lift coefficient.

The situation that prevailed on a portion of the finite-span wing of the present investigation is illustrated by the summary data presented in figure 12. The transition Reynolds numbers indicated in this figure were obtained by taking the maximum values from the separate curves for the various angles of attack and angles of sweep in figure 9. It is to be noted that, in all cases of finite sweep angle, there is one angle of attack where these maximum values of transition Reynolds number in turn reach a maximum. This is the optimum condition described above.

In order to provide a comparison of the pressure and velocity gradients required for optimum boundary-layer stability characteristics on the wing at various sweep angles, the chordwise distributions of pressure coefficient (in streamwise direction) and velocity (normal to leading edge) at the angles of attack for the maximum values of  $(R_{trans})_{max}$  shown in figure 12 are presented in figure 13. The velocity distributions were obtained from the corresponding pressure distributions which were obtained from the experimental pressure distributions at the outboard wing station by interpolation. Since no maximum value is believed to exist at  $0^\circ$  sweep (except as might possibly result due to stream turbulence effects in a wind tunnel), there is no single value of pressure gradient which is optimum in this case. This is in accord with the generally accepted rule that more negative pressure gradients result in increased boundary-layer stability on unswept surfaces.

#### SUMMARY OF RESULTS

The boundary layer on a swept wing is governed by two types of instability, viscous instability and inflectional instability. Viscous instability is the type that is associated with the development of Tollmien-Schlichting waves (laminar oscillations) on unswept surfaces under proper conditions of stream turbulence. Inflectional instability is the type that exists when the boundary-layer velocity profile contains an inflection point. This type of profile is found in the laminar boundary layer on both swept and unswept surfaces in the presence of an adverse (positive) pressure gradient and also in a direction normal to the potential-flow streamlines on swept surfaces in the presence of either a positive or negative pressure gradient. Inflectional instability may lead to the formation of discrete vortices parallel to the potential-flow streamlines in the case of swept wings. It has been suggested in previous studies that a useful parameter which may be used as a criterion for the onset of vortex formation is the crossflow Reynolds number. This parameter is based on the local boundary-layer thickness and the maximum component of velocity in the transverse direction (normal to the potential-flow streamlines).

From an investigation of the effects of sweep on the boundary-layer stability and transition characteristics of an untapered wing having an NACA 64<sub>2</sub>A015 section normal to the leading edge, the following results are obtained.

1. There was found to be a deleterious effect of sweep in causing premature transition to take place on either surface of the wing under certain conditions. This effect generally resulted in an abrupt forward

movement of the location of beginning transition with increasing stream Reynolds number, accompanied by a marked reduction in the transition Reynolds number.

2. Flow-visualization and boundary-layer surveys have demonstrated that vortices did exist on the wing and were the cause of the premature transition behavior. It is believed that, in general, the initial development of vortices, with increasing Reynolds number, immediately preceded the forward movement of beginning transition.

3. It was found that the stream Reynolds number at which vortices first develop depends on the angle of sweep and the pressure distribution on the surface. The results indicate that, for a given two-dimensional wing, the minimum stream Reynolds number at which vortices appear occurs at a sweep angle close to  $50^\circ$ . Since strong pressure gradients on swept surfaces are more conducive to vortex development than are weak gradients, the effects of sweep in causing premature transition forward of the minimum pressure station are generally first encountered on the lower surfaces of wings operating at positive angles of attack or lift coefficients. When conditions suitable for the formation of vortices are not present, as is often the case on the upper surface of swept wings, transition results from viscous instability or adverse-gradient-type inflectional instability as in the case of unswept wings.

A  
2  
2  
2

4. The crossflow Reynolds number was found to correlate the onset of vortex development and subsequent beginning transition very well. The critical values of this parameter obtained for vortex formation and for beginning transition at sweep angles of  $20^\circ$  to  $50^\circ$  range from about 135 to 190 and from about 190 to 260, respectively. The lower values in these ranges were obtained with a light coating of biphenyl crystals on the surface of the wing (for flow-visualization purposes), suggesting that this material may have induced premature vortex development and premature beginning transition at a given location. The critical values of crossflow Reynolds number for vortex development are in good agreement with those reported in previous investigations.

5. An approximate method is presented for computing the distribution of crossflow Reynolds number on any two-dimensional swept surface for which the pressure distribution is known. Using this distribution together with "critical" crossflow Reynolds number values of 180 and 240 (for vortex development and beginning transition, respectively), it is possible to obtain an estimate of the stream Reynolds number at which vortices will develop and induce the beginning of transition.

Ames Research Center  
National Aeronautics and Space Administration  
Moffett Field, Calif., July 19, 1960

## APPENDIX

## APPROXIMATE CALCULATION OF CROSSFLOW REYNOLDS NUMBER

Determination of Boundary-Layer Profile Normal  
to Potential-Flow Streamline

A  
2  
2  
2

According to the usual definition, the crossflow Reynolds number at any location on a swept surface is based on the maximum boundary-layer velocity component normal to the potential-flow streamline and on the boundary-layer thickness (as well, of course, as on the kinematic viscosity of the fluid). The following determination of the boundary-layer velocity profile normal to the potential-flow streamline is based on the approximate two-dimensional boundary-layer theory of Pohlhausen (see ref. 9) and on the approximate swept-wing boundary-layer theory given by Rott and Crabtree in reference 10.

If it is assumed, according to reference 10, that the boundary-layer velocity profile in the  $x$  direction (normal to the leading edge of the wing) is independent of the spanwise flow (i.e., that it depends only on the component of the flow normal to the leading edge of the wing), then, according to Pohlhausen

$$\frac{u}{U} = F(\eta_x) + \lambda G(\eta_x) \quad (A1)$$

where

$$\left. \begin{aligned} F(\eta_x) &= 2\eta_x - 2\eta_x^3 + \eta_x^4 \\ G(\eta_x) &= \frac{\eta_x}{6} (1 - \eta_x)^3 \end{aligned} \right\} \quad (A2)$$

and

$$\lambda = \frac{\delta_x^2}{\nu} \frac{dU}{ds}$$

$$\eta_x = \frac{z}{\delta_x}$$

$\delta_x$  = boundary-layer thickness based on  
chordwise velocity profile

The functions  $F(\eta_x)$  and  $G(\eta_x)$  are shown in figure 14.

If it is also assumed, according to reference 10, that the boundary-layer velocity profile in the  $y$  direction (parallel to the leading edge of the wing) is constant and equal to the Blasius or flat-plate profile, then

$$\begin{aligned} \frac{u}{v} &= F(\eta_y) \\ &= 2\eta_y - 2\eta_y^3 + \eta_y^4 \end{aligned} \quad (A3)$$

where

$$\eta_y = \frac{z}{\delta_y}$$

$\delta_y$  = boundary-layer thickness based on spanwise velocity profile

It follows that

$$\eta_y = \frac{\delta_x}{\delta_y} \eta_x \quad (A4)$$

From the flow diagram shown in figure 15(a) it is apparent that the resultant potential-flow velocity is given by

$$W = \sqrt{U^2 + V^2} \quad (A5)$$

and that

$$\frac{V}{U} = \tan \theta \quad (A6)$$

If  $w_n$  is now defined as the boundary-layer velocity component normal to the potential streamline, it is readily seen from figure 15(b) that

$$w_n = u \sin \theta - v \cos \theta \quad (A7)$$

where

$$u = U[F(\eta_x) + \lambda G(\eta_x)]$$

$$v = VF(\eta_y) = VF\left(\frac{\delta_x}{\delta_y} \eta_x\right)$$

Thus

$$\begin{aligned}
 w_n &= U[F(\eta_x) + \lambda G(\eta_x)] \sin \theta - VF \left( \frac{\delta_x}{\delta_y} \eta_x \right) \cos \theta \\
 &= U \sin \theta \left[ F(\eta_x) + \lambda G(\eta_x) - F \left( \frac{\delta_x}{\delta_y} \eta_x \right) \right] \\
 &= \frac{UV}{\sqrt{U^2+V^2}} \left[ F(\eta_x) + \lambda G(\eta_x) - F \left( \frac{\delta_x}{\delta_y} \eta_x \right) \right] \quad (A8)
 \end{aligned}$$

Introducing now the local static-pressure coefficient  $C_{p_{\Lambda=0}}$ , which can be assumed to depend only on the component of flow in the  $x$  direction, so that in low-speed flow

$$C_{p_{\Lambda=0}} = 1 - \left( \frac{U}{U_\infty} \right)^2 \quad (A9)$$

it is found that

$$\begin{aligned}
 \frac{UV}{\sqrt{U^2+V^2}} &= \frac{U_\infty \sqrt{1-C_{p_{\Lambda=0}}} \sin \Lambda}{\sqrt{1-C_{p_{\Lambda=0}}} \cos^2 \Lambda} \\
 &= \frac{W_\infty \sqrt{1-C_{p_{\Lambda=0}}} \sin 2\Lambda}{2\sqrt{1-C_{p_{\Lambda=0}}} \cos^2 \Lambda} = \frac{W_\infty}{2} f(C_{p_{\Lambda=0}}, \Lambda) \quad (A10)
 \end{aligned}$$

Thus, equation (A8) can be written as

$$\begin{aligned}
 w_n &= \frac{W_\infty \sqrt{1-C_{p_{\Lambda=0}}} \sin 2\Lambda}{2\sqrt{1-C_{p_{\Lambda=0}}} \cos^2 \Lambda} \left[ F(\eta_x) + \lambda G(\eta_x) - F \left( \frac{\delta_x}{\delta_y} \eta_x \right) \right] \\
 &= \frac{W_\infty}{2} f(C_{p_{\Lambda=0}}, \Lambda) \left[ F(\eta_x) + \lambda G(\eta_x) - F \left( \frac{\delta_x}{\delta_y} \eta_x \right) \right] \quad (A11)
 \end{aligned}$$

The variation of the function  $f\left(C_{p_{\Lambda=0}}, \Lambda\right)$  with angle of sweep  $\Lambda$  for several values of pressure coefficient  $C_{p_{\Lambda=0}}$  is shown in figure 16.

#### Determination of Maximum Value of $w_n$

Although an expression has been developed in the previous section for the component of velocity normal to the potential-flow streamline at any distance from the surface in the boundary layer, we are only concerned with the maximum value of velocity in this profile for the calculation of crossflow Reynolds number. In order to find the value of  $\eta_x (= \eta_x')$  at which  $w_n$  is a maximum, we first set the derivative of  $w_n$  with respect to  $\eta_x$  equal to 0.

$$\frac{d}{d\eta_x} \left[ F(\eta_x) + \lambda G(\eta_x) - F\left(\frac{\delta_x}{\delta_y} \eta_x\right) \right] = 0 \quad (A12)$$

When equations (A2) are used in conjunction with equation (A12) and the resulting expression rearranged to group terms in equal powers of  $\eta_x'$  together, the following equation is obtained

$$\left[ \frac{\lambda}{6} + 2 - 2 \left( \frac{\delta_x}{\delta_y} \right) \right] - \lambda \eta_x' + \left[ \frac{3}{2} \lambda - 6 + 6 \left( \frac{\delta_x}{\delta_y} \right)^3 \right] \eta_x'^2 - \left[ \frac{2}{3} \lambda - 4 + 4 \left( \frac{\delta_x}{\delta_y} \right)^4 \right] \eta_x'^3 = 0 \quad (A13)$$

with  $\lambda$  and  $\delta_x/\delta_y$  considered to be constants for any given case. It is possible to find roots of this cubic equation in terms of  $\lambda$  and  $\delta_x/\delta_y$ . However, it is more convenient to calculate  $\lambda$  for different values of  $\eta_x'$  and  $\delta_x/\delta_y$ . If equation (A13) is solved for  $\lambda$ , we obtain

$$\lambda = \frac{-\left[ 2 - 2 \left( \frac{\delta_x}{\delta_y} \right) \right] + \left[ 6 - 6 \left( \frac{\delta_x}{\delta_y} \right)^3 \right] \eta_x'^2 - \left[ 4 - 4 \left( \frac{\delta_x}{\delta_y} \right)^4 \right] \eta_x'^3}{\frac{1}{6} - \eta_x' + \frac{3}{2} \eta_x'^2 - \frac{2}{3} \eta_x'^3} \quad (A14)$$

This function is plotted versus  $\eta_x'$  with  $\delta_x/\delta_y$  as a parameter in figure 17. In order to determine the value of  $\eta_x'$  for a given value of  $\lambda$ , it is first necessary to evaluate  $\delta_x/\delta_y$  at the given surface

location. The method used to obtain the values of  $\delta_x/\delta_y$  in the present calculations is based on the approximate theory of reference 10.

### Calculation of $R_*/R^{1/2}$

If the crossflow Reynolds number is written as

$$R_* = \frac{w_{n_{max}} \delta_x}{\nu}$$

and the stream Reynolds numbers based on flow in the streamwise and chordwise direction, respectively, as

$$R = \frac{W_\infty c}{\nu}$$

$$R_\perp = \frac{U_\infty c_\perp}{\nu} = R \cos^2 \Lambda$$

then, using equation (A11) and the relationship

$$\begin{aligned} \lambda &= \frac{\delta_x^2}{\nu} \frac{dU}{ds} \\ &= \left( \frac{\delta_x}{c_\perp} \right)^2 R_\perp \frac{d(U/U_\infty)}{d(s/c_\perp)} \end{aligned}$$

it is found that

$$\begin{aligned} R_* &= \frac{1}{2} \left( \frac{\delta_x}{c_\perp} \right) R \cos \Lambda \left[ \left( \frac{\delta_x}{c_\perp} \right)^2 R_\perp \frac{d(U/U_\infty)}{d(s/c_\perp)} G(\eta_{x'}) + F(\eta_{x'}) \right. \\ &\quad \left. - F \left( \frac{\delta_x}{\delta_y} \eta_{x'} \right) \right] f(C_{p_{\Lambda=0}}, \Lambda) \end{aligned} \quad (A15)$$

where  $\eta_{x'}$  indicates the value of  $\eta_x$  for the condition of  $w_{n_{max}}$ . As a final form of this expression we write

$$\frac{R_*}{R^{1/2}} = \frac{1}{2} \left( \frac{\delta_x}{c_l} \right) R_1^{1/2} \left[ \left( \frac{\delta_x}{c_l} \right)^2 R_1 \frac{d(U/U_\infty)}{d(s/c_l)} G(\eta_{x'}) \right. \\ \left. + F(\eta_{x'}) - F \left( \frac{\delta_x}{\delta_y} \eta_{x'} \right) \right] f \left( C_{p_{\Lambda=0}}, \Lambda \right) \quad (A16)$$

where the functions  $F$ ,  $G$ , and  $f$  are evaluated using equations (A2) and (A10), respectively, along with the values of  $\eta_{x'}$  and  $\delta_x/\delta_y$ . The value of  $(\delta_x/c_l)R_1^{1/2}$  which is proportional to the boundary-layer thickness in the  $x$  direction may be calculated by any one of several approximate methods (e.g., see ref. 9). The calculated chordwise distributions of  $R_*/R^{1/2}$  for the wing of the present investigation at several angles of sweep and at several values of unswept section lift coefficient,  $c_{l_{\Lambda=0}}$ , are presented in figures 18 and 19. The variation of  $R_* R^{1/2}$  with  $c_{l_{\Lambda=0}}$  for several chordwise locations on the wing at a sweep angle of  $30^\circ$  is presented in figure 20. In order to determine the value of  $c_{l_{\Lambda=0}}$  corresponding to a given angle of attack, the following relationship between the angle of attack of a swept wing (measured in the streamwise plane) and the angle of attack for the corresponding unswept wing (measured in a plane normal to the leading edge)

$$\alpha = \alpha_{\Lambda=0} \cos \Lambda$$

may be used in conjunction with the value of section lift-curve slope (0.092 for the wing of the present investigation) to obtain the expression

$$c_{l_{\Lambda=0}} = c_{l_\alpha} \left( \frac{\alpha}{\cos \Lambda} \right)$$

A  
2  
2  
2

## REFERENCES

1. Owen, P. R., and Randall, D. G.: Boundary Layer Transition on a Sweptback Wing. RAE Tech. Memo. Aero 277, May 1952.
2. Gregory, N., and Walker, W. S.: Brief Wind Tunnel Tests on the Effect of Sweep on Laminar Flow. British A.R.C. 14,928 (Perf. 934, FM 1728) May 1952.
- A 3. Gregory, N., Stuart, J. T., and Walker, W. S.: On the Stability of  
2 Three-Dimensional Boundary Layers with Application to the Flow Due  
2 to a Rotating Disk. Phil. Trans. Royal Soc. of London, ser. A,  
2 no. 943, vol. 248, July 14, 1955, pp. 155-199.
4. Loftin, Lawrence K., Jr.: Theoretical and Experimental Data for a Number of NACA 6A-Series Airfoil Sections. NACA Rep. 903, 1948.
5. Boltz, Frederick W., Kenyon, George C., and Allen, Clyde Q.: The Boundary-Layer Transition Characteristics of Two Bodies of Revolution, a Flat Plate, and an Unswept Wing in a Low-Turbulence Wind Tunnel. NASA TN D-309, 1960.
6. Herriot, John G.: Blockage Corrections for Three-Dimensional-Flow Closed-Throat Wing Tunnels, with Consideration of the Effect of Compressibility. NACA Rep. 995, 1950.
7. Schubauer, G. B., and Skramstad, H. K.: Laminar-Boundary-Layer Oscillations and Transition on a Flat Plate. NACA Rep. 909, 1948.
8. Abbott, Ira H., von Doenhoff, Albert E., and Stivers, Louis S., Jr.: Summary of Airfoil Data. NACA Rep. 824, 1945.
9. Schlichting, Hermann: Boundary Layer Theory. McGraw-Hill Book Co., Inc., 1st Eng. ed., 1955.
10. Rott, Nicholas, and Crabtree, L. F.: Simplified Laminar Boundary-Layer Calculations for Bodies of Revolution and for Yawed Wings. Jour. Aero. Sci., vol. 19, no. 8, Aug. 1952, pp. 553-565.

TABLE I.- NACA 64<sub>2</sub>A015 WING COORDINATES  
(All dimensions given in percent length)

Station	Ordinate	Station	Ordinate
0	0	40.00	7.487
.50	1.193	45.00	7.313
.75	1.436	50.00	6.978
1.25	1.815	55.00	6.517
2.50	2.508	60.00	5.956
5.00	3.477	65.00	5.311
7.50	4.202	70.00	4.600
10.00	4.799	75.00	3.847
15.00	5.732	80.00	3.084
20.00	6.423	85.00	2.321
25.00	6.926	90.00	1.558
30.00	7.270	95.00	.795
35.00	7.463	100.00	.032

L. E. radius 1.561 percent, 0.749 inch  
T. E. radius 0.037 percent, 0.018 inch

A  
2  
2  
2

TABLE II.- STATIC-PRESSURE ORIFICE LOCATIONS (45 AND 80 PERCENT SPAN)  
[All dimensions given in percent length]

Upper and lower surface meridians	
Station	Station
1.4	49.9*
4.1	54.9*
7.0*	59.9*
10.1*	65.0*
15.9*	69.0*
20.8*	75.0*
23.9*	80.0*
29.9*	85.0*
34.8*	89.0*
39.8*	94.8*
44.8*	

\*Microphone at inboard and outboard  
upper surface orifice station

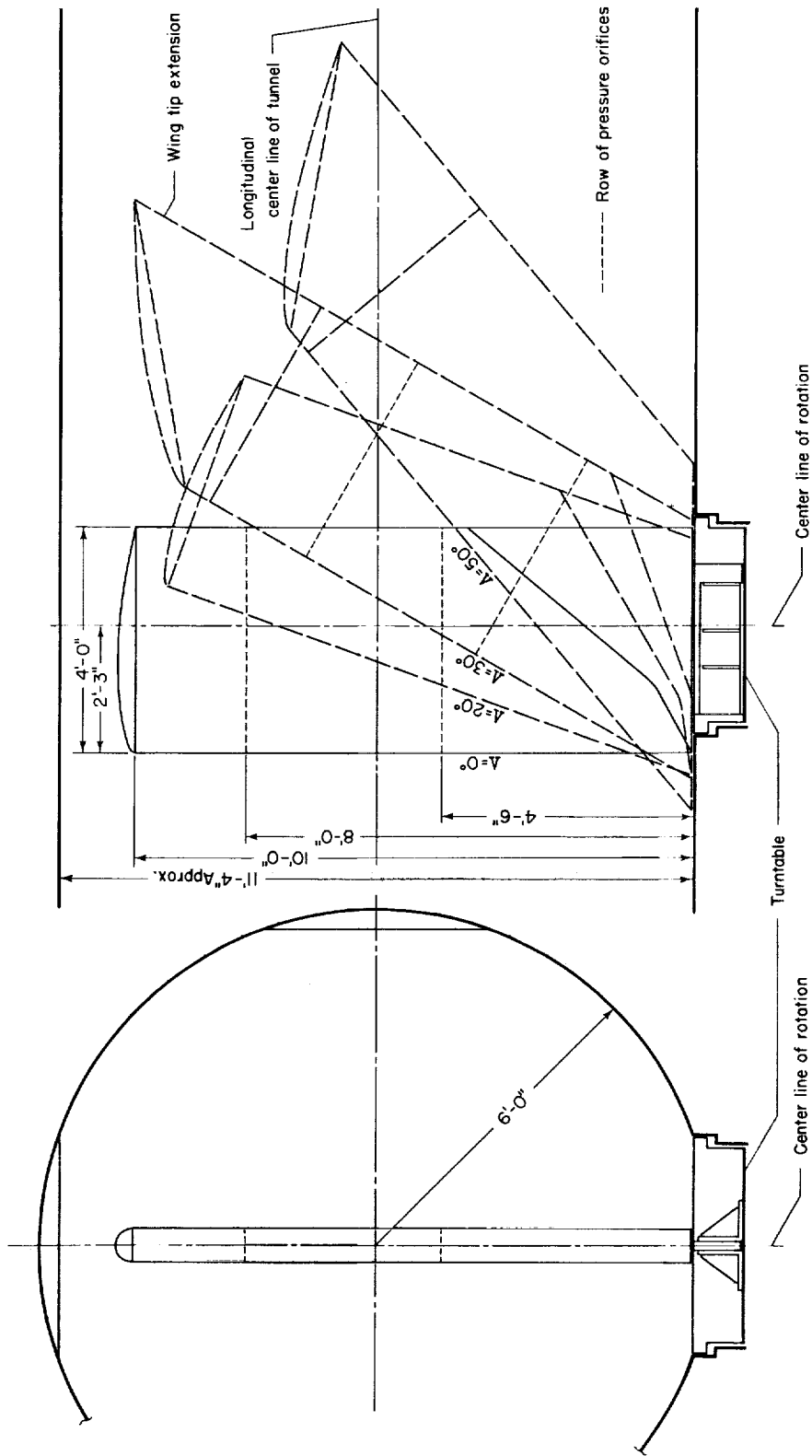
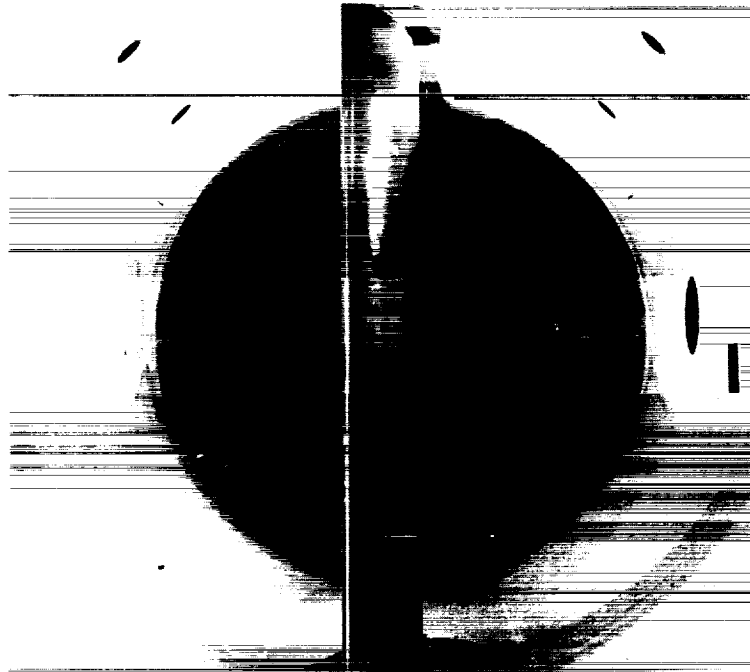


Figure 1.- The model orientation in the test section for several angles of sweep.

(a)  $\Lambda = 0^\circ$ 

A-25580

(b)  $\Lambda = 40^\circ$ 

A-26901

Figure 2.- The model mounted in the test section at  $0^\circ$  and  $40^\circ$  of sweep.

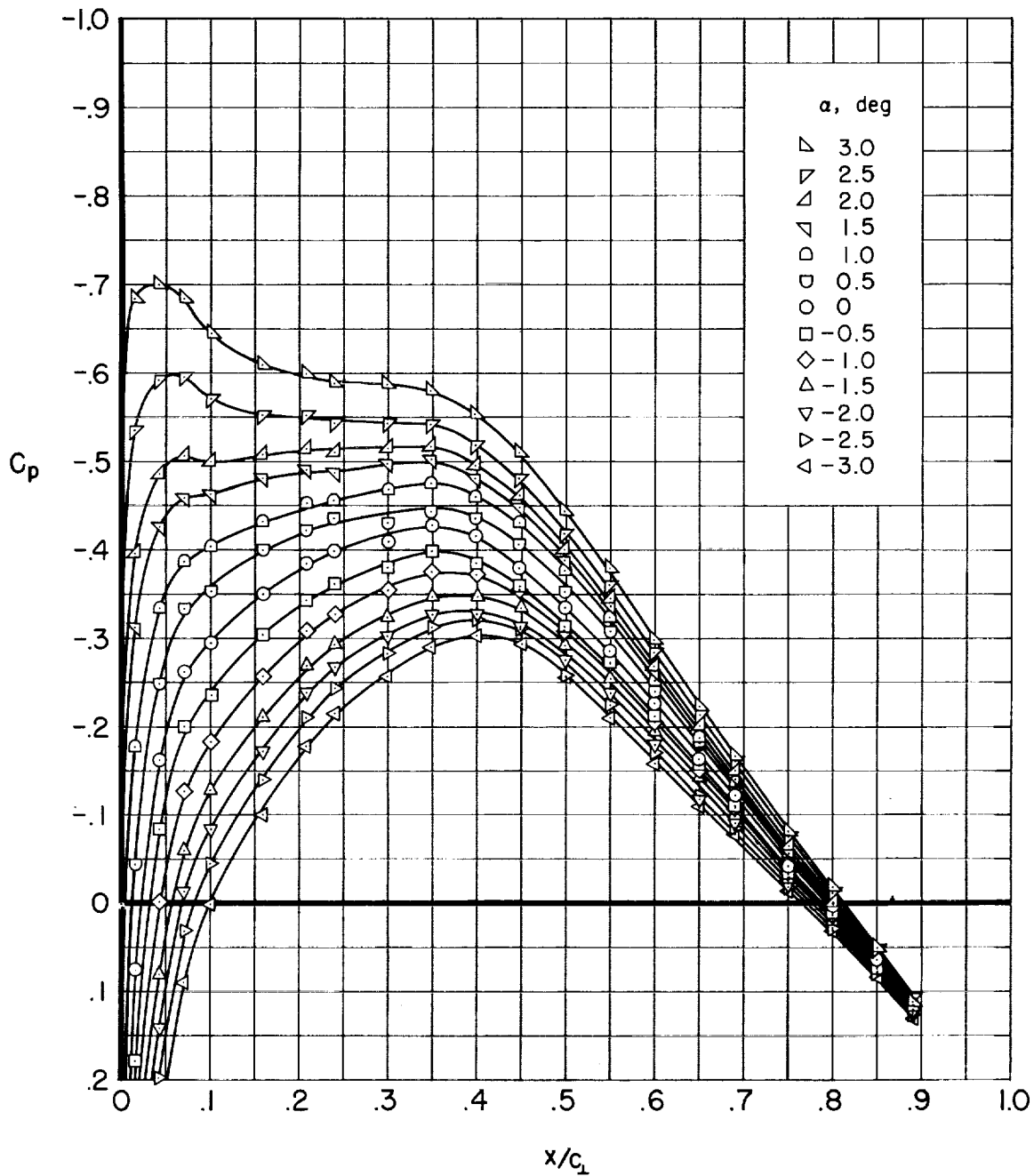
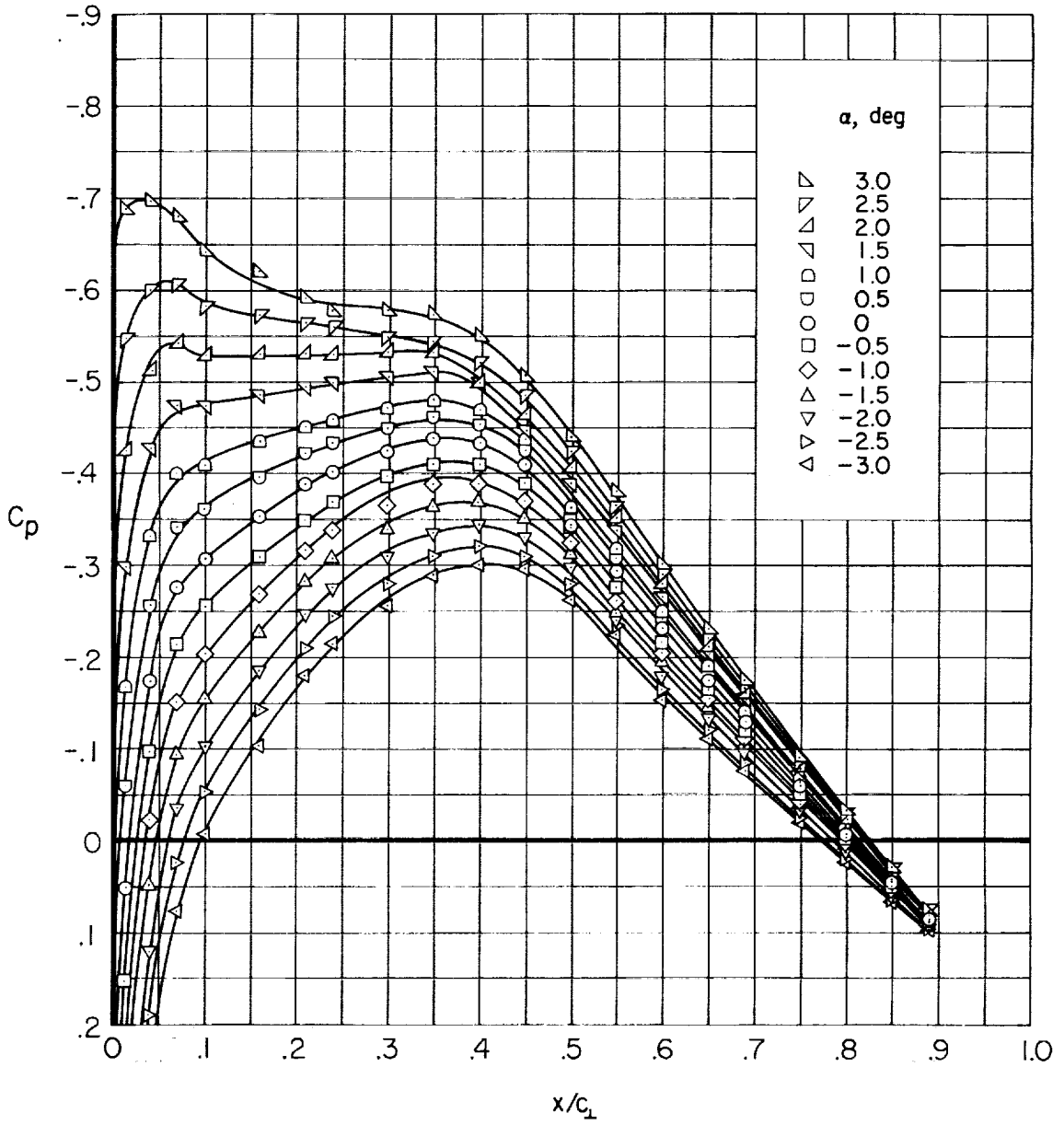
(a)  $\Lambda = 0^\circ$ 

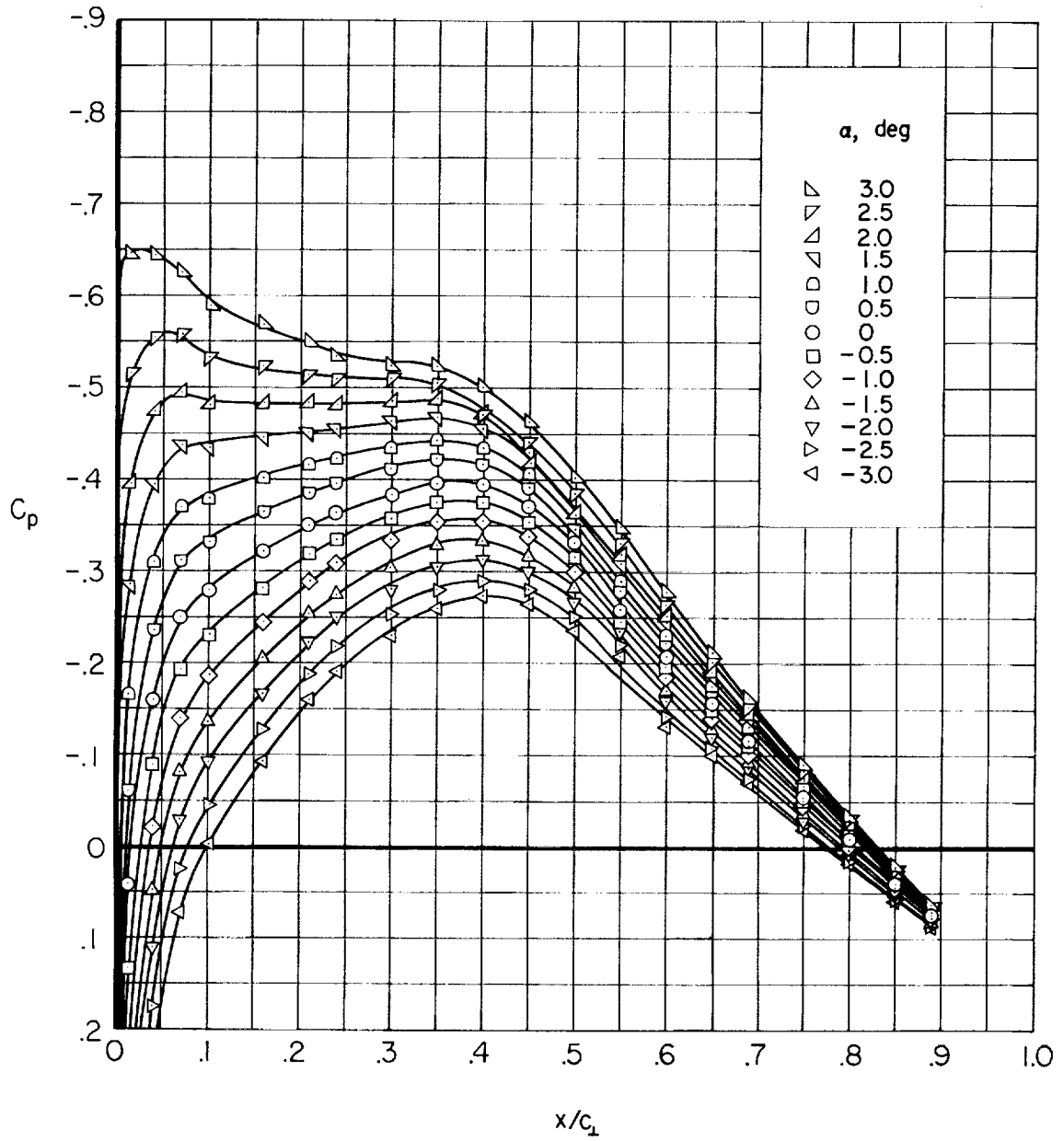
Figure 3.- The chordwise distributions of static-pressure coefficient on the upper surface of the wing at the inboard station.



(b)  $\Lambda = 10^\circ$

Figure 3.- Continued.

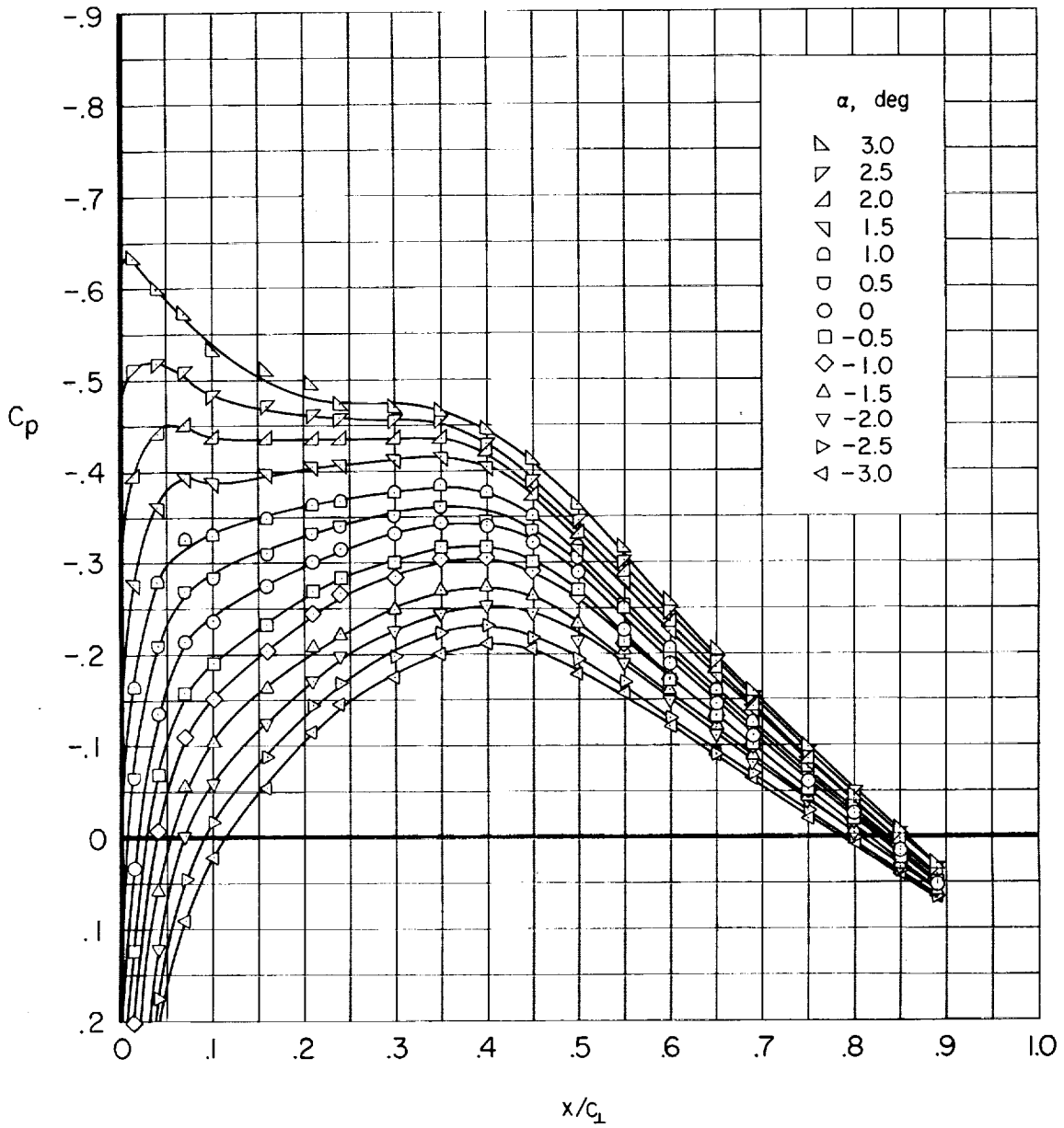
A  
2  
2  
2



(c)  $\Lambda = 20^\circ$

Figure 3.- Continued.

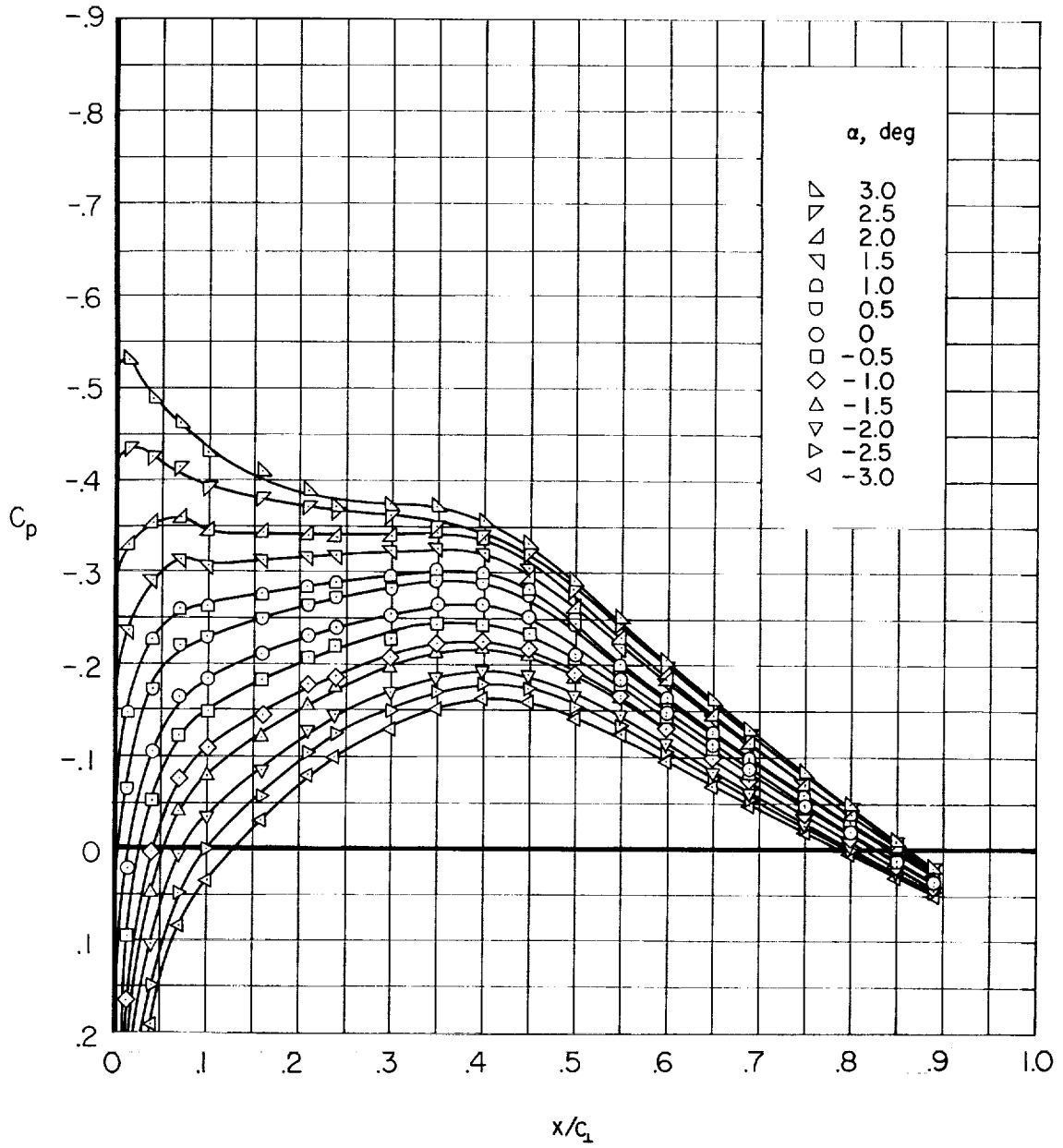
A  
2  
2  
2



(d)  $\Lambda = 30^\circ$

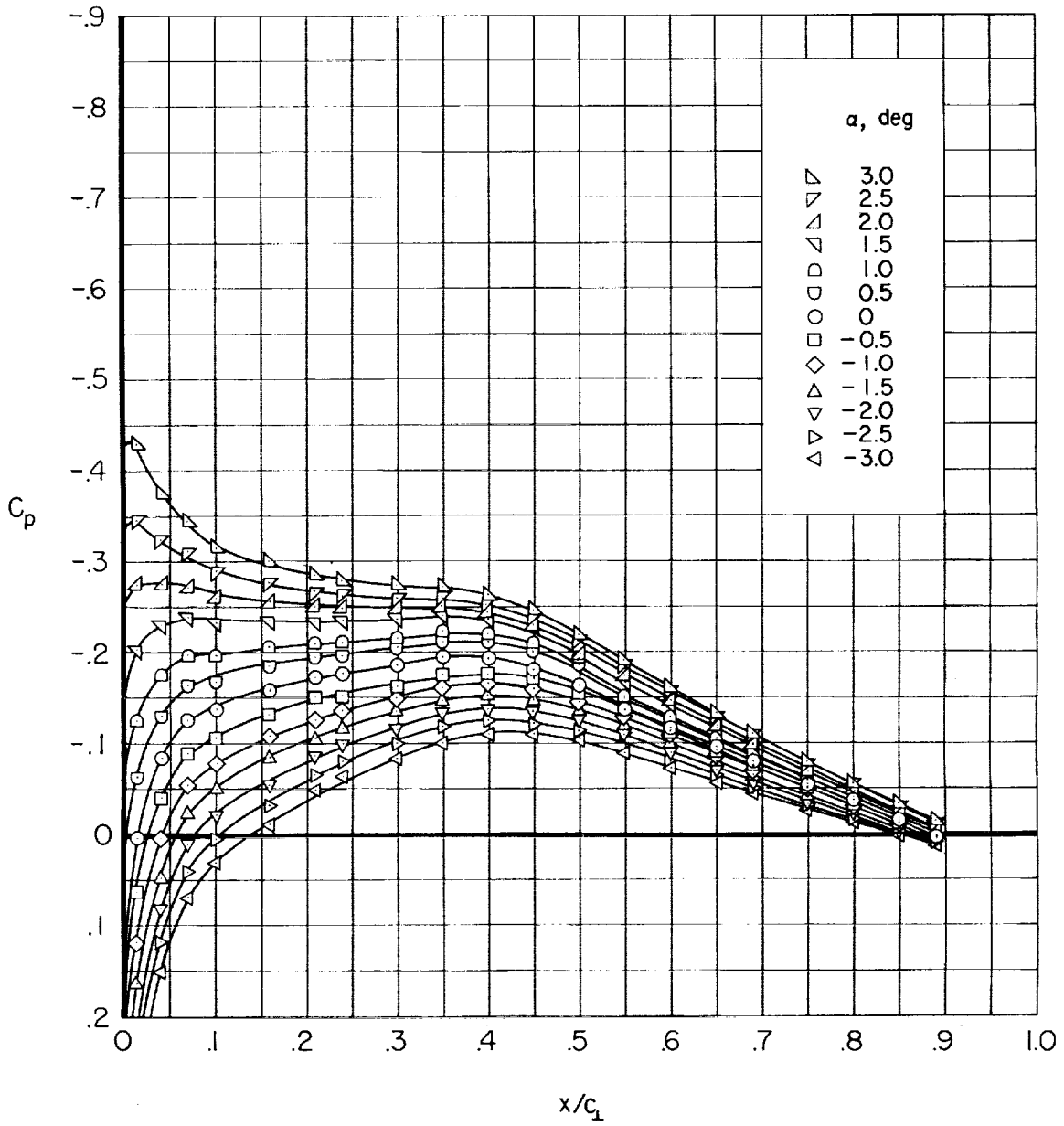
Figure 3.- Continued.

A  
2  
2  
2



(e)  $\Lambda = 40^\circ$

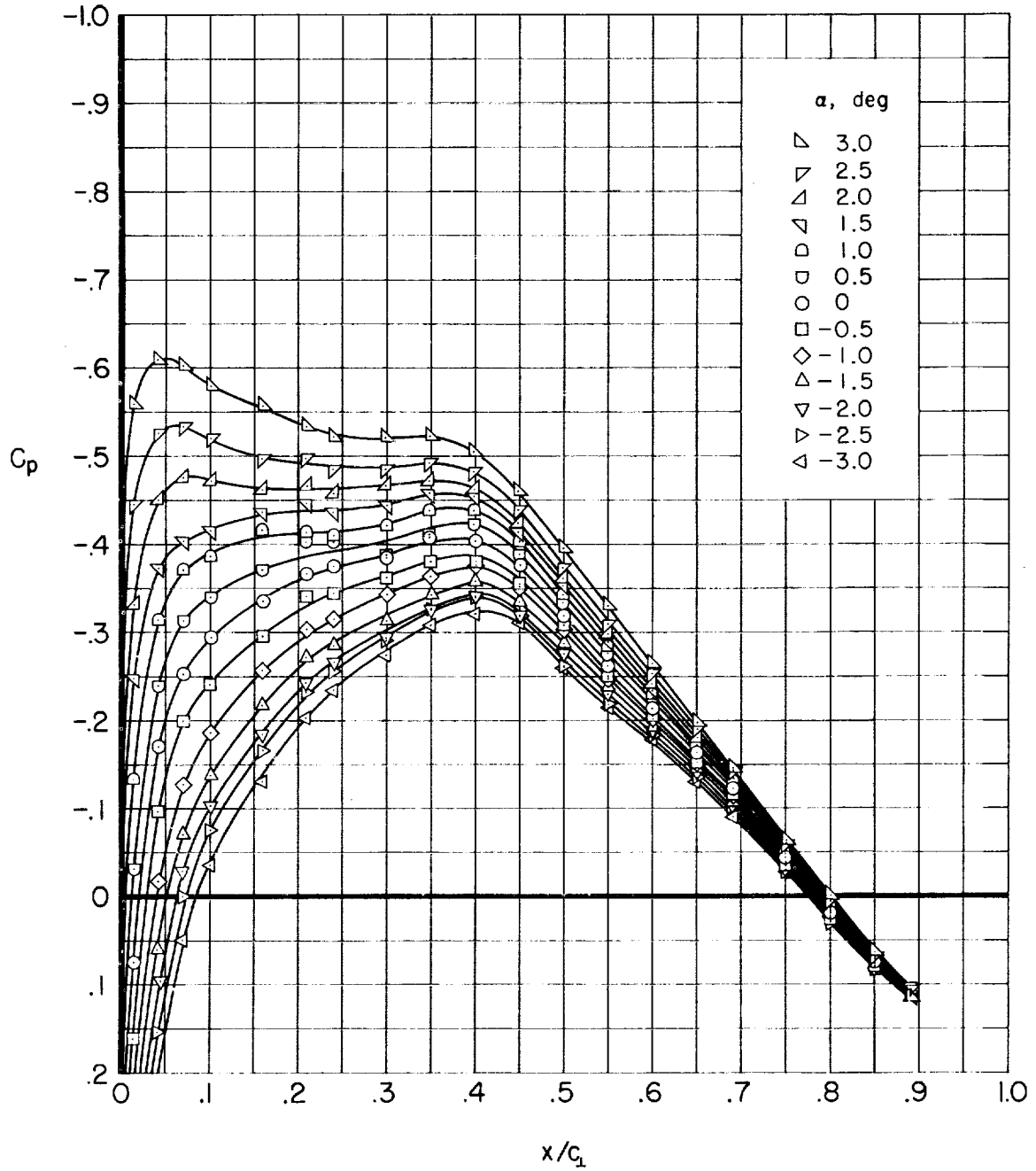
Figure 3.- Continued.



(f)  $\Lambda = 50^\circ$

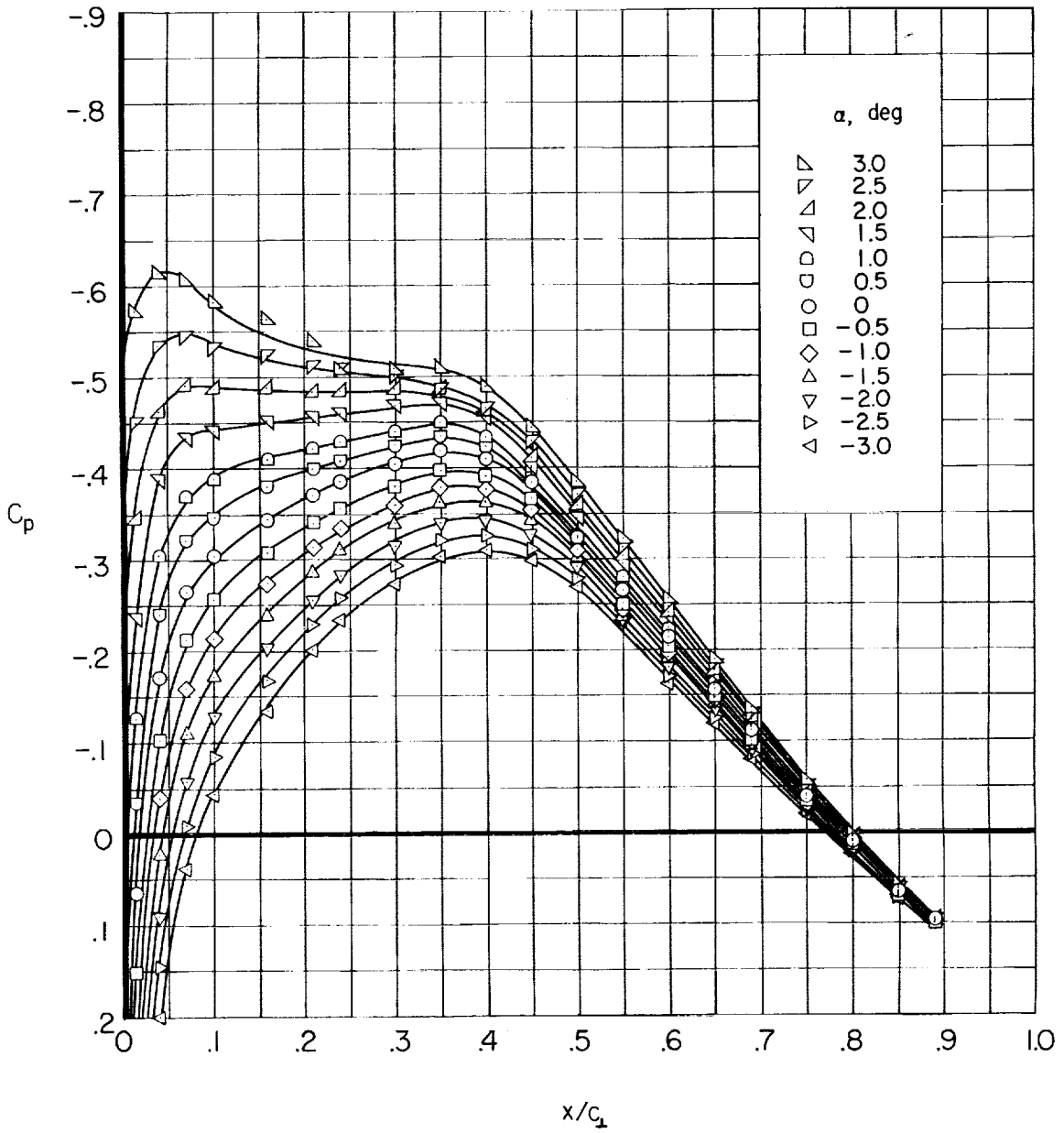
Figure 3.- Concluded.

A  
2  
2  
2



(a)  $\Lambda = 0^\circ$

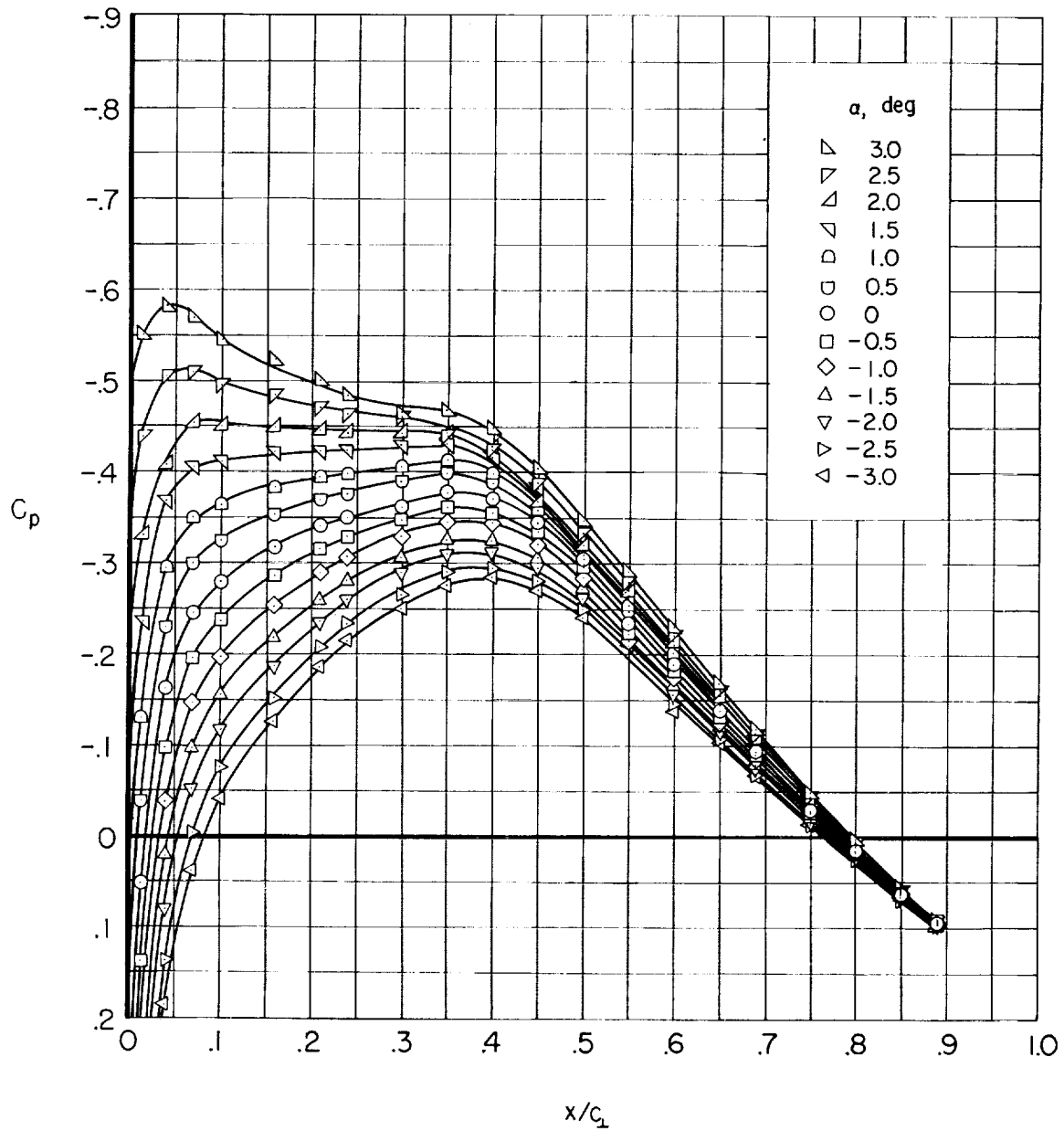
Figure 4.- The chordwise distributions of static-pressure coefficient on the upper surface of the wing at the outboard station.



(b)  $\Lambda = 10^\circ$

Figure 4.- Continued.

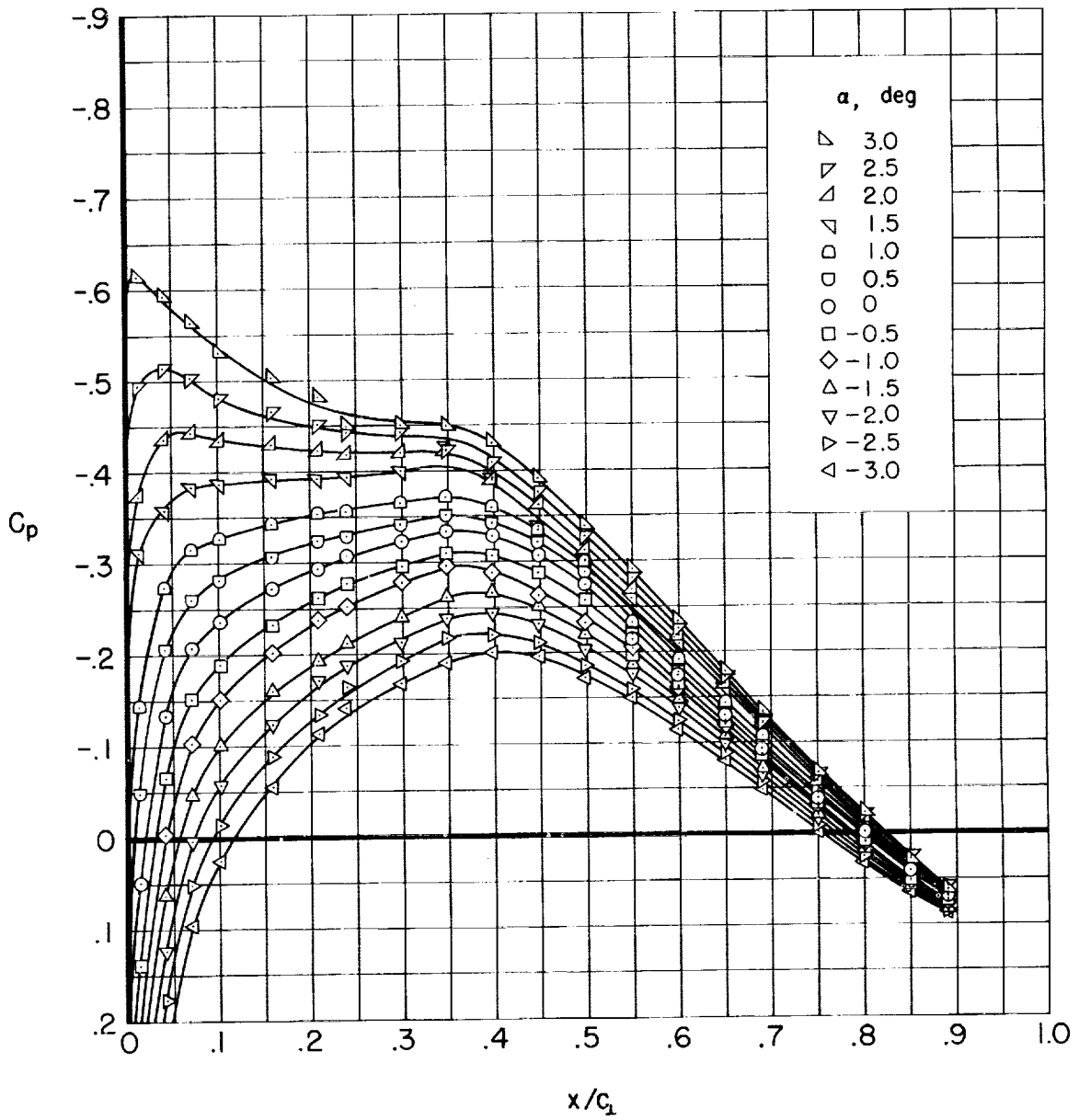
A  
2  
2  
2



(c)  $\Lambda = 20^\circ$

Figure 4.- Continued.

A  
2  
2  
2

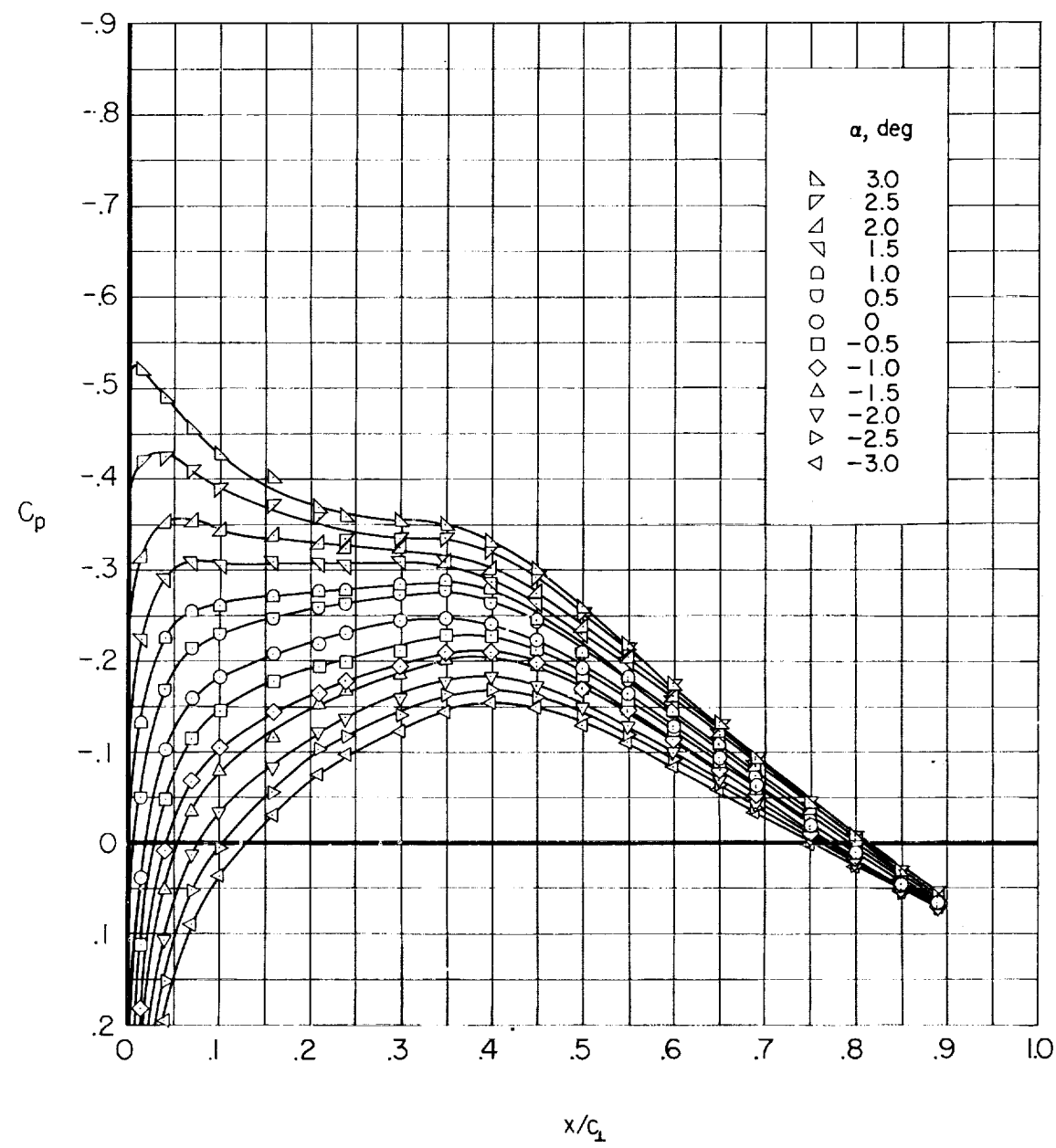


(d)  $\Lambda = 30^\circ$

Figure 4.- Continued.

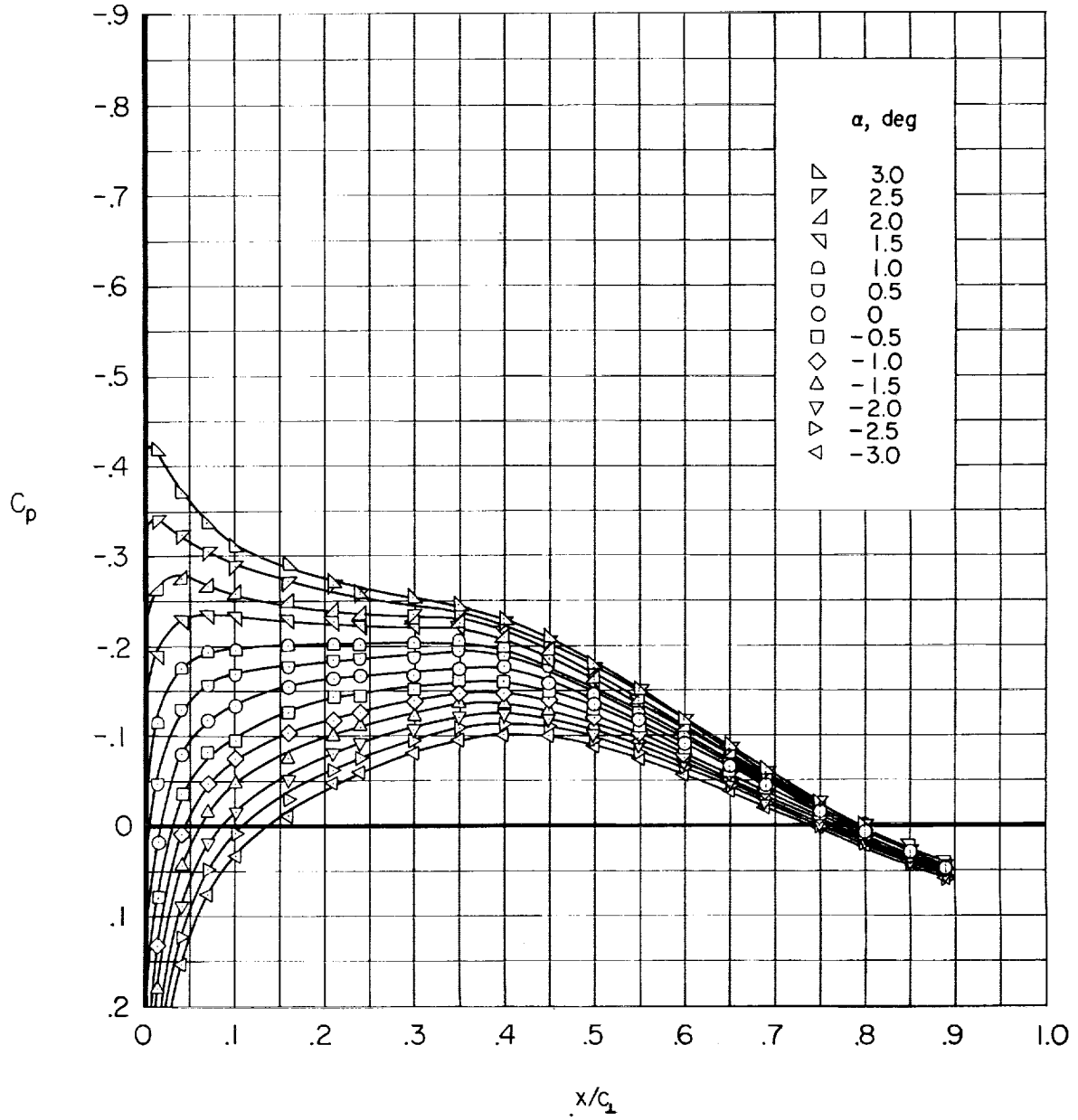
A  
2  
2  
2

A  
2  
2  
2



(e)  $\Lambda = 40^\circ$

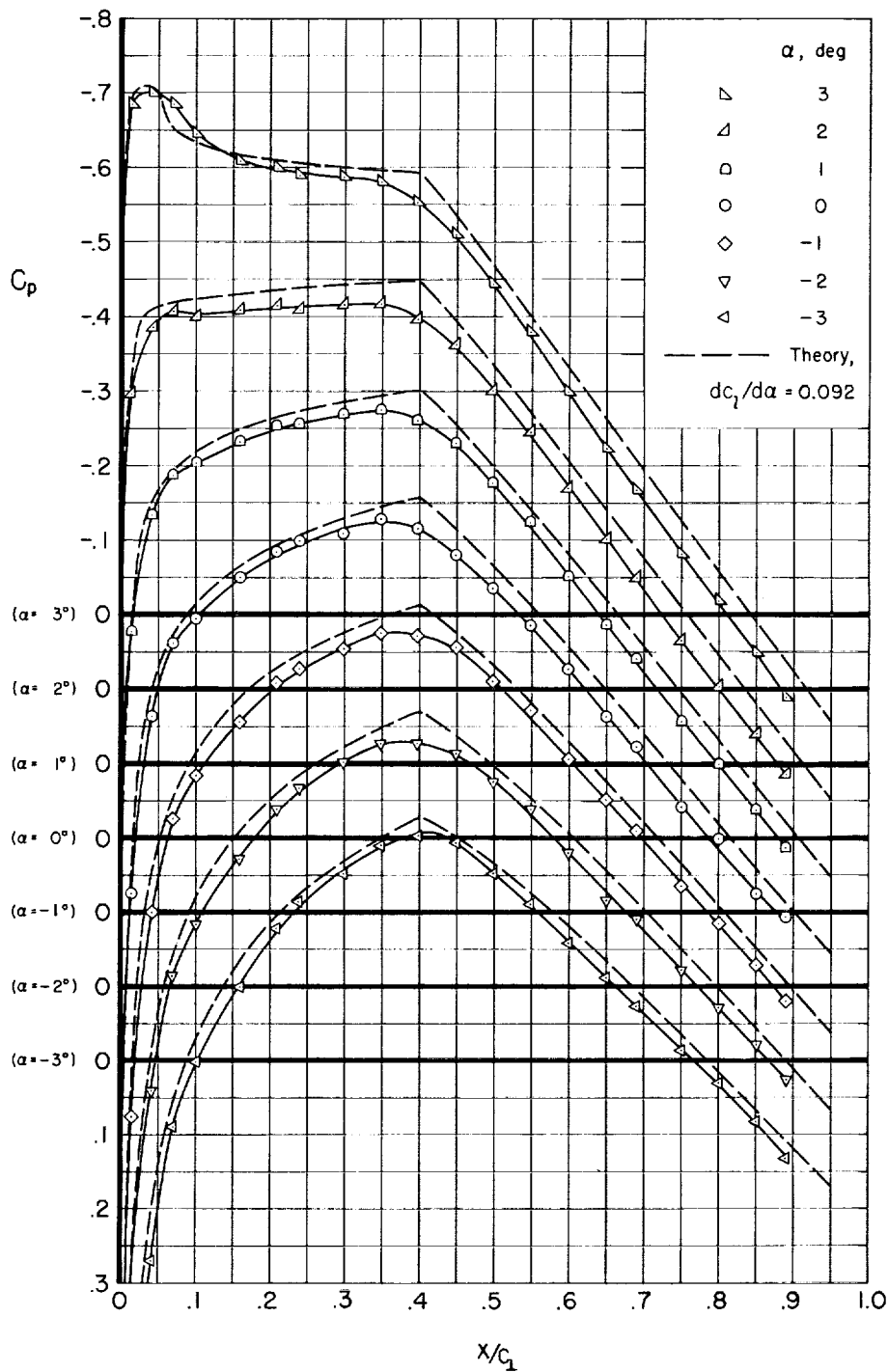
Figure 4.- Continued.



(f)  $\Lambda = 50^\circ$

Figure 4.- Concluded.

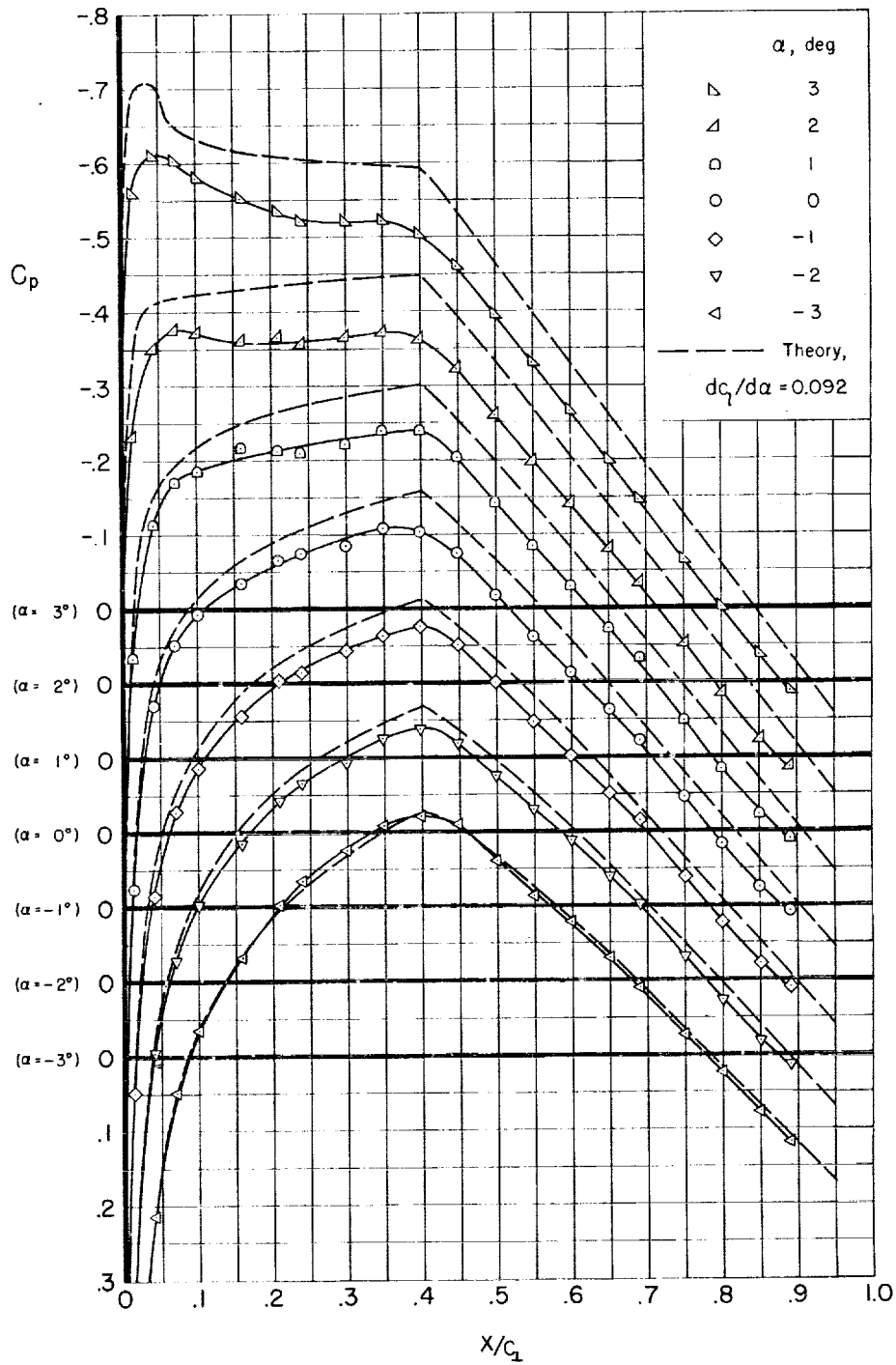
A  
2  
2  
2



(a) Inboard station.

Figure 5.- Comparisons of the experimental and theoretical pressure distributions on the upper surface of the wing at  $0^\circ$  of sweep.

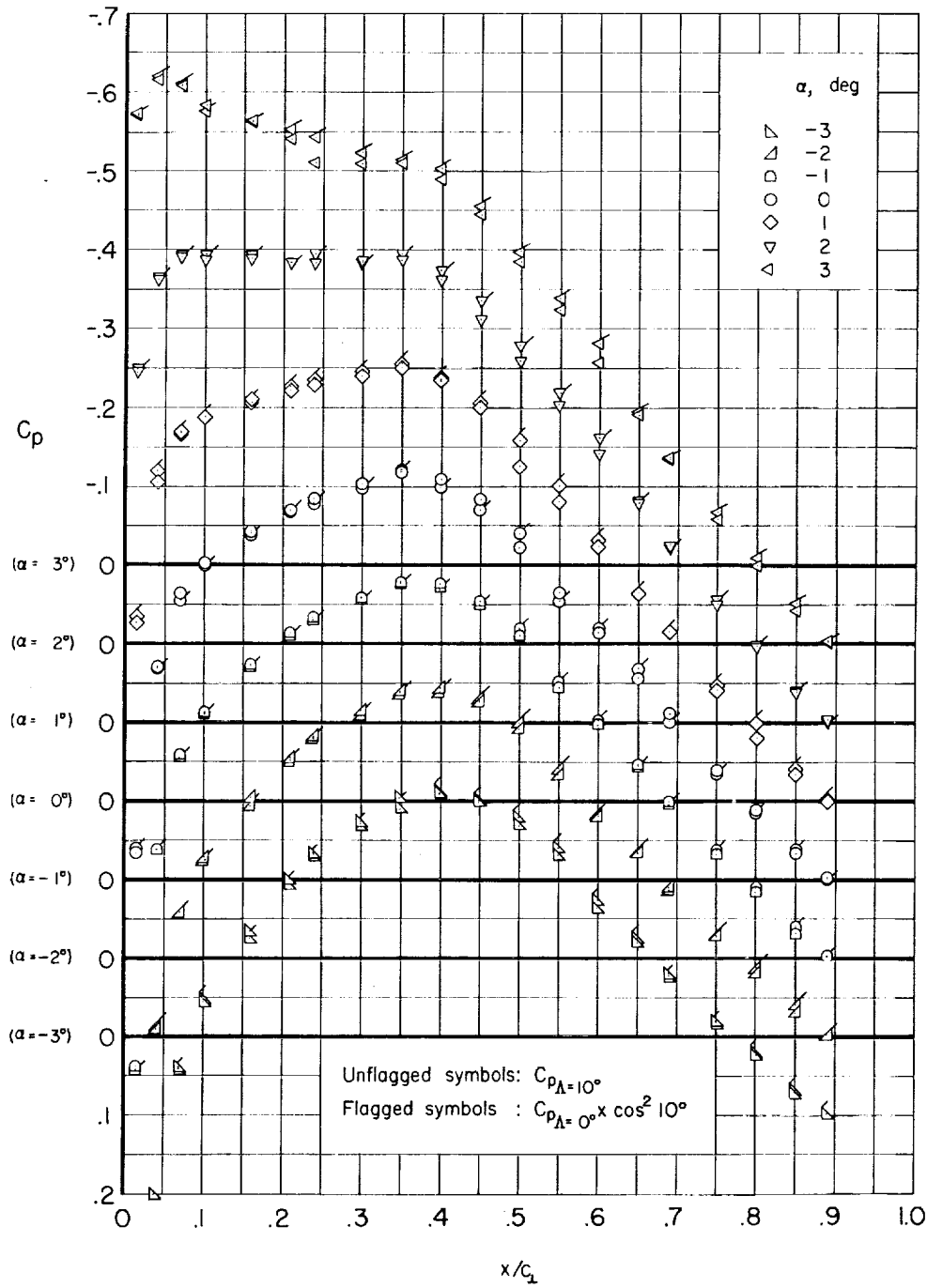
A  
2  
2  
2



A  
2  
2  
2

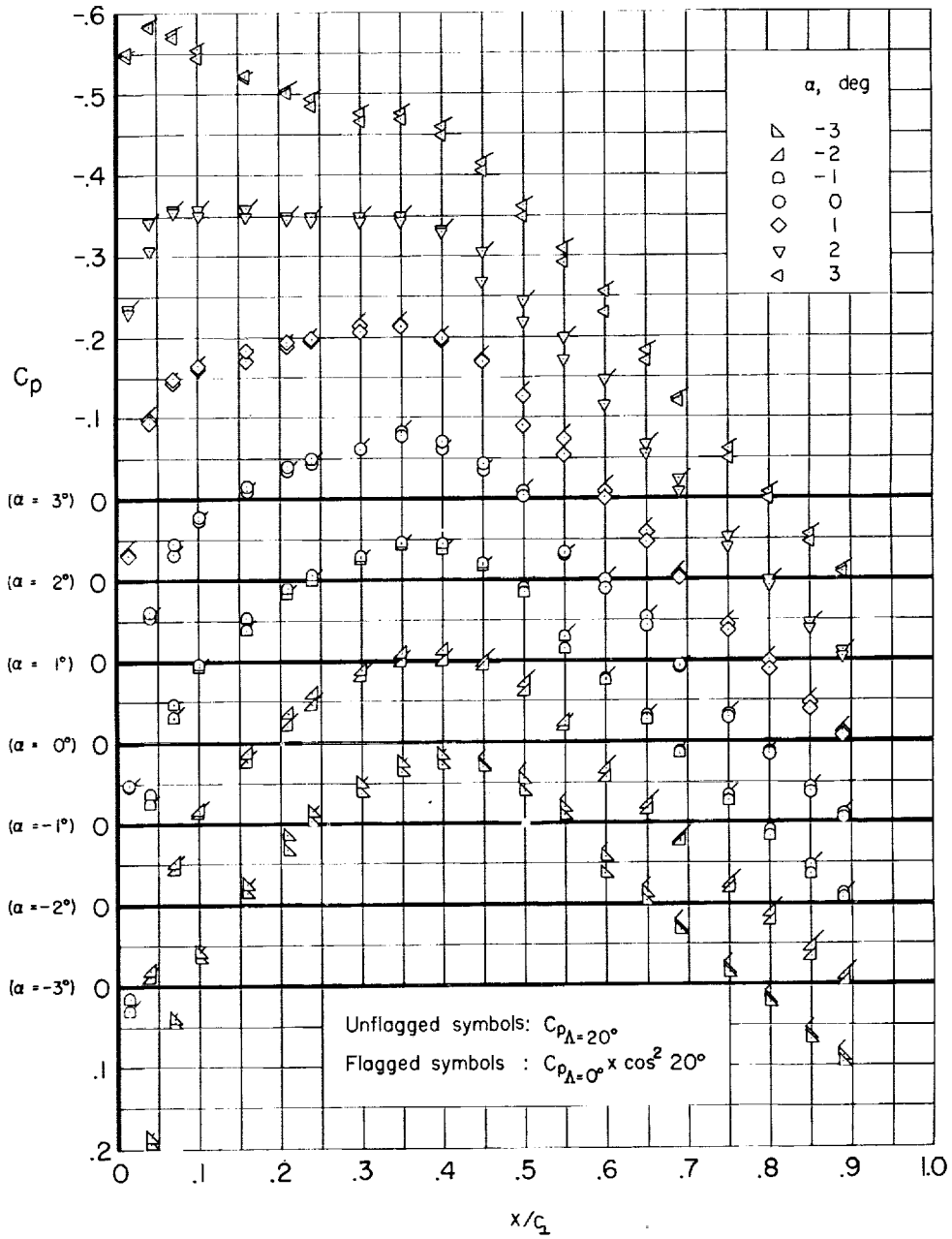
(b) Outboard station.

Figure 5.- Concluded.



(a)  $\Lambda = 10^\circ$

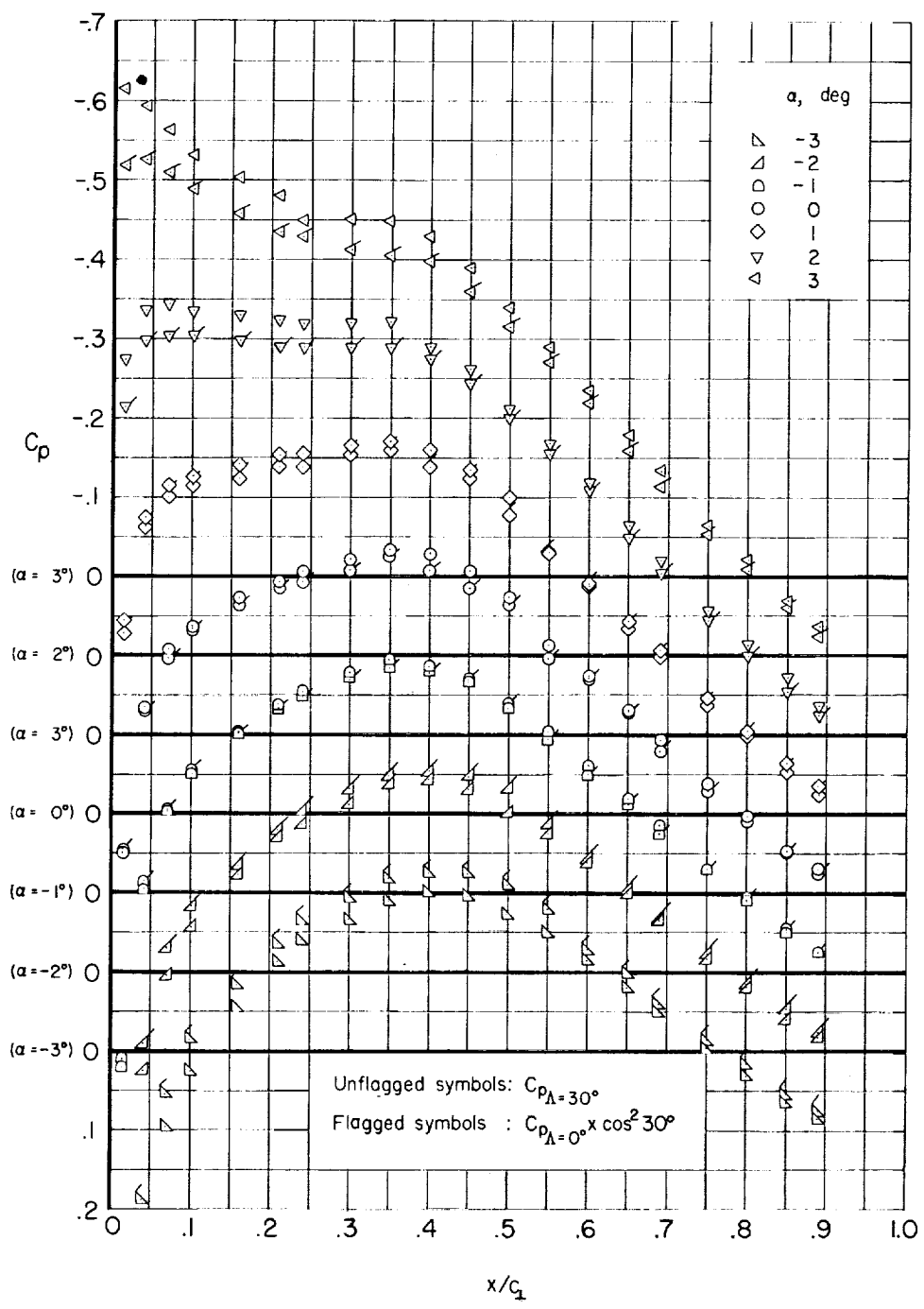
Figure 6.- Comparisons of the experimental pressure distributions on the upper surface of the wing at the outboard station with those derived using simple-sweep theory.



(b)  $\Lambda = 20^\circ$

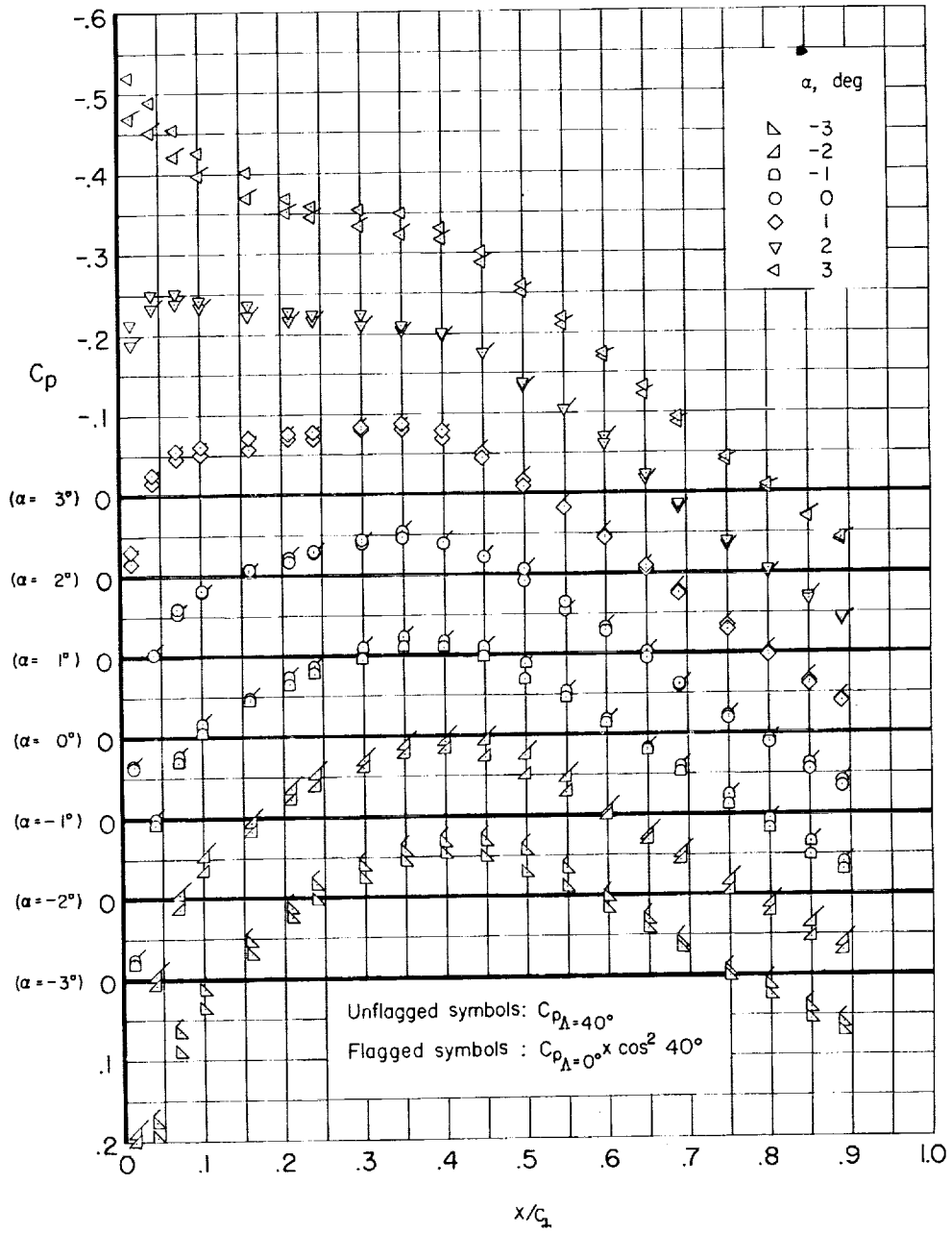
Figure 6.- Continued.

A  
N  
N  
N  
N



(c)  $\Lambda = 30^\circ$

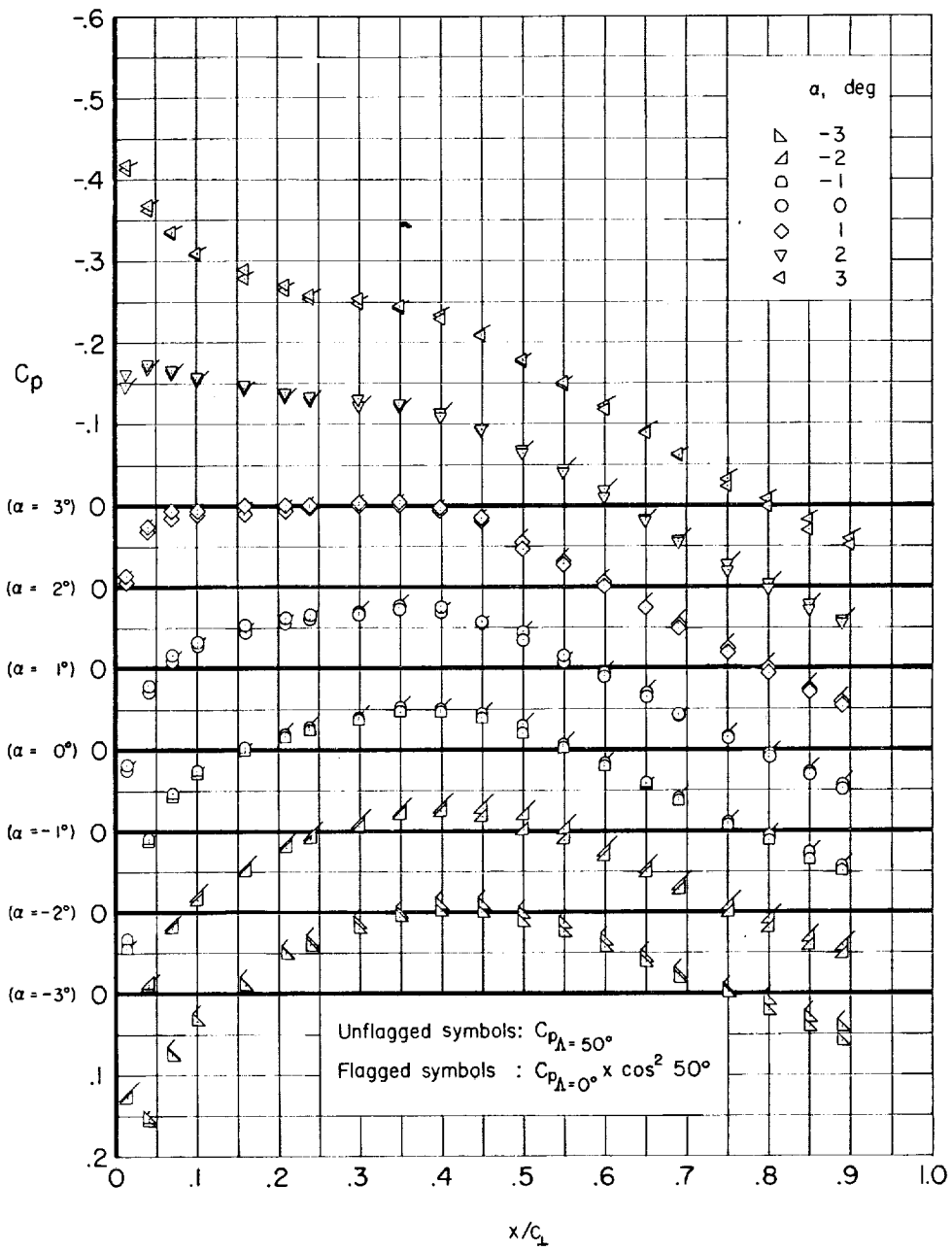
Figure 6.- Continued.



(a)  $\Lambda = 40^\circ$

Figure 6.- Continued.

A  
2  
2  
2



(e)  $\Lambda = 50^\circ$

Figure 6.- Concluded.

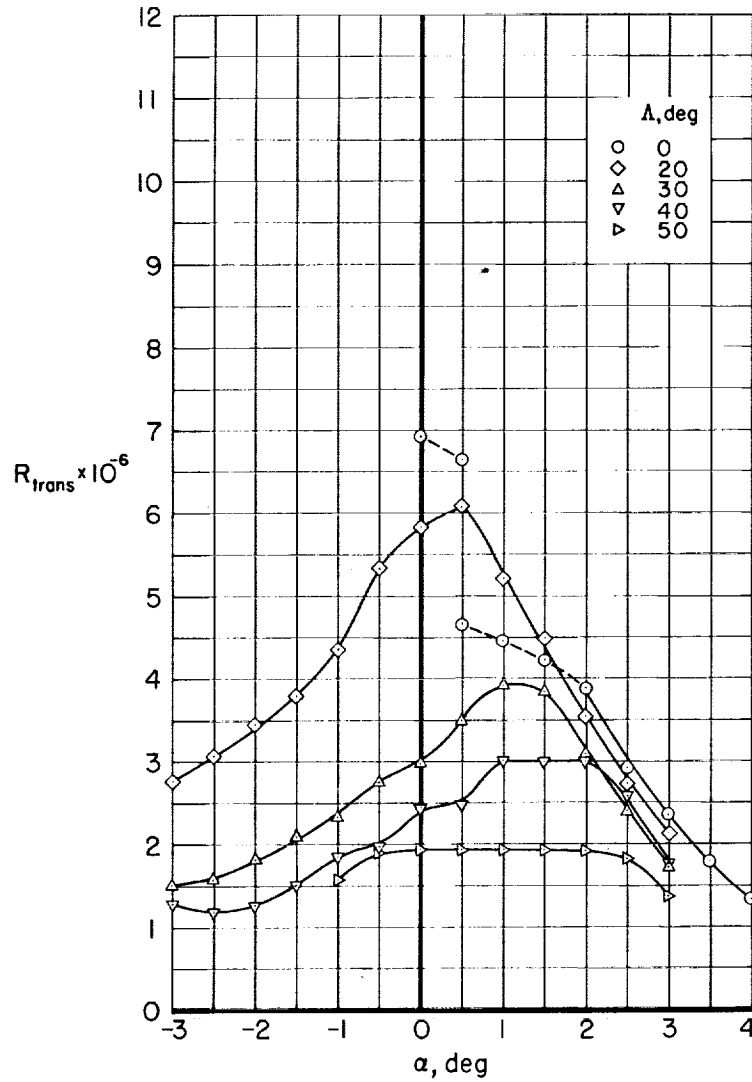
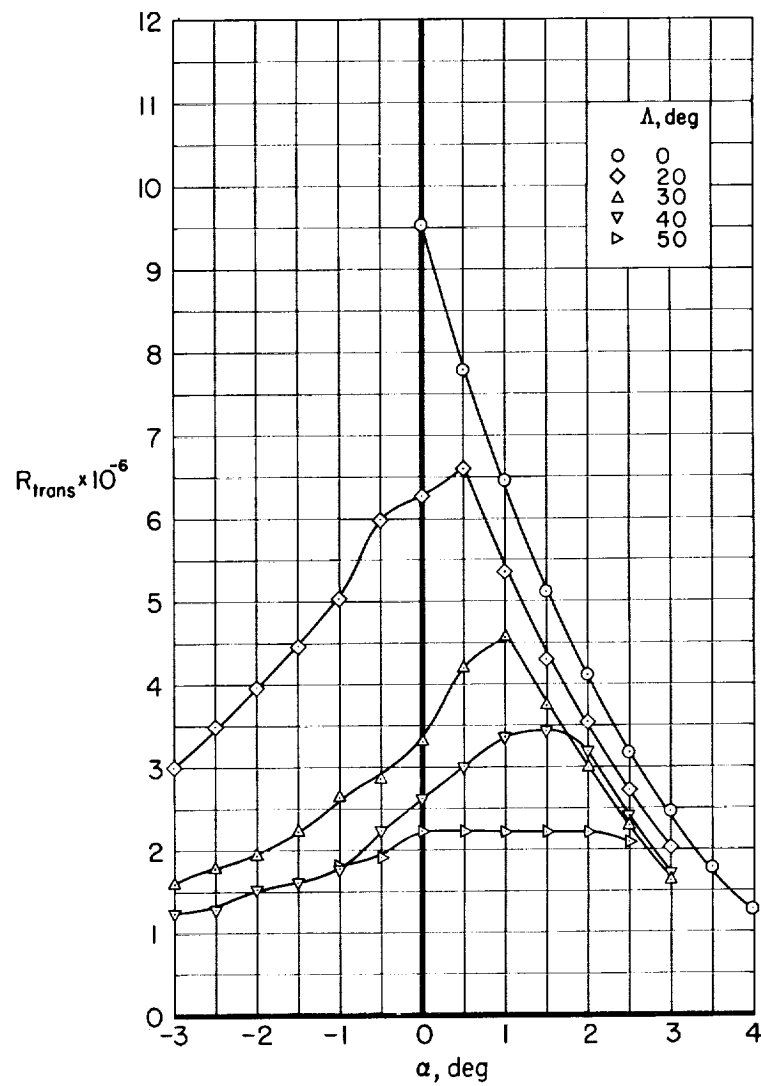
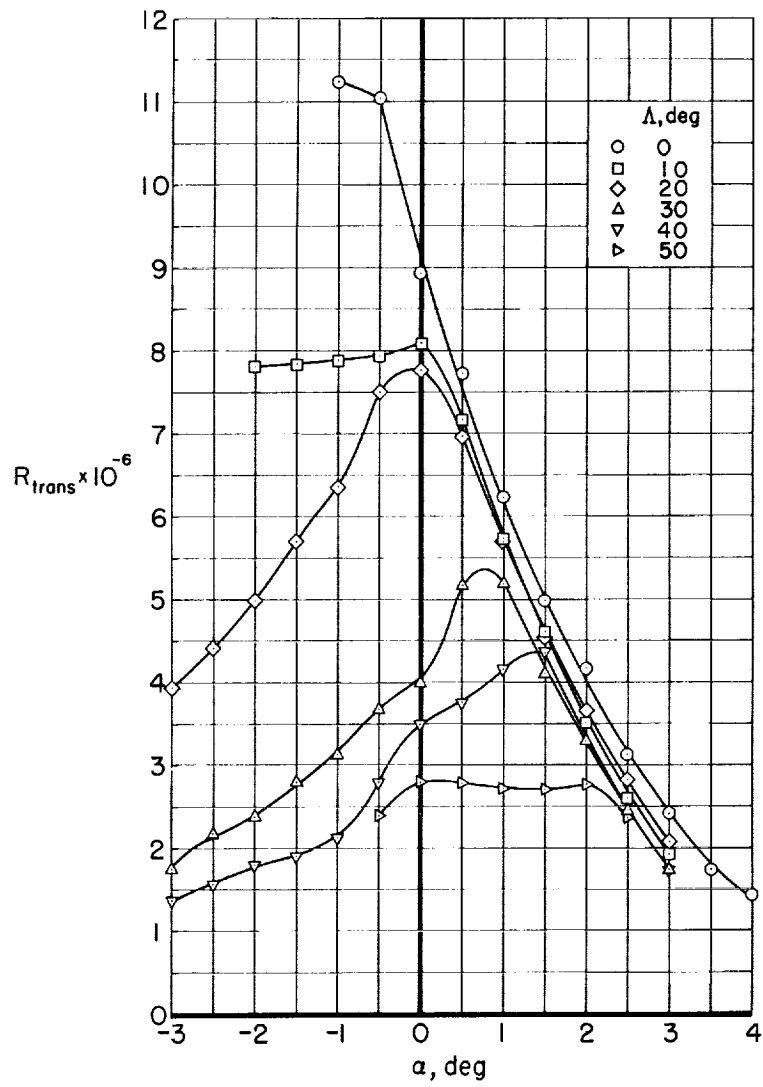
(a)  $x/c_1 = 0.21$ 

Figure 7.- The variation of transition Reynolds number with angle of attack at several chordwise locations on the upper surface of the wing.



(b)  $x/c_1 = 0.24$

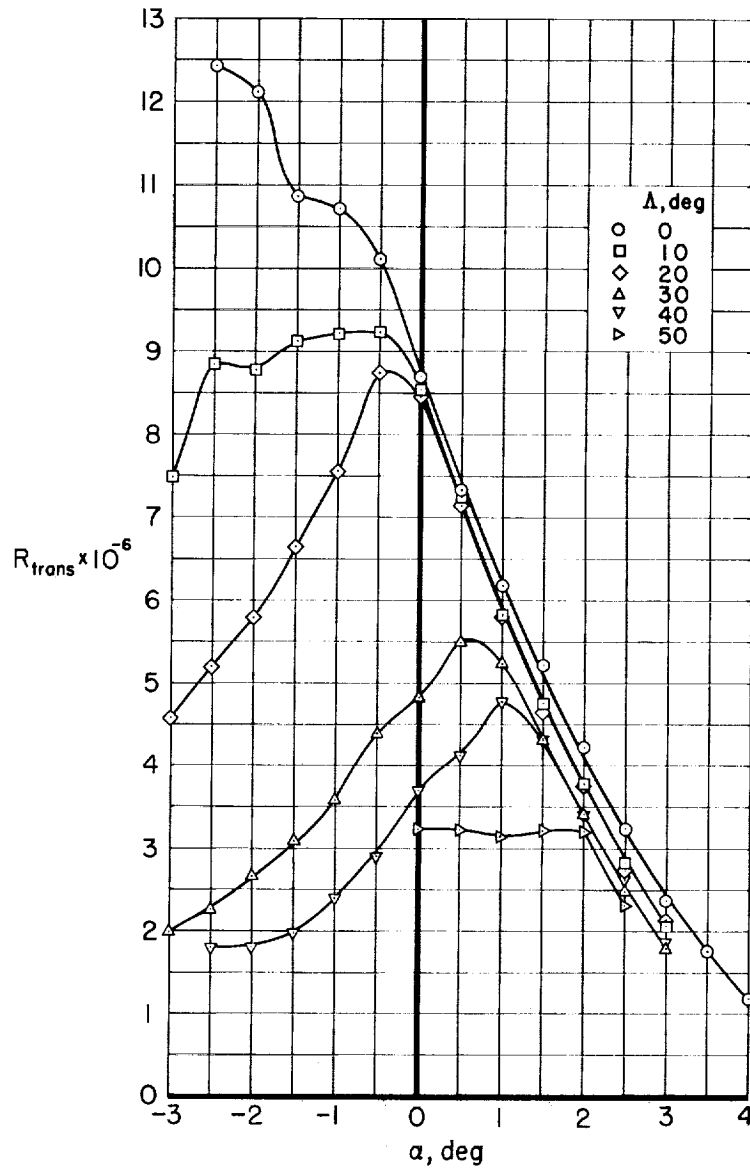
Figure 7.- Continued.



(c)  $x/c_{\perp} = 0.30$

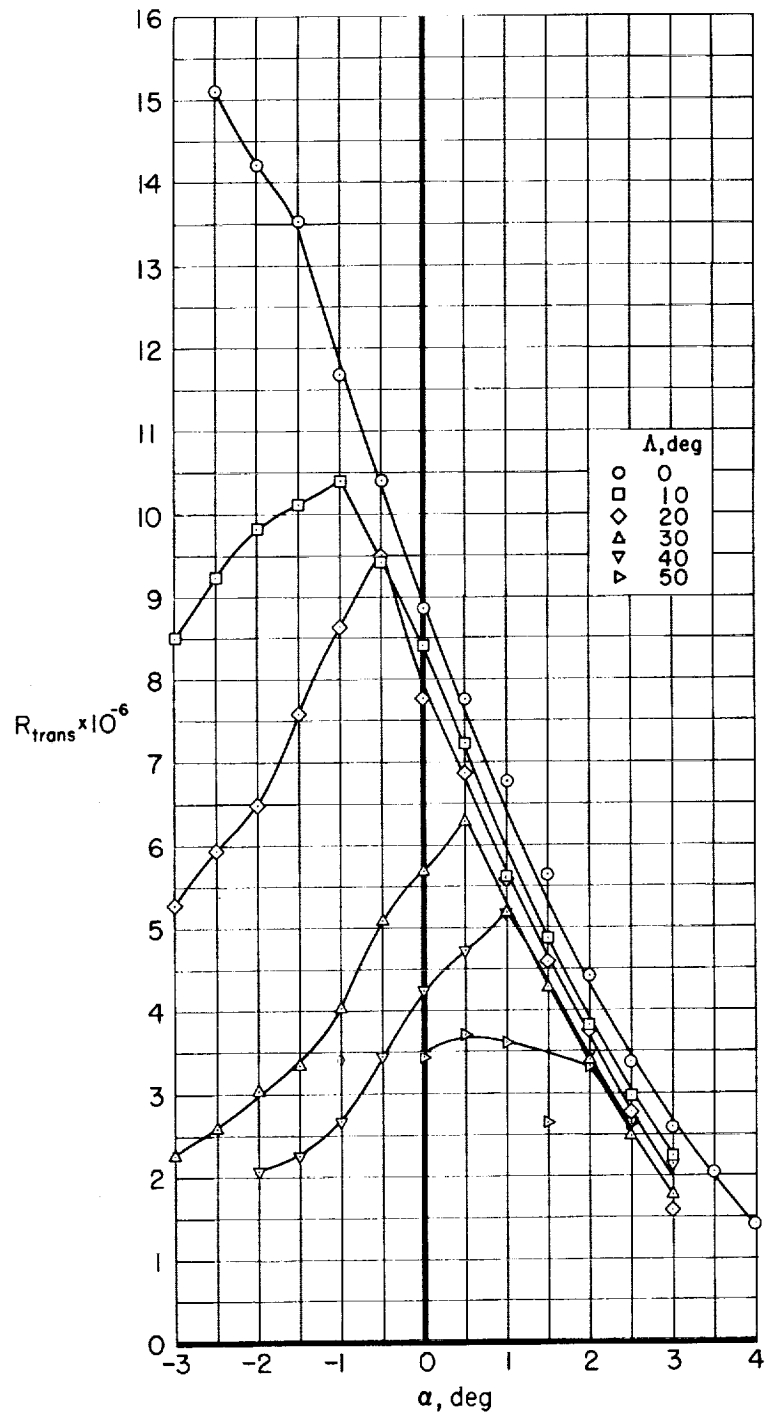
Figure 7.- Continued.

A  
2  
2  
2



(d)  $x/c_1 = 0.35$

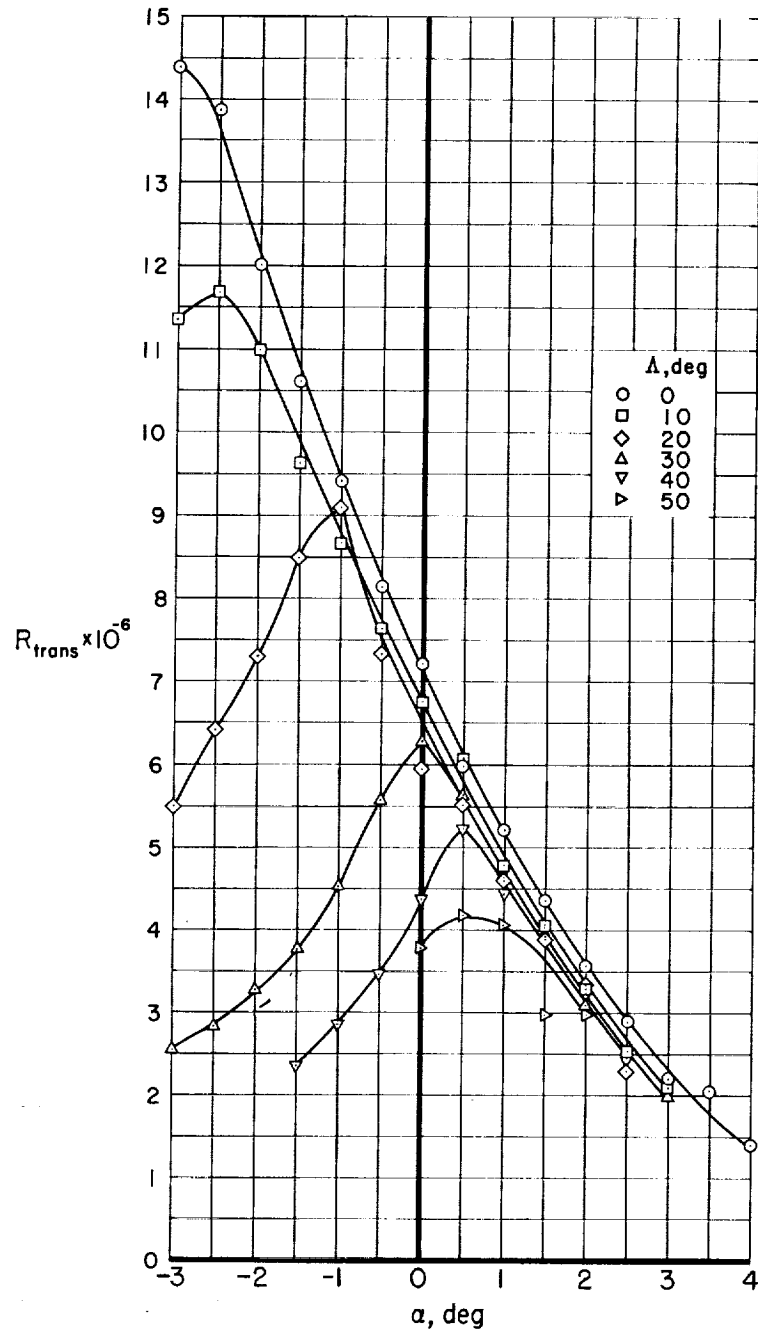
Figure 7.- Continued.



(e)  $x/c_{\perp} = 0.40$

Figure 7.- Continued.

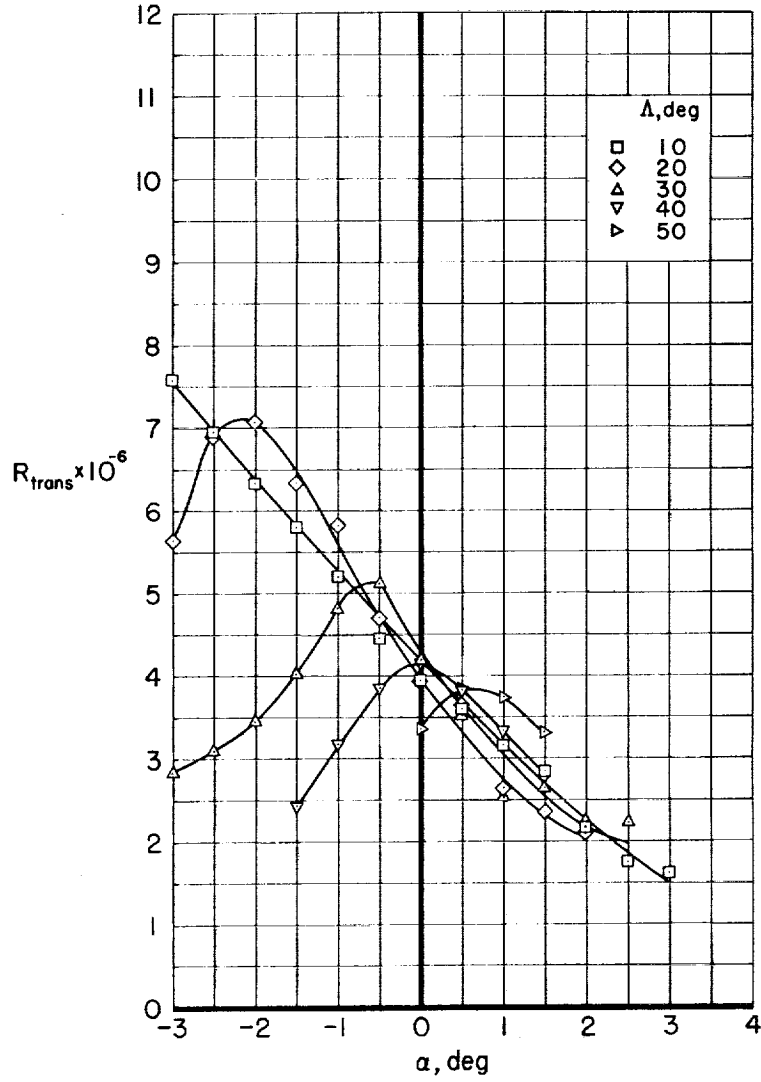
A  
2  
2  
2



(f)  $x/c_{\perp} = 0.45$

Figure 7.- Continued

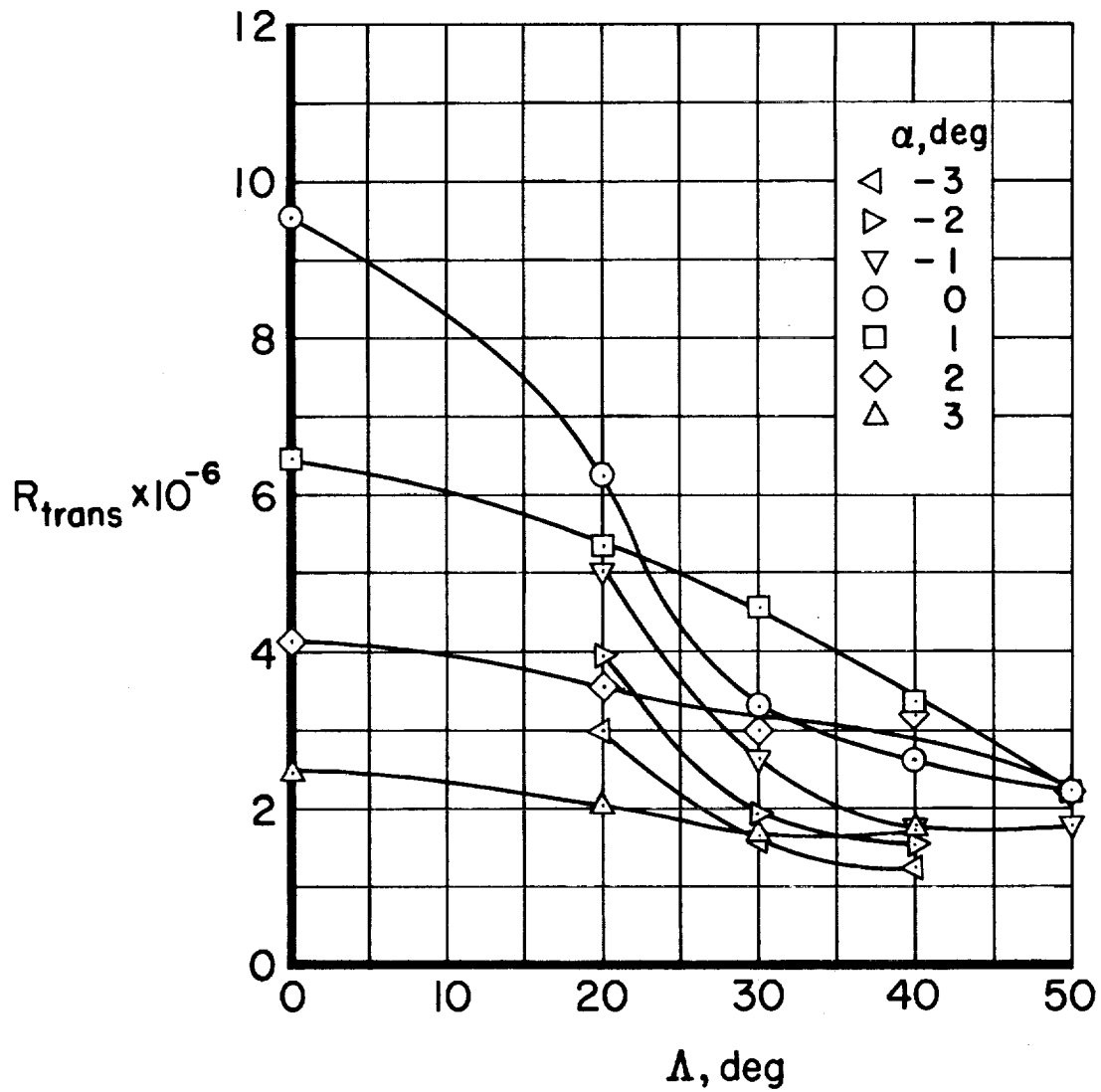
A  
2  
2  
2



(g)  $x/c_1 = 0.50$

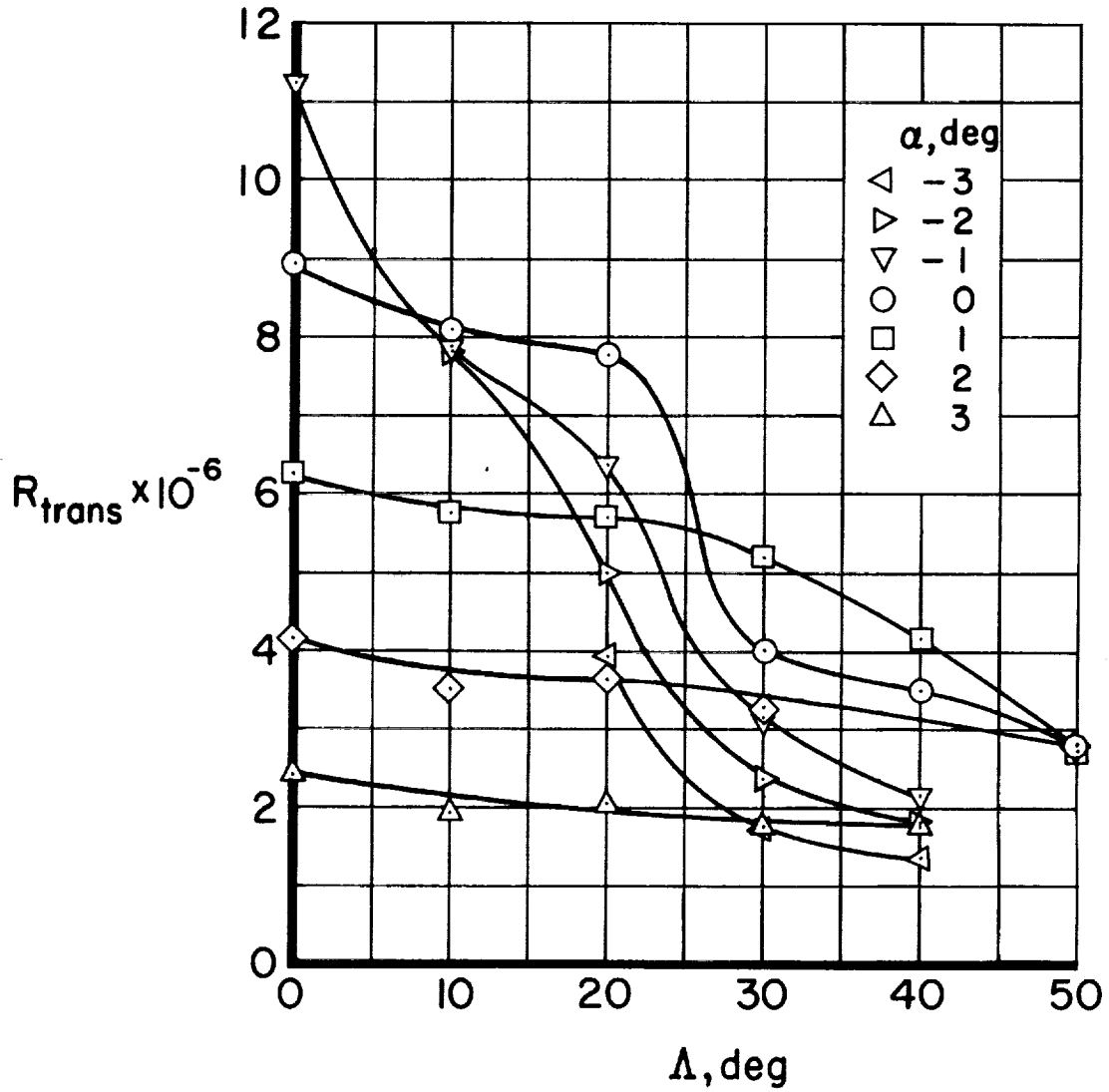
Figure 7.- Concluded.

A  
2  
2  
2



(a)  $x/c_{\perp} = 0.24$

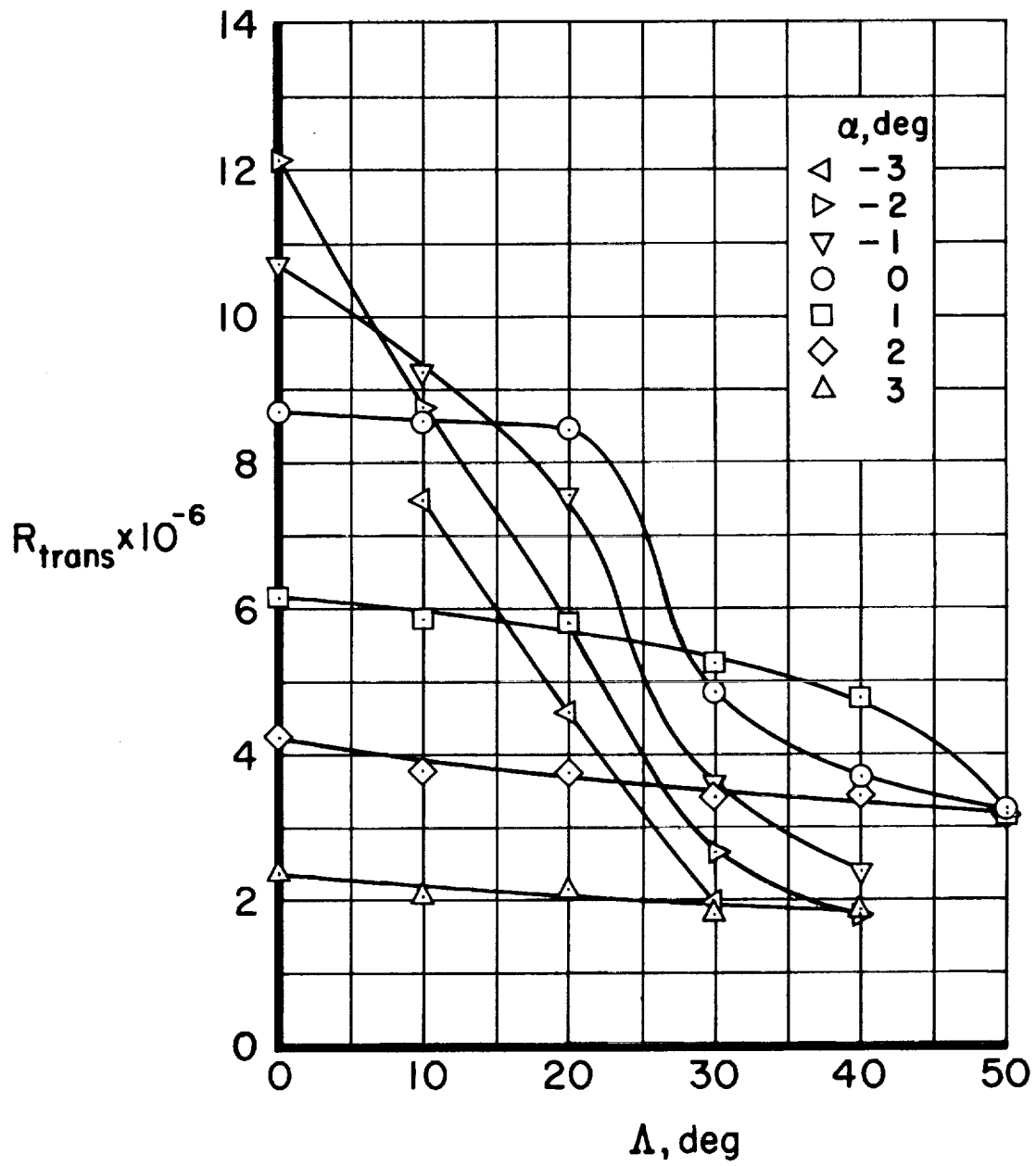
Figure 8.- The variation of transition Reynolds number with sweep angle at several chordwise locations on the upper surface of the wing.



(b)  $x/c_1 = 0.30$

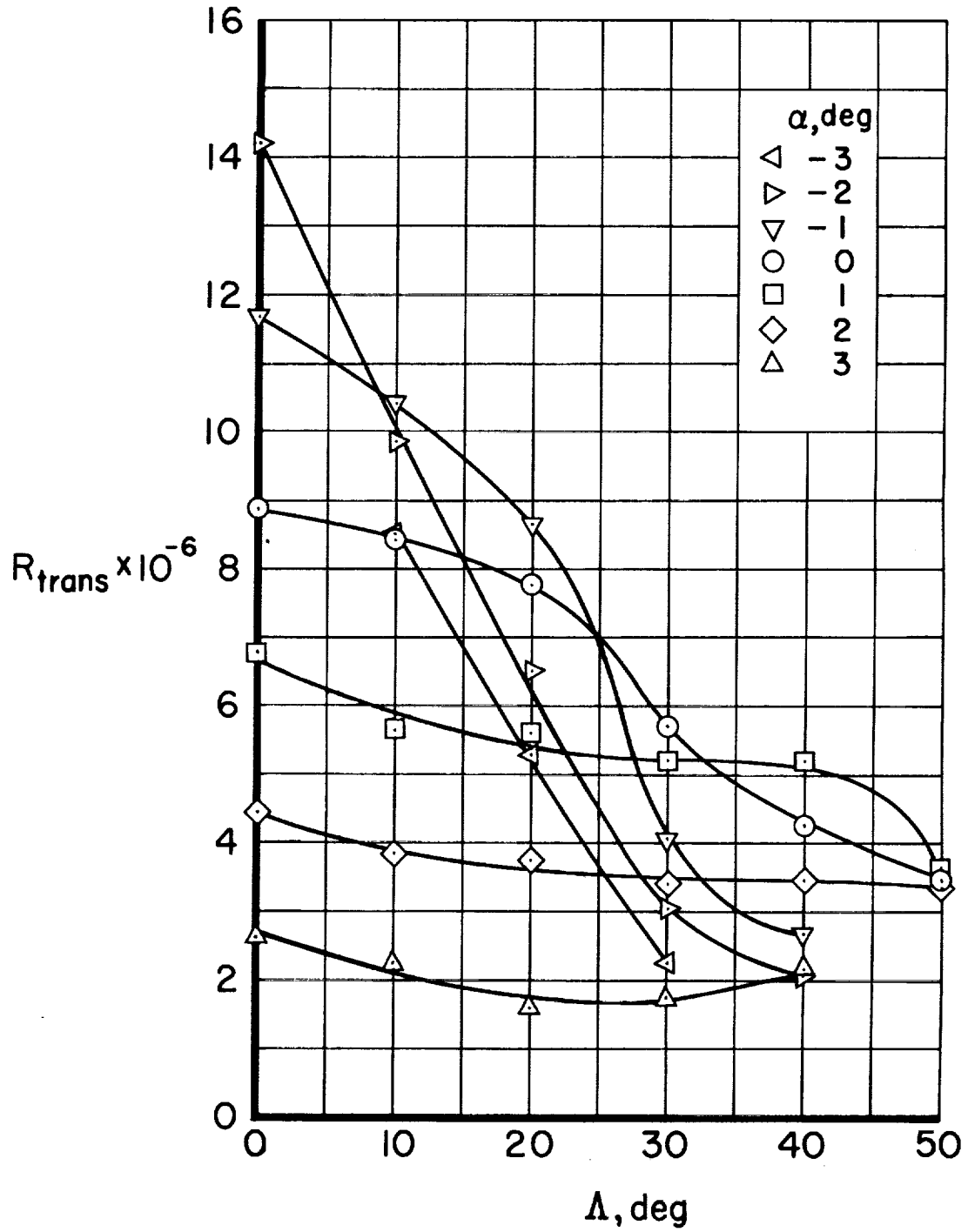
Figure 8.- Continued.

A  
2  
2  
2



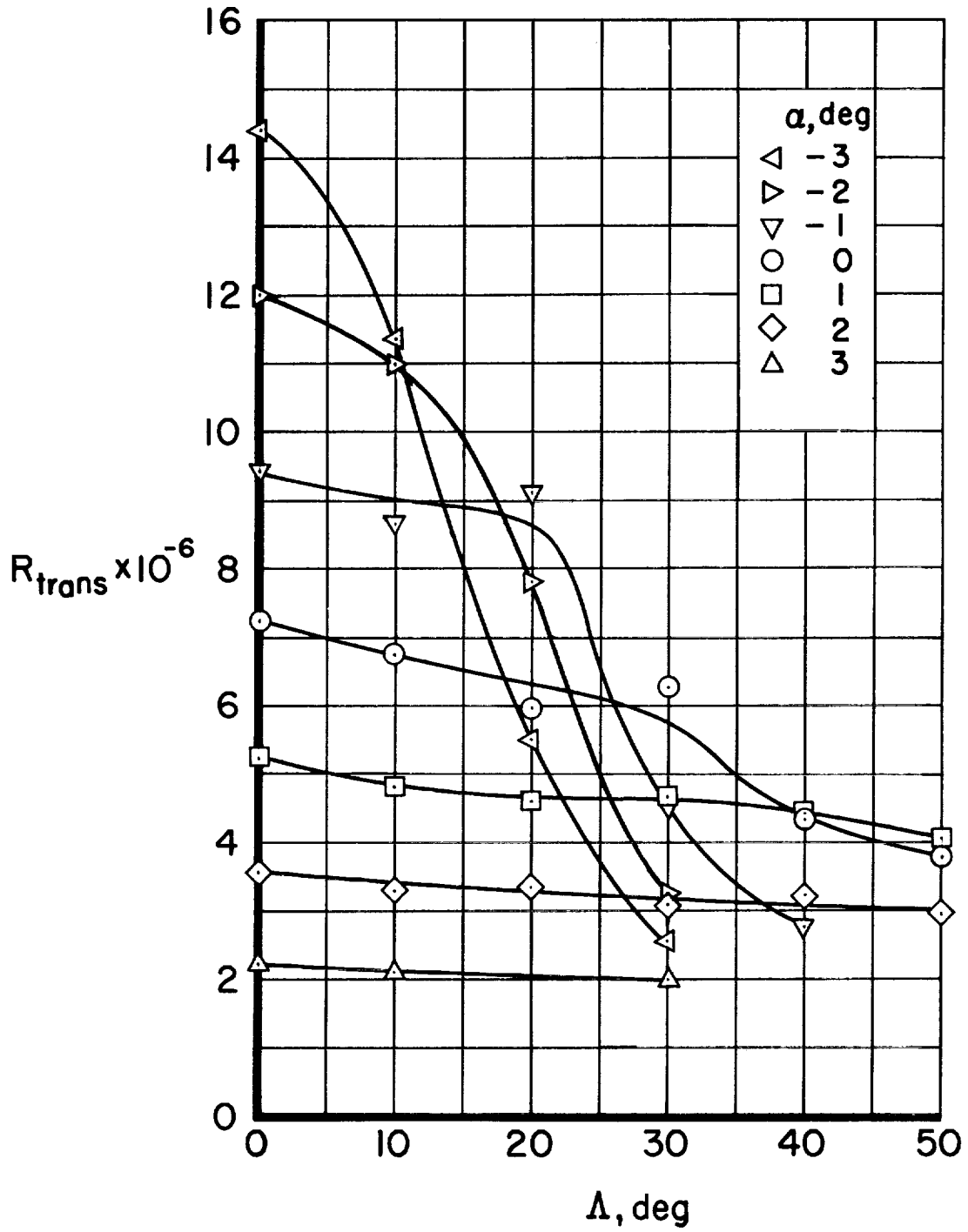
(c)  $x/c_{\perp} = 0.35$

Figure 8.- Continued.



(d)  $x/c_L = 0.40$

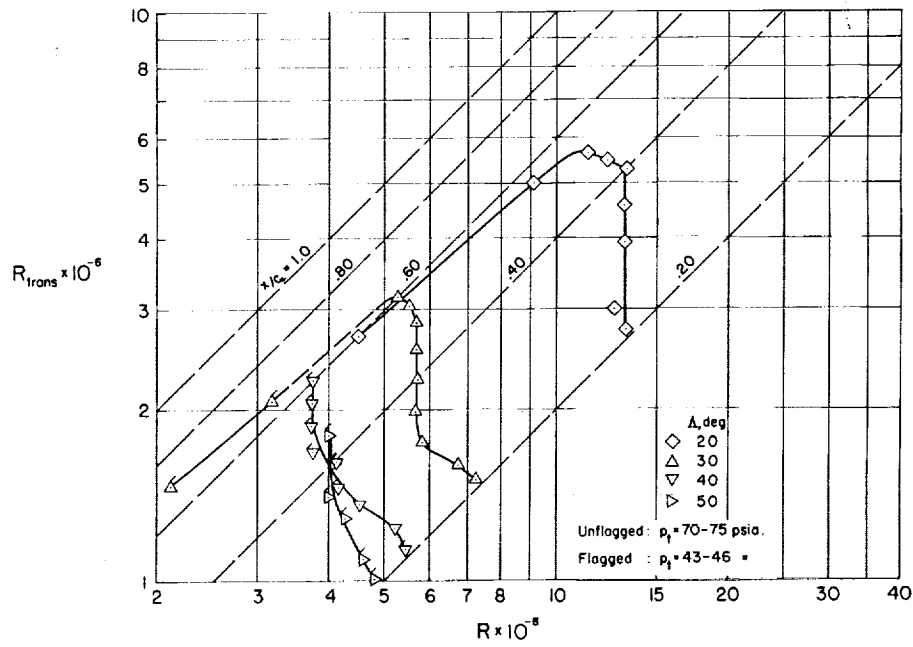
Figure 8.- Continued.



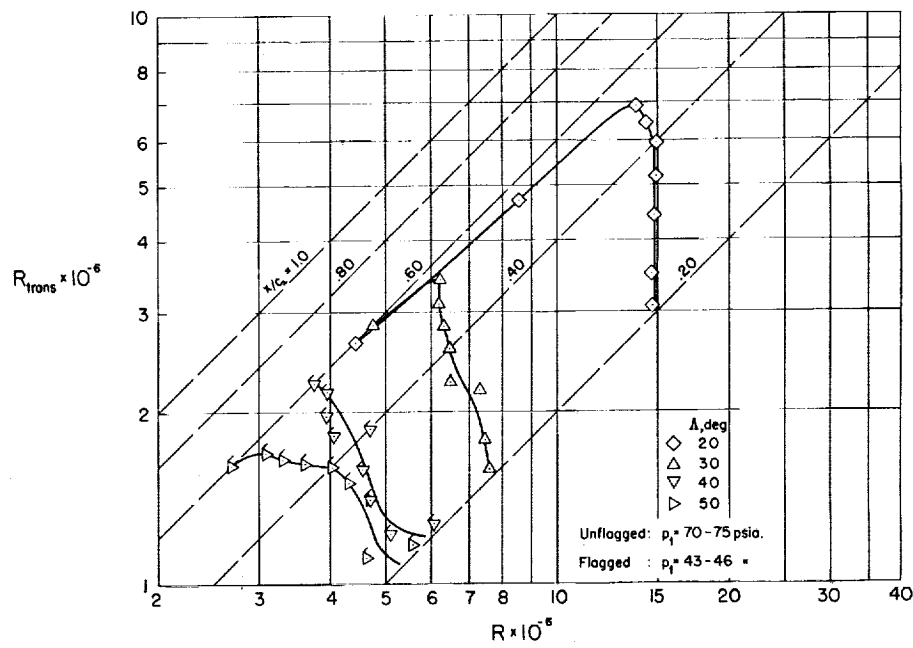
(e)  $x/c_{\perp} = 0.45$

Figure 8.- Concluded.

A  
2  
2  
2



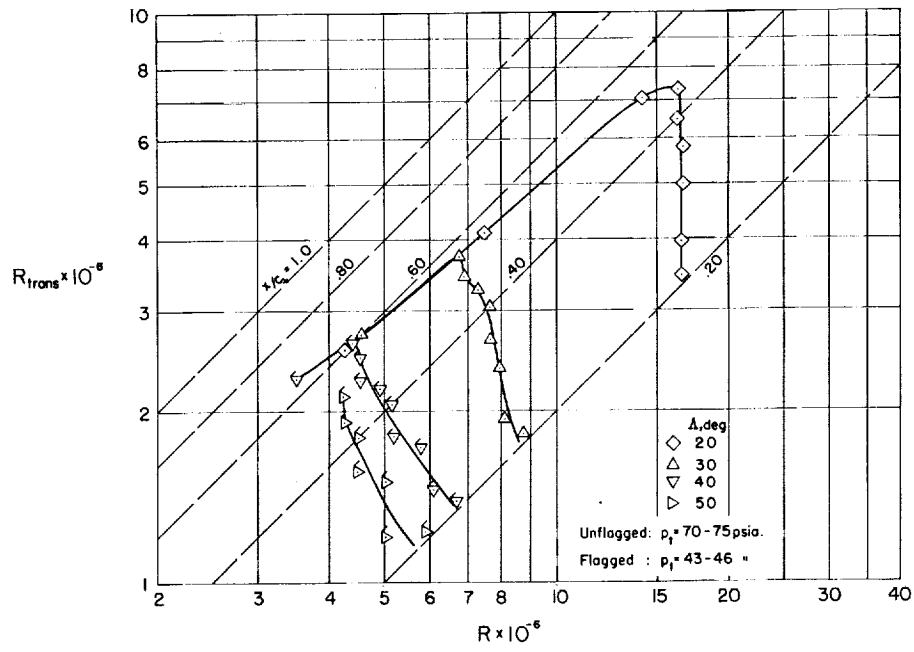
(a)  $\alpha = -3^\circ$



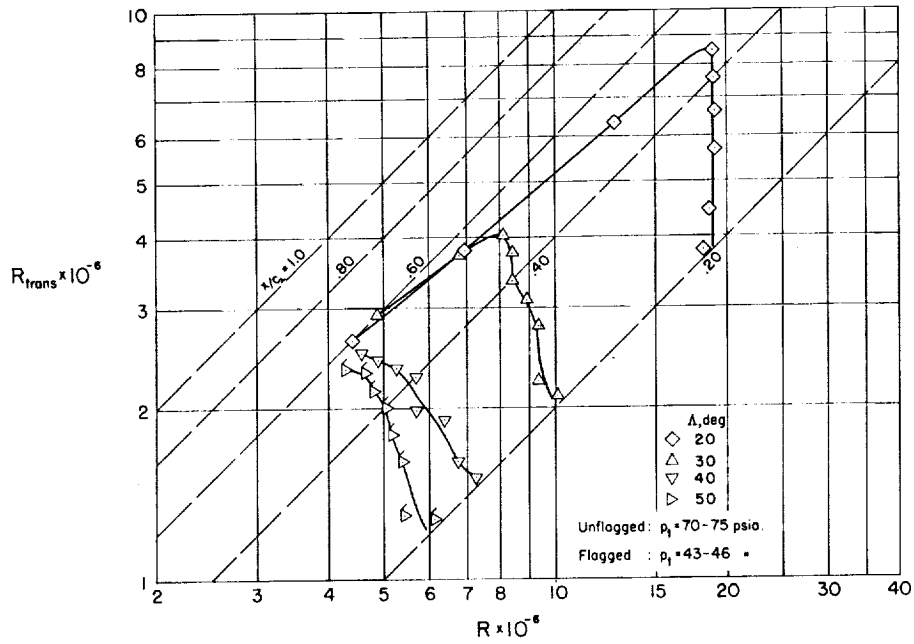
(b)  $\alpha = -2.5^\circ$

Figure 9.- The variation of transition Reynolds number on the upper surface of the wing with chord Reynolds number for several angles of attack and angles of sweep.

A  
2  
2  
2



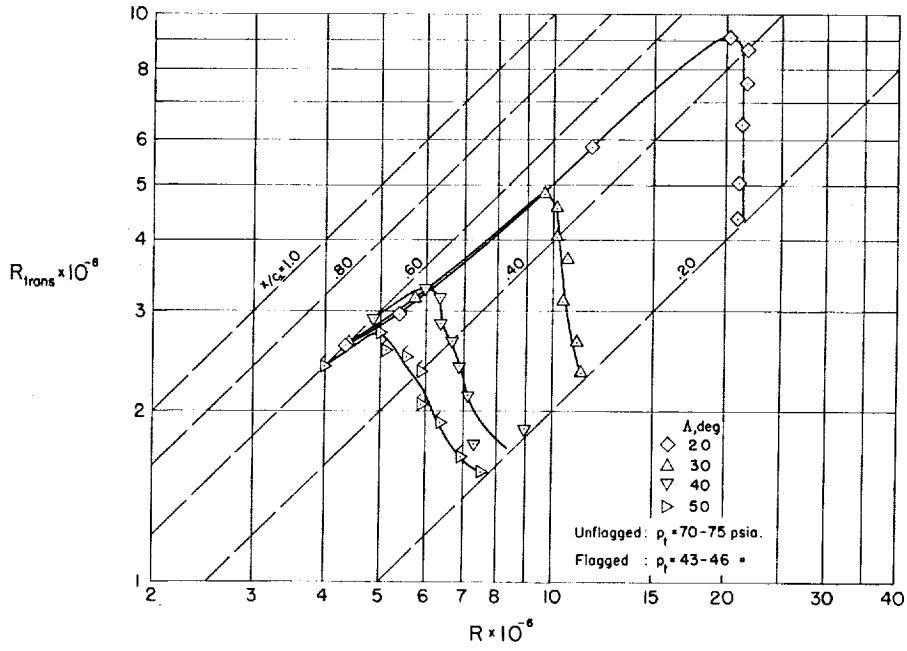
(c)  $\alpha = -2^\circ$



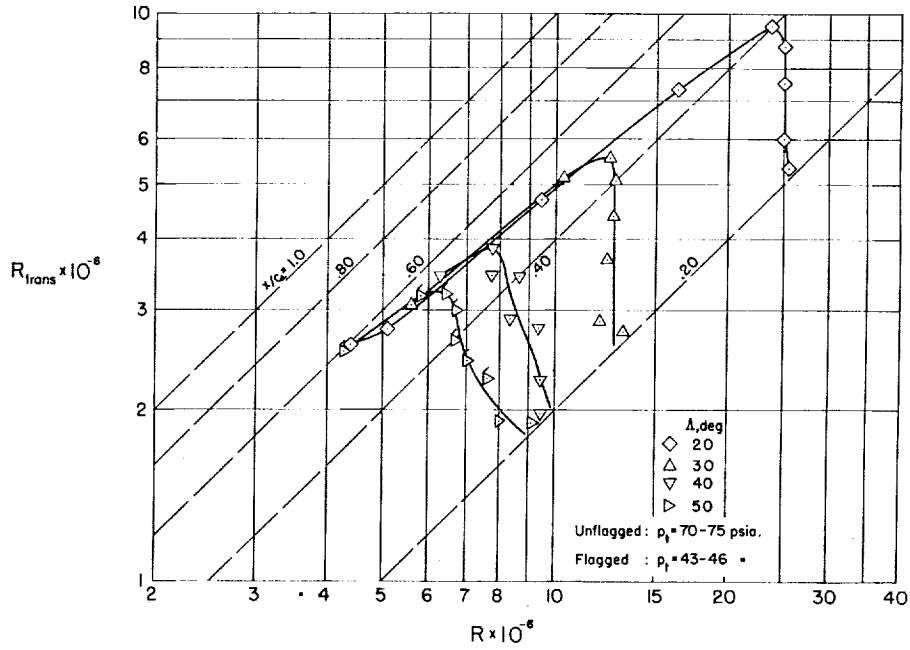
(d)  $\alpha = -1.5^\circ$

Figure 9.- Continued.

A  
2  
2  
2



(e)  $\alpha = -1^\circ$

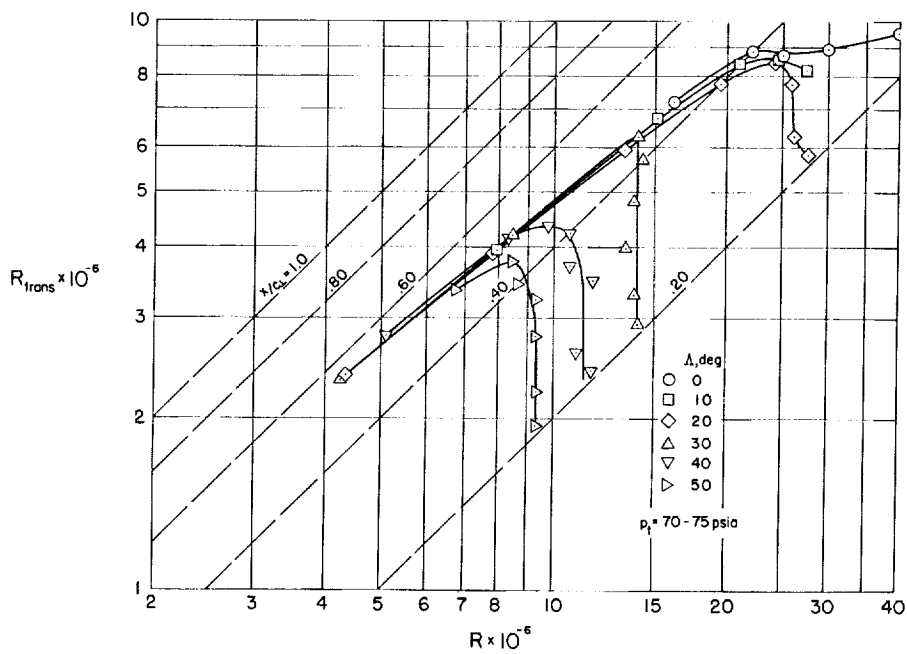


(f)  $\alpha = -0.5^\circ$

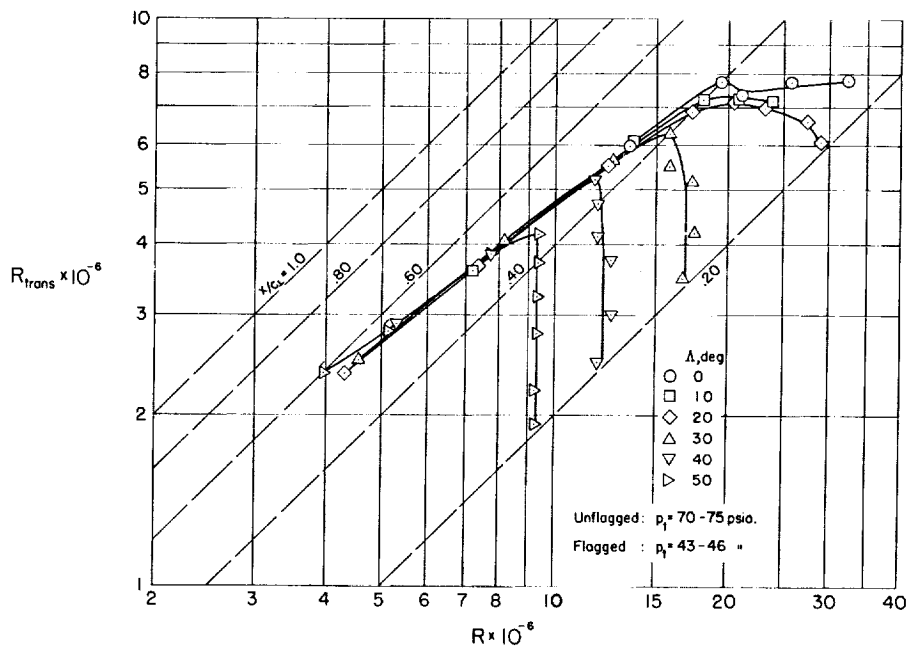
Figure 9.- Continued.

A  
2  
2  
2

A  
2  
2  
2

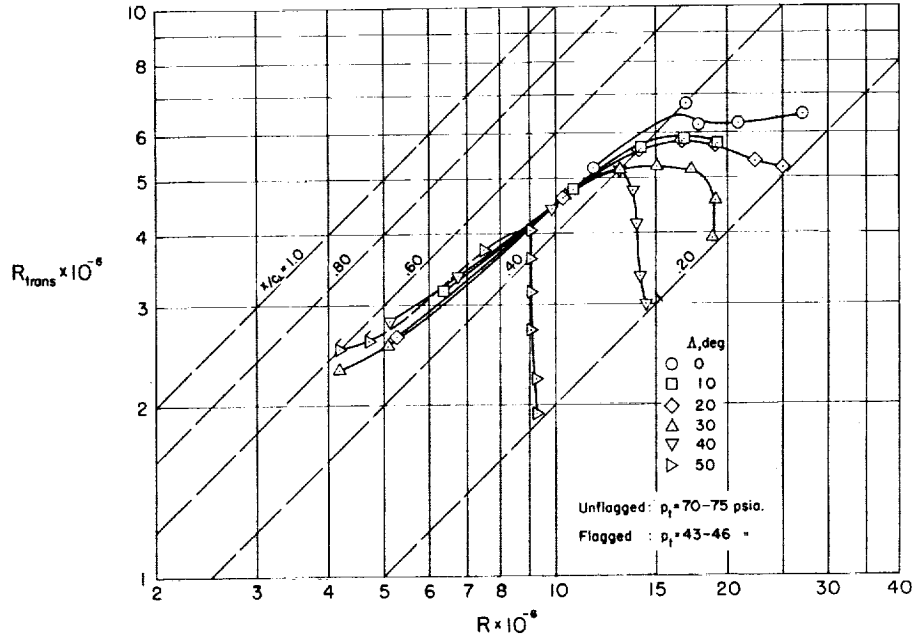


(g)  $\alpha = 0^\circ$

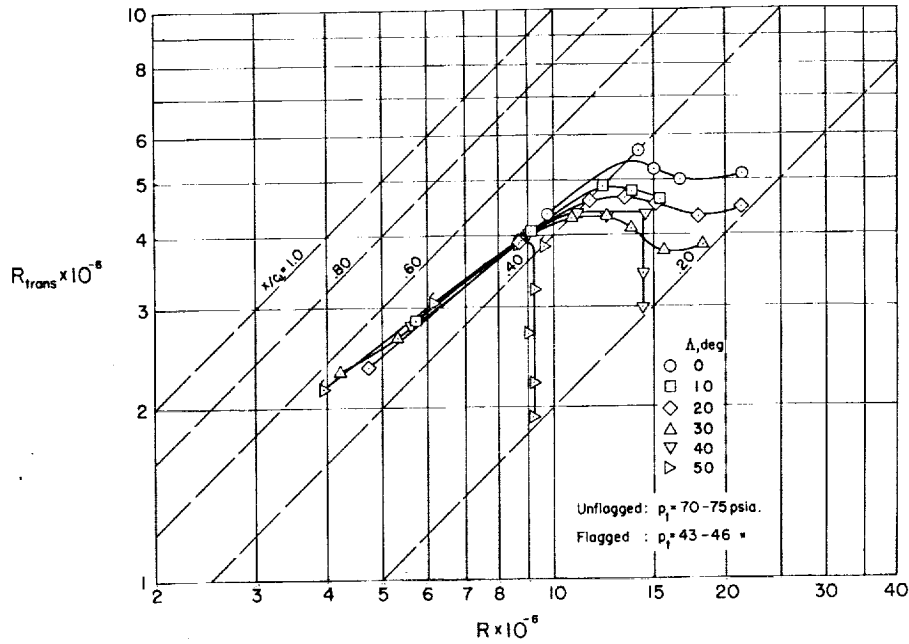


(h)  $\alpha = 0.5^\circ$

Figure 9.- Continued.



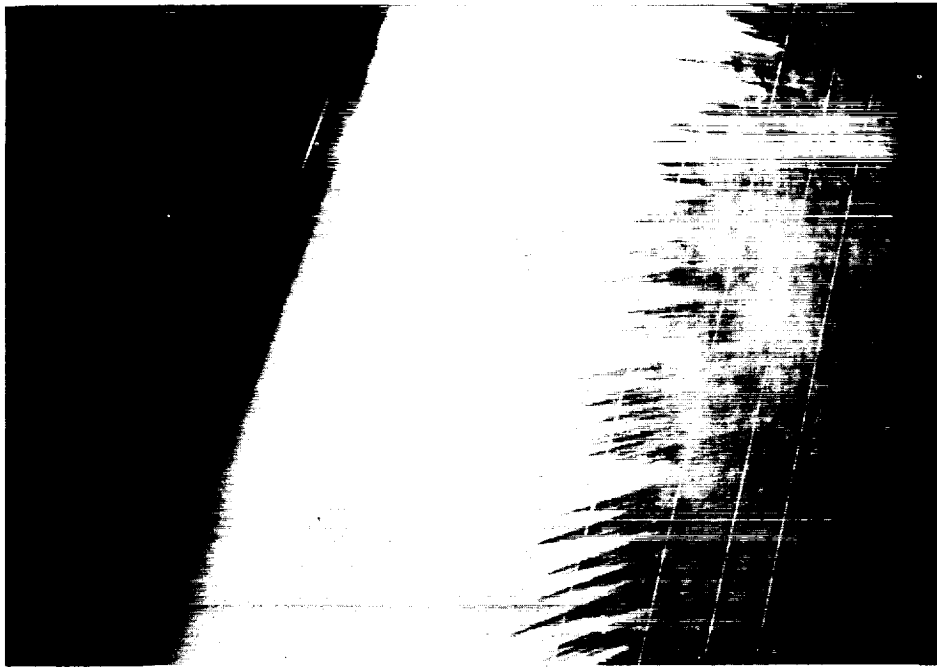
(i)  $\alpha = 1^\circ$



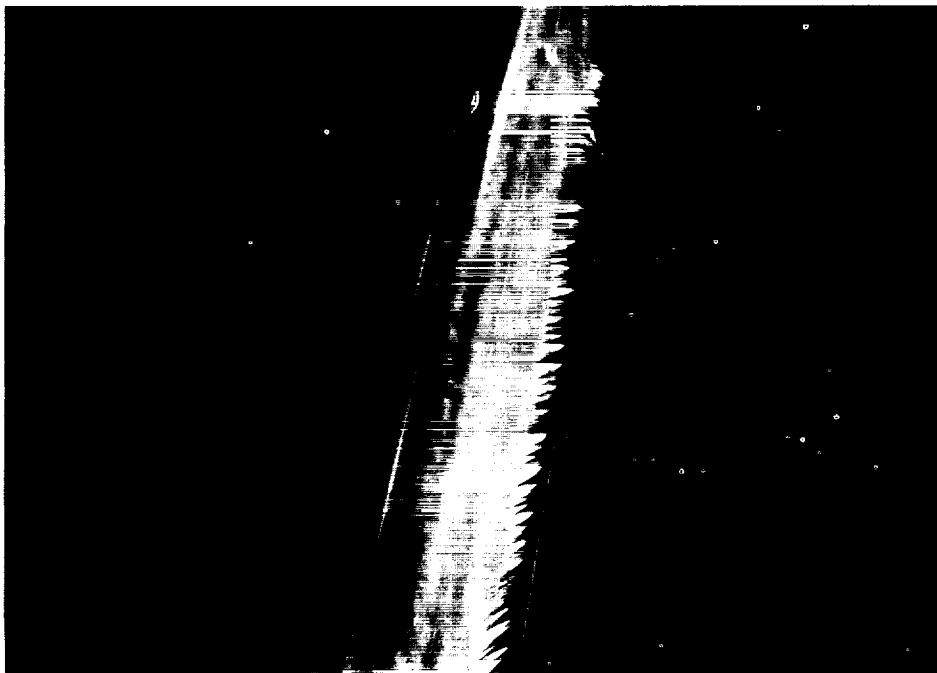
(j)  $\alpha = 1.5^\circ$

Figure 9.- Concluded.

A  
2  
2  
2

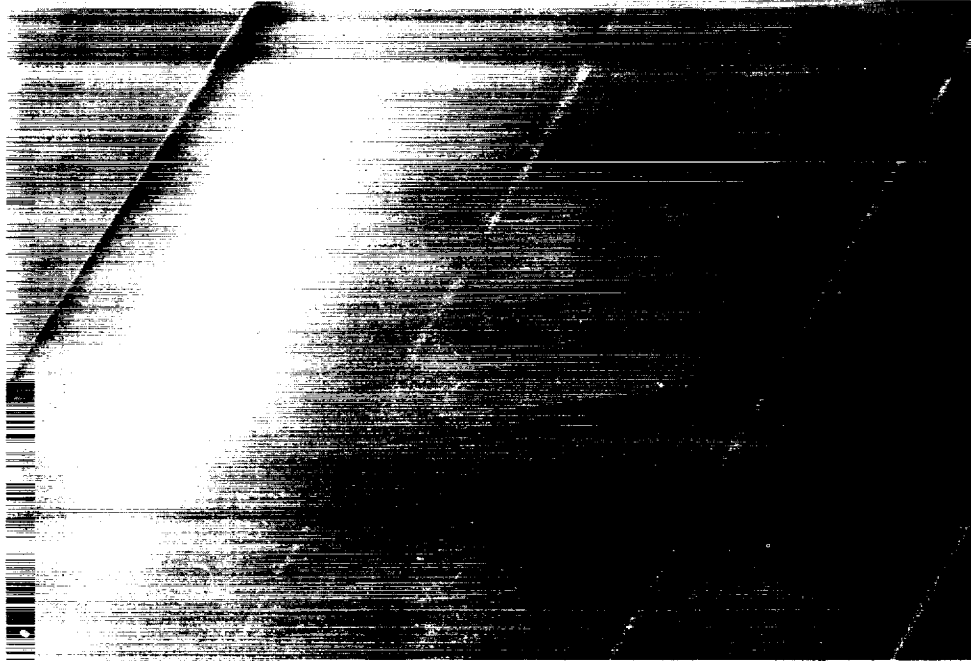


(a) Three-fourths front view of model;  $\alpha = -12^\circ$ ,  $R = 2.3 \times 10^6$ .

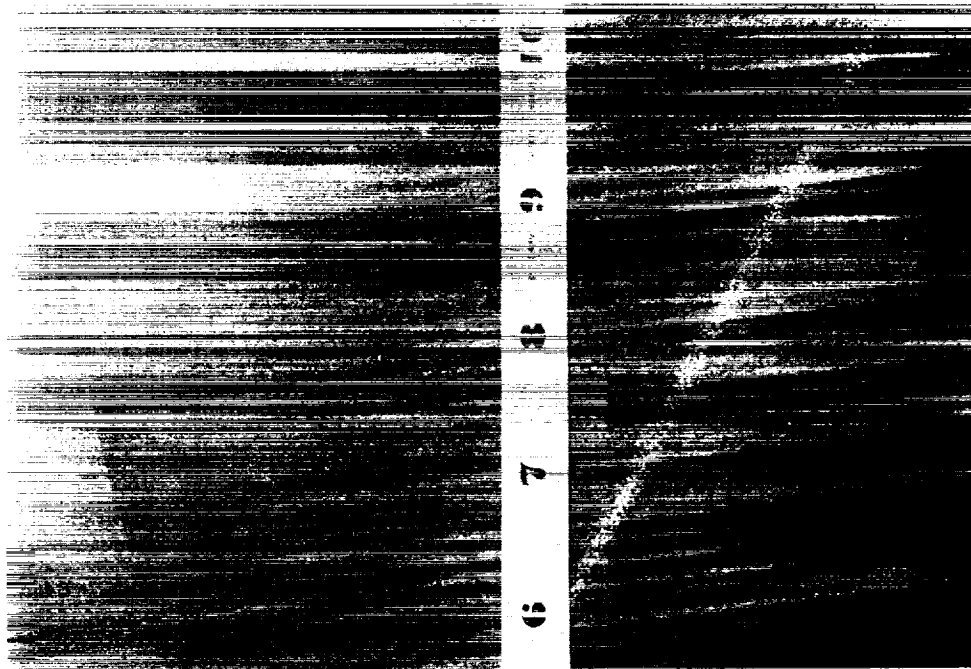


(b) Seven-eighths front view of model;  $\alpha = -8^\circ$ ,  $R = 3.2 \times 10^6$ .

Figure 10.- Several representative photographs of the effects of vortex activity in the boundary layer on the wing,  $\Lambda = 30^\circ$ .

A  
2  
2  
2

(c) Side view of model;  $\alpha = -10^\circ$ ,  $R = 3.2 \times 10^6$ .



(d) Side view of model near leading edge;  $\alpha = -12^\circ$ ,  $R = 3.2 \times 10^6$ .

Figure 10.- Concluded.

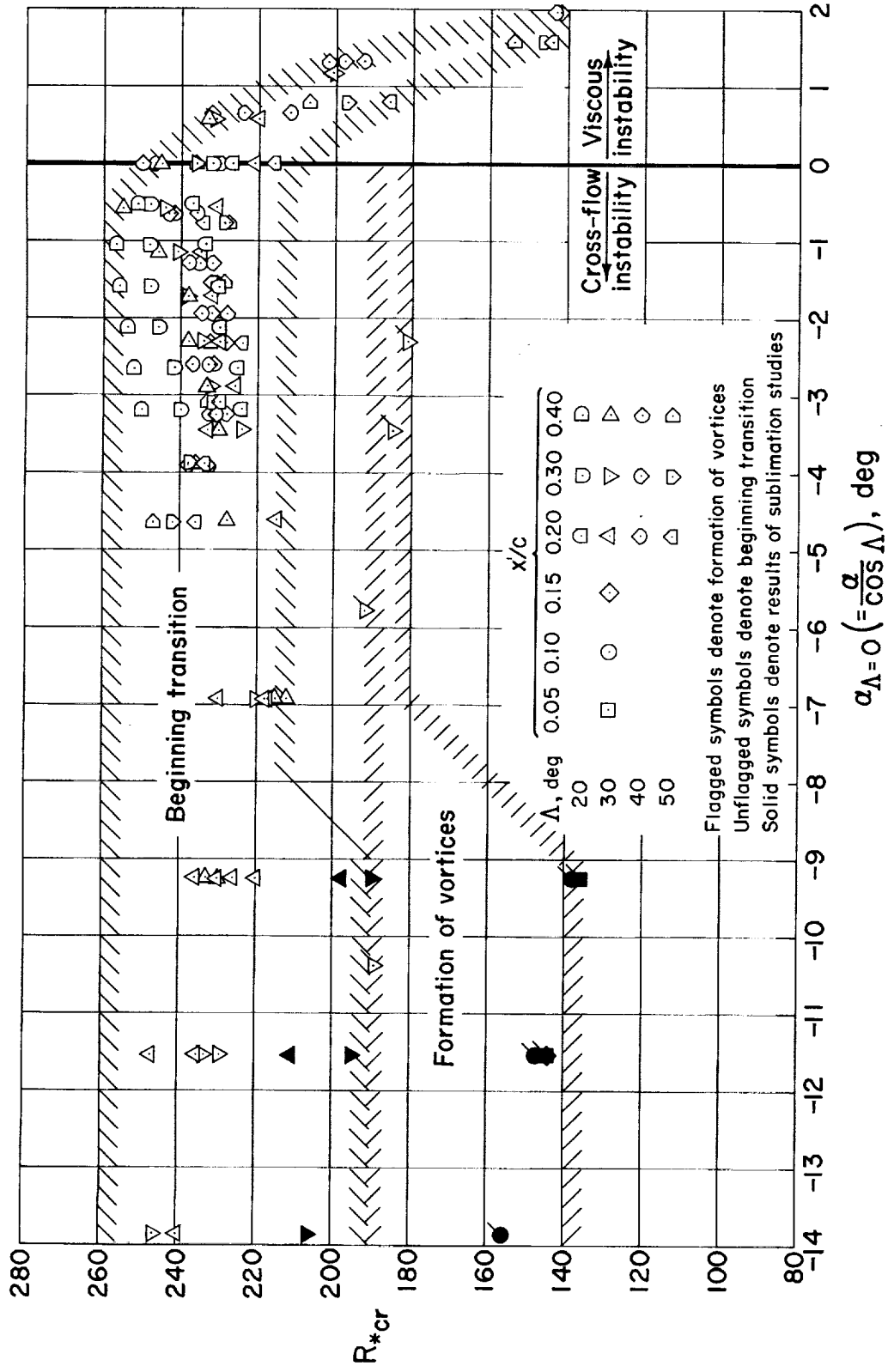


Figure 11.- Critical bands of crossflow Reynolds number.

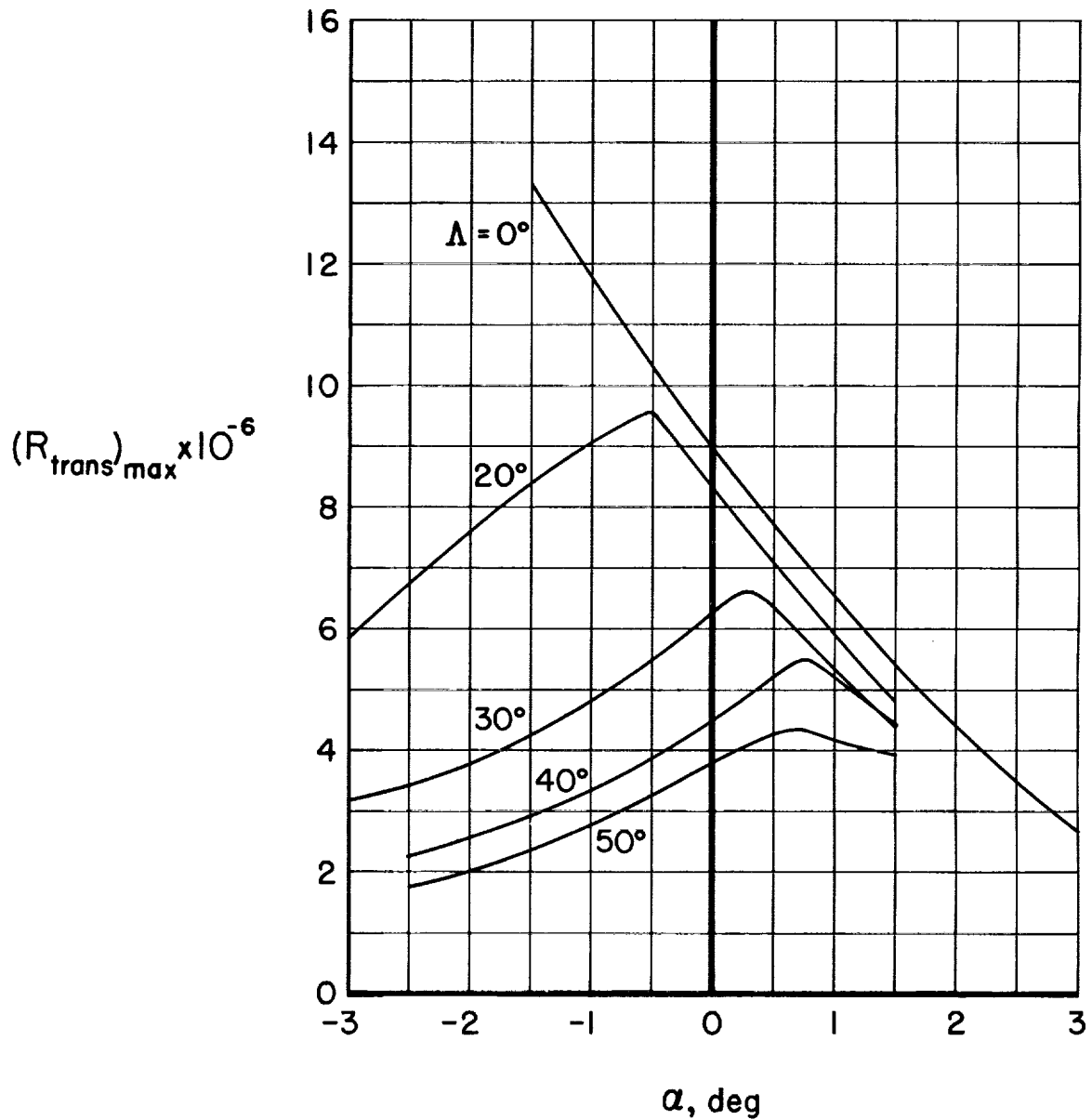
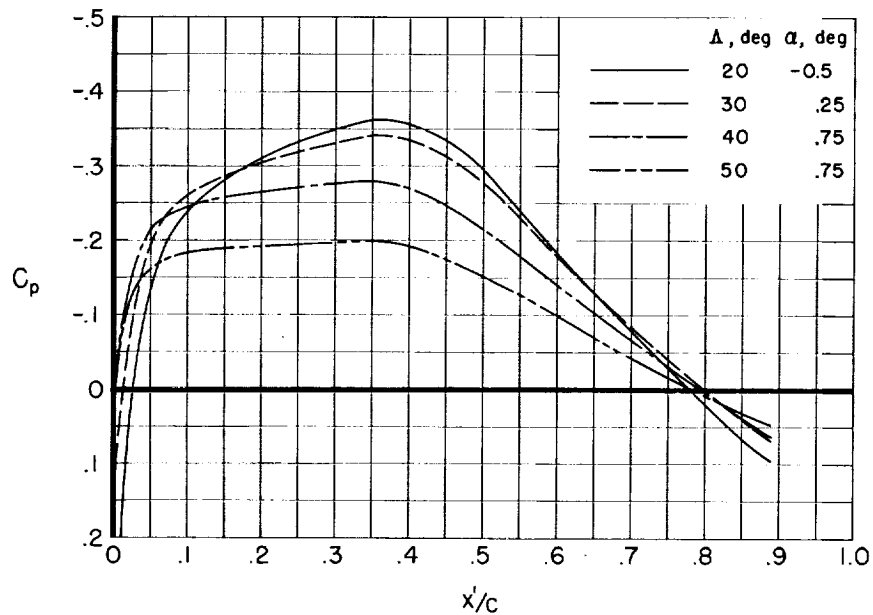
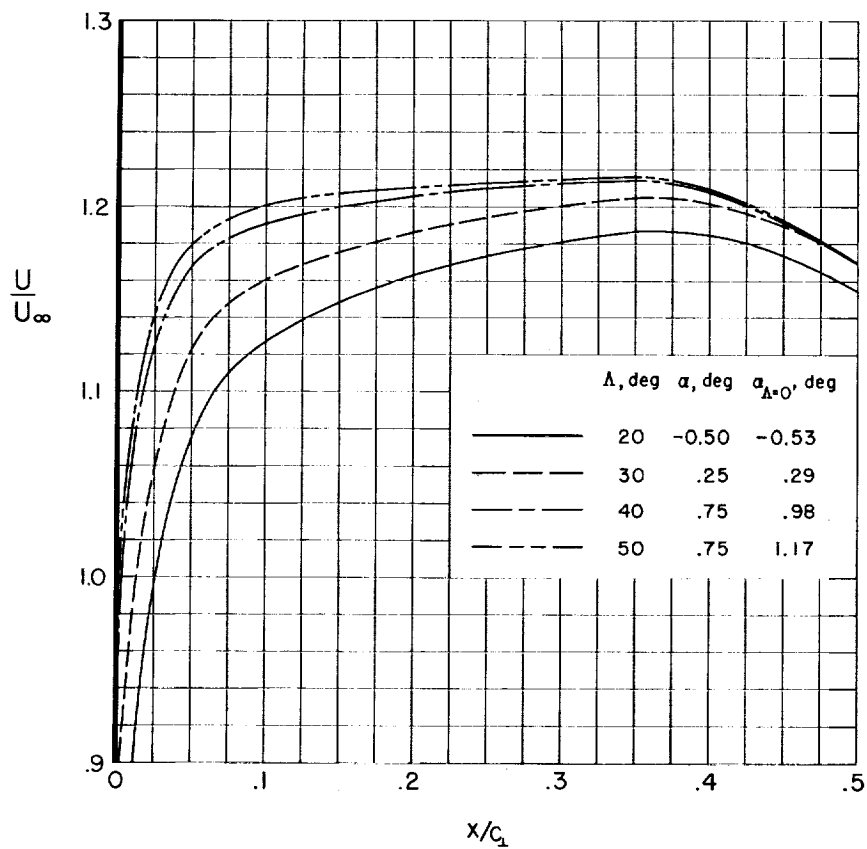


Figure 12.- The variation of the maximum value of transition Reynolds number obtained on the upper surface of the wing with angle of attack for several angles of sweep.



(a) Chordwise pressure distribution.



(b) Chordwise velocity distribution.

Figure 13.- The chordwise pressure and velocity distributions on the wing for the maximum values of transition Reynolds' number at several angles of sweep (pressure coefficient based on flow in streamwise direction and velocity ratio based on flow normal to leading edge of wing).

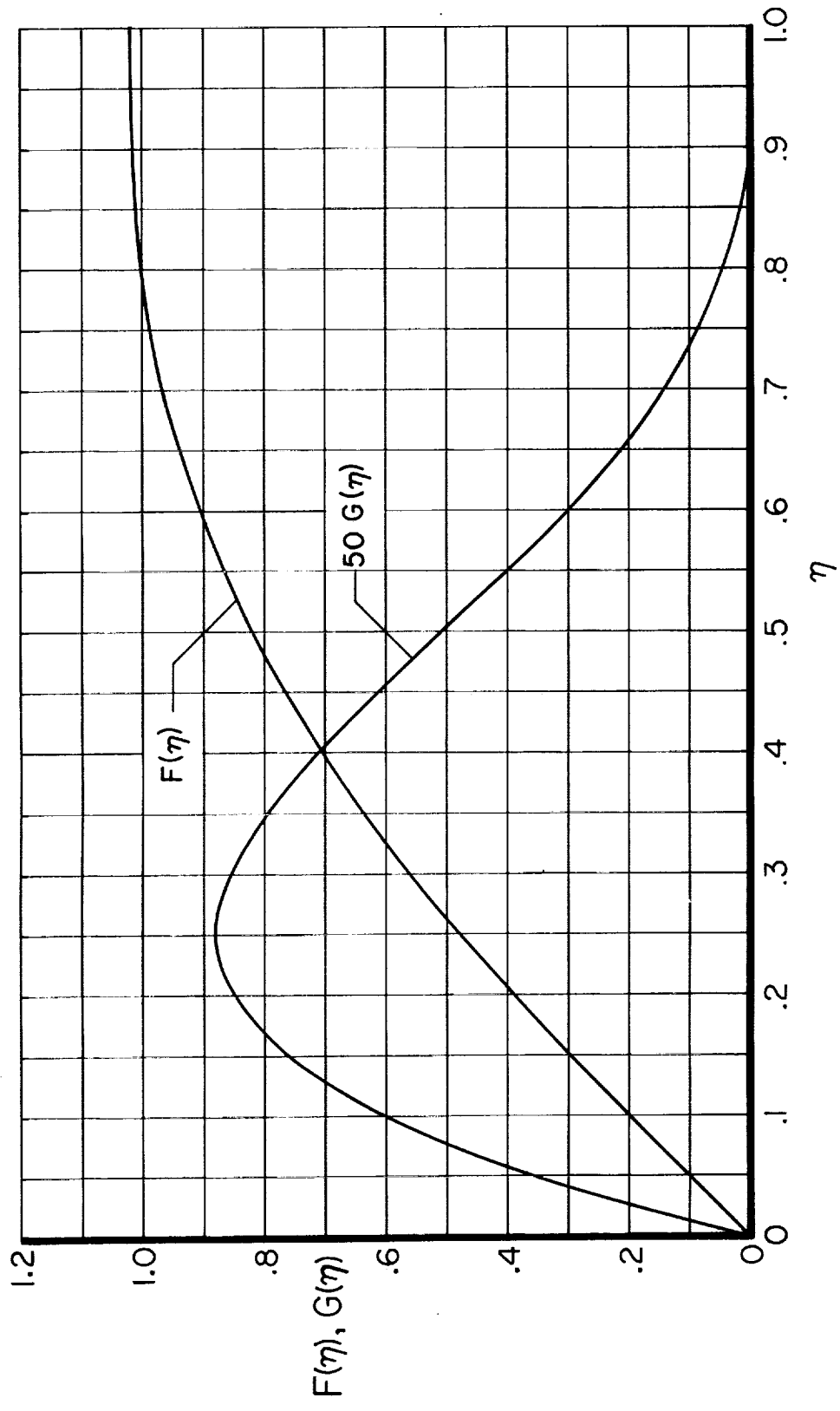
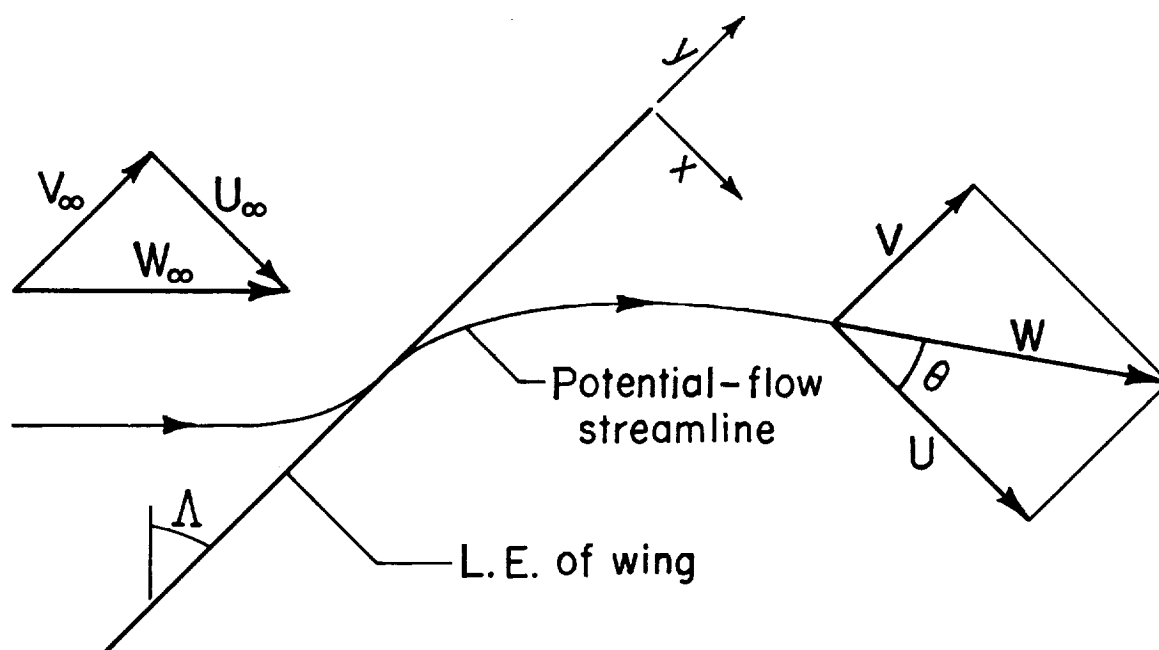
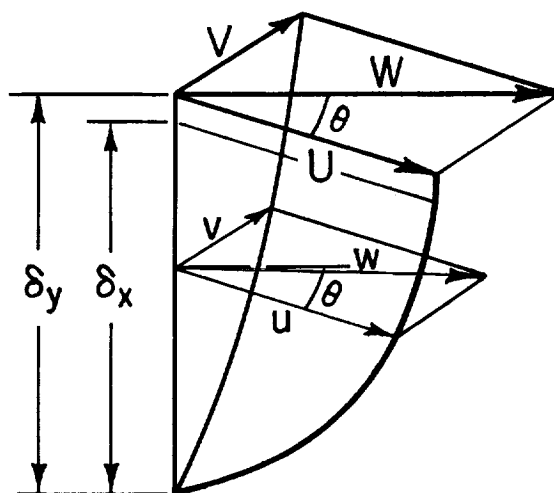


Figure 14.- The functions  $F(\eta)$  and  $G(\eta)$  for the velocity distribution in the boundary layer.

A  
2  
2  
2

(a) Components of potential flow on swept wing.



(b) Components of boundary-layer flow on swept wing.

Figure 15.- Components of potential flow and boundary-layer flow on swept wing.

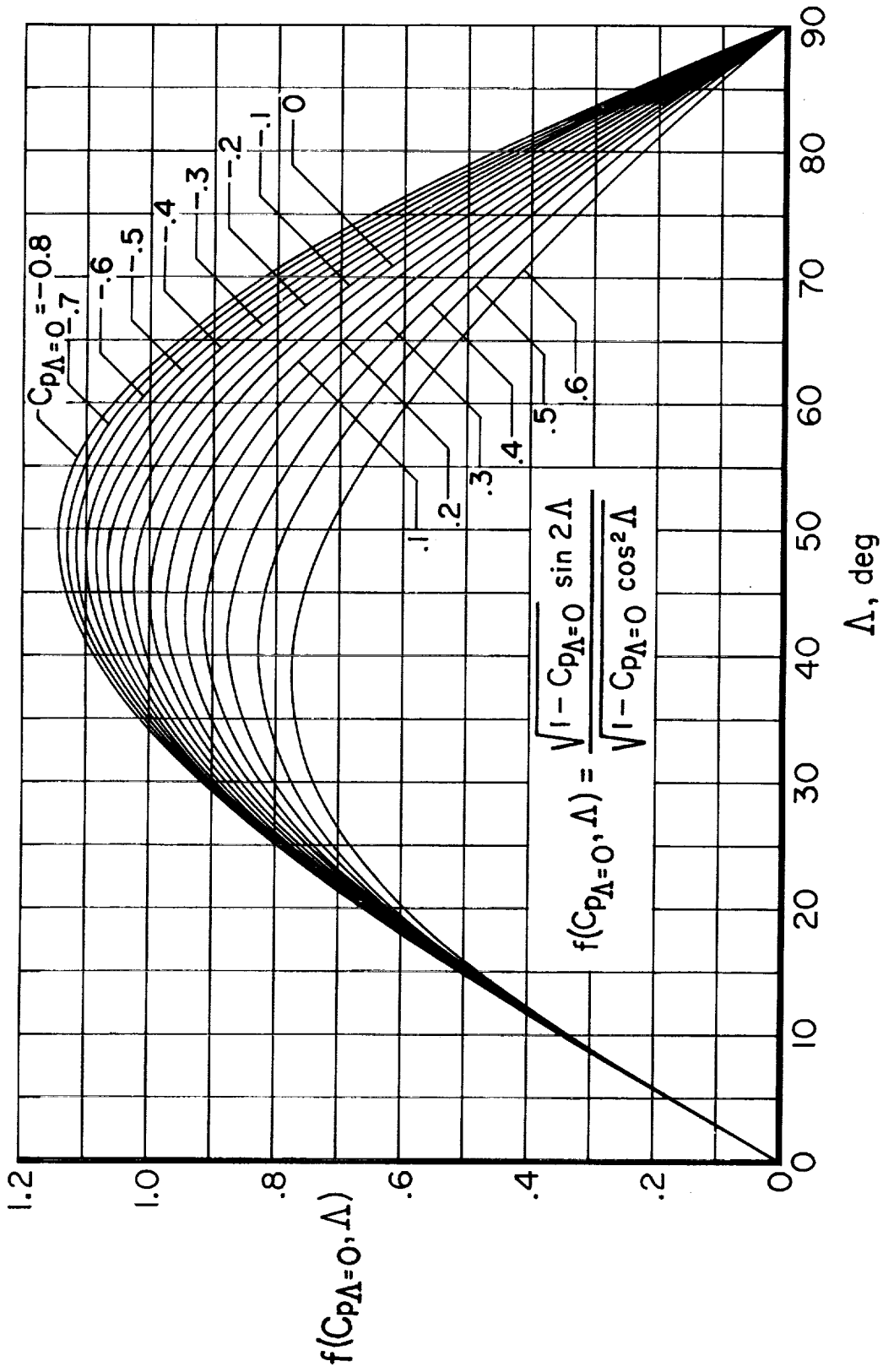


Figure 16.- The function  $f(C_{p\Lambda=0}, \Delta)$  used in the computation of crossflow Reynolds number.

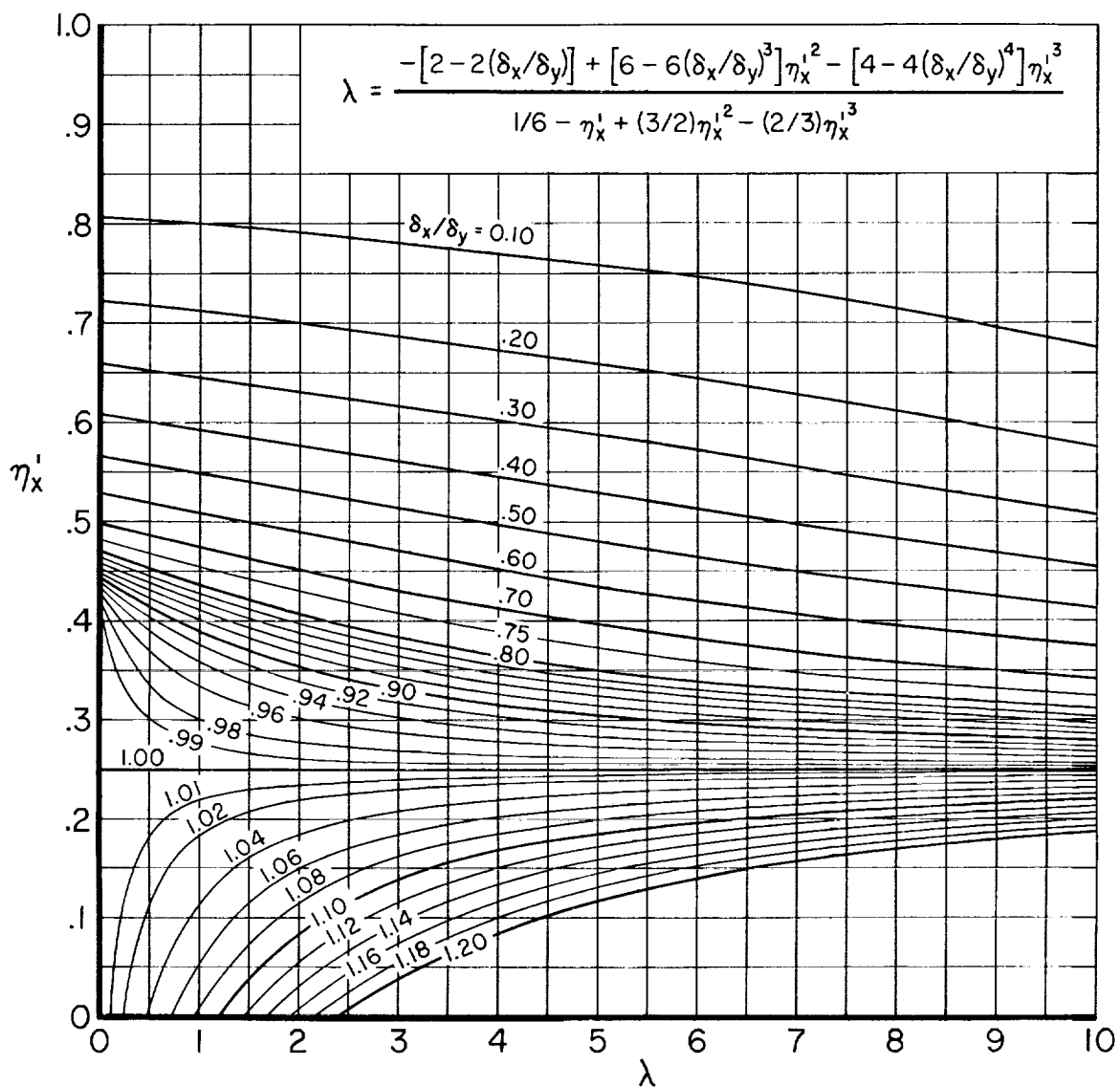


Figure 17.- The variation of  $\eta_{ix}$  for  $w_{\eta_{max}}$  with  $\lambda$  at various values of  $\delta_x/\delta_y$ .

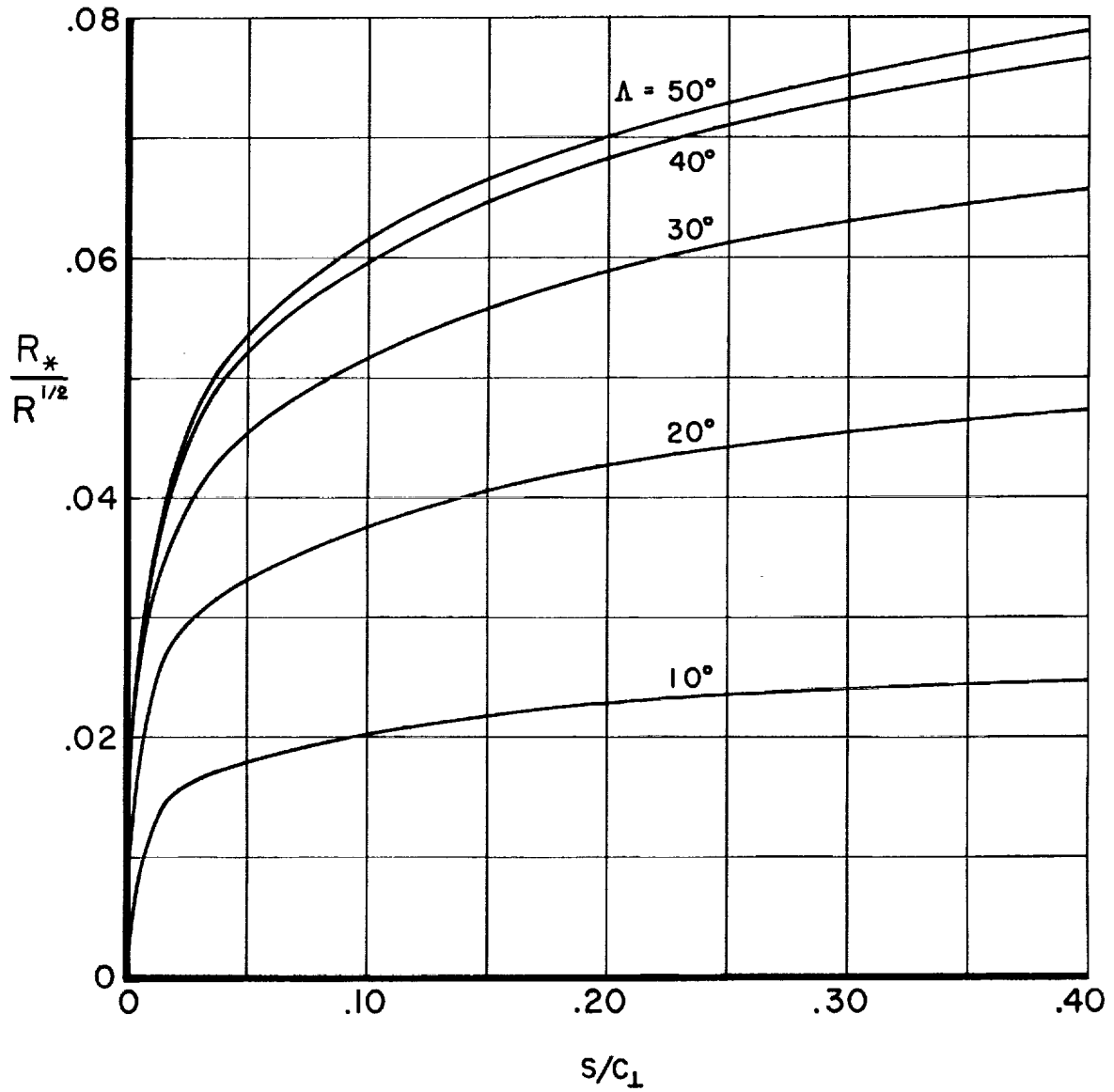


Figure 18.- The distribution of crossflow Reynolds number on the wing in the chordwise direction at zero lift for several angles of sweep.

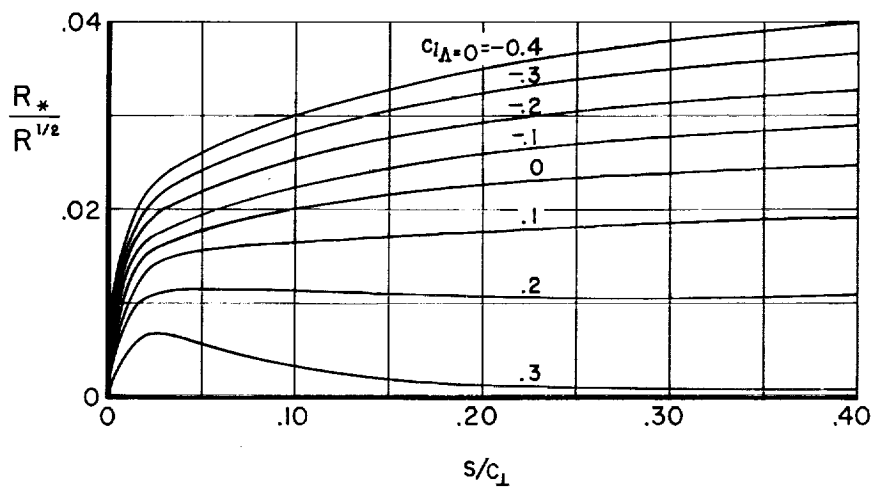
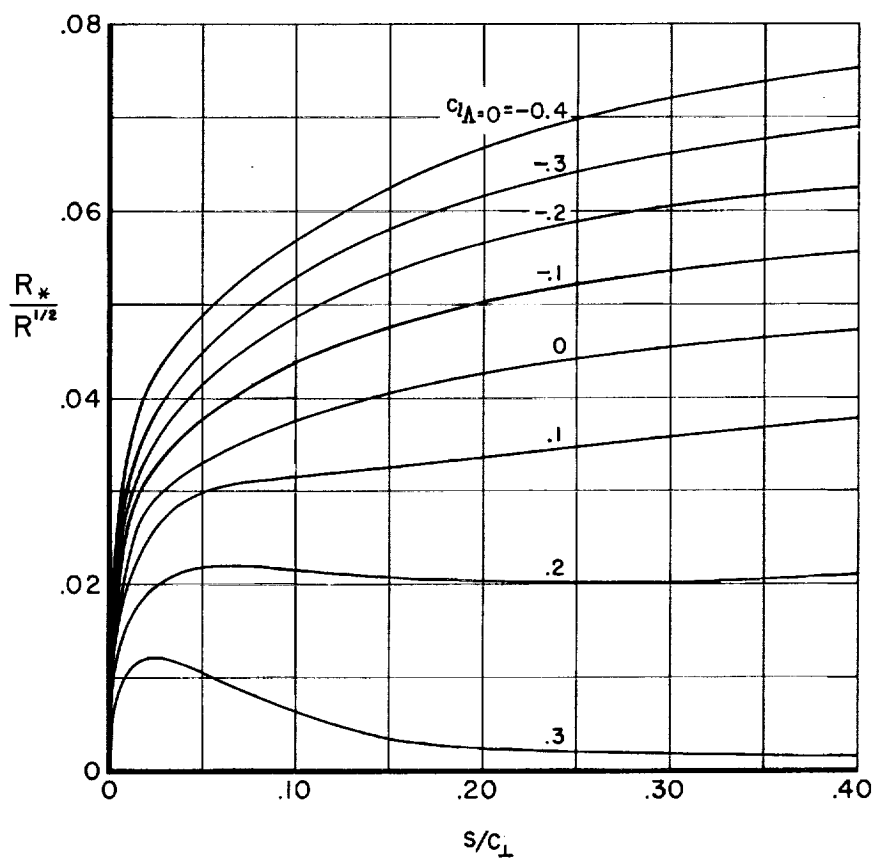
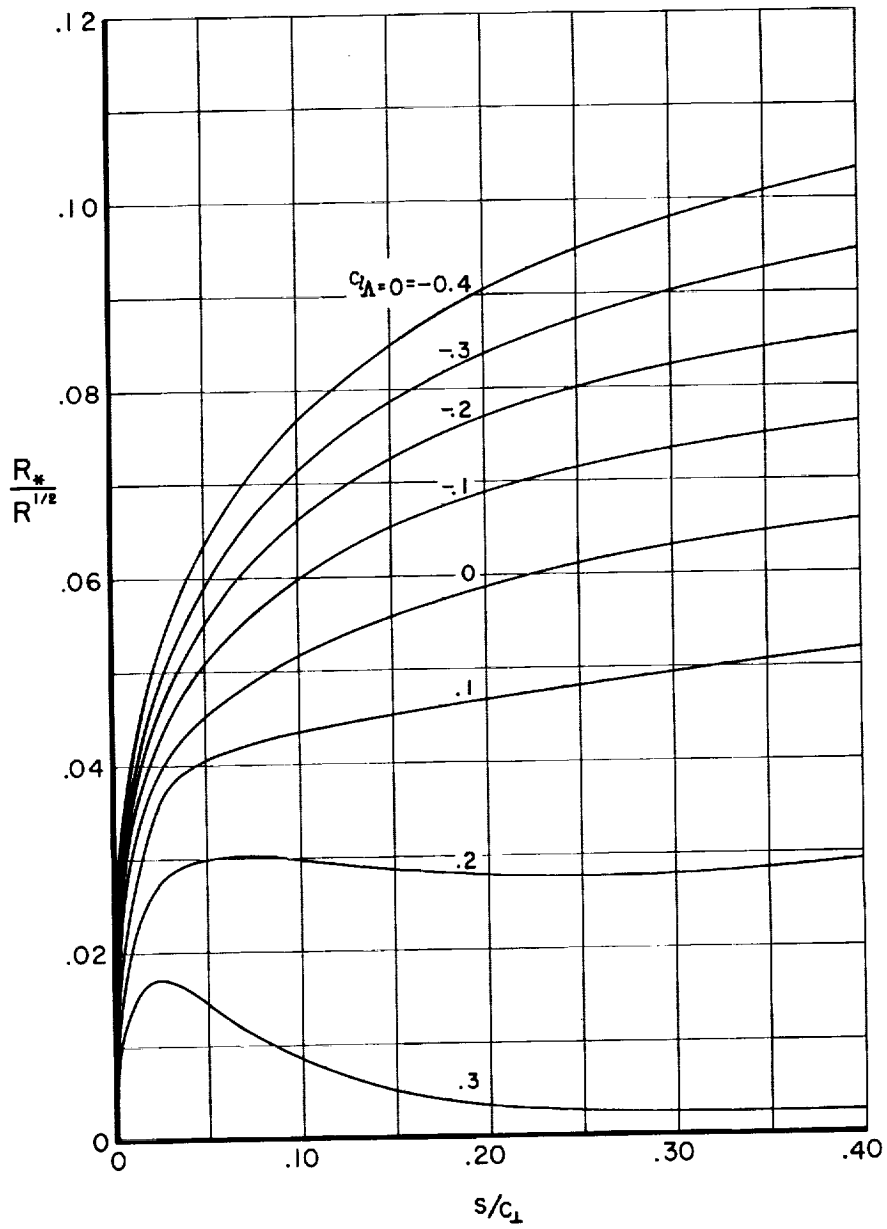
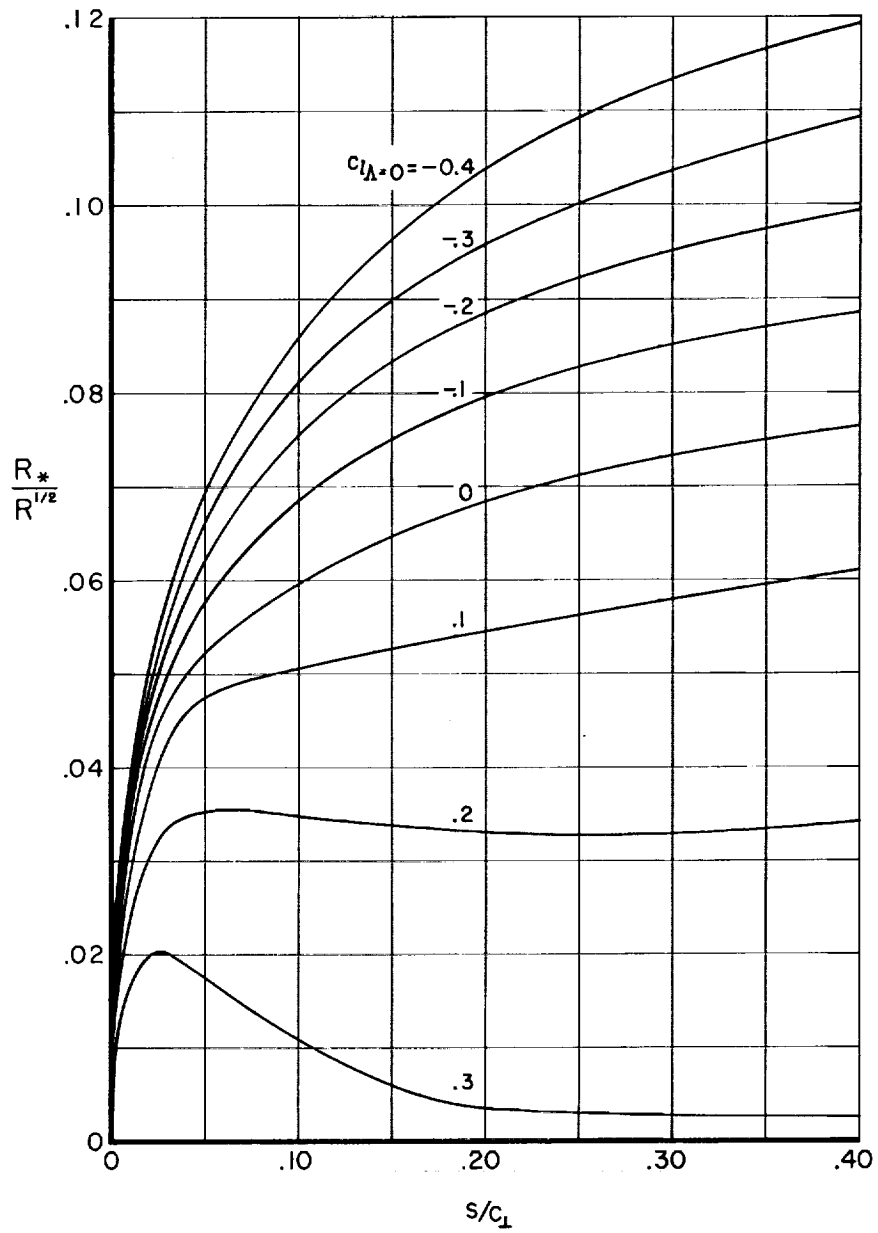
(a)  $\Lambda = 10^\circ$ (b)  $\Lambda = 20^\circ$ 

Figure 19.- The distribution of crossflow Reynolds number in the chordwise direction on the upper surface of the wing for several values of section lift coefficient at several angles of sweep.



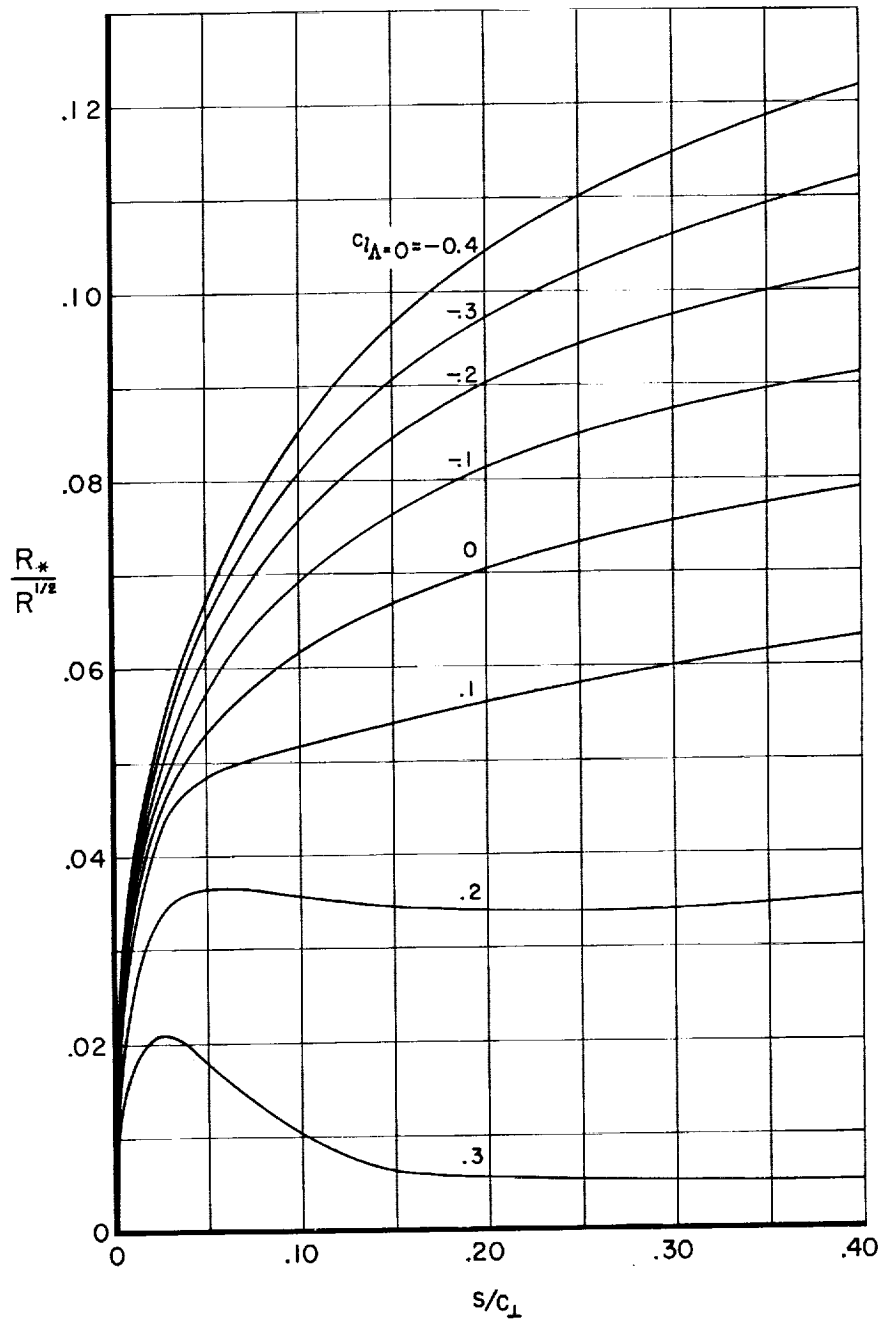
(c)  $\Lambda = 30^\circ$

Figure 19.- Continued.



(d)  $\Lambda = 40^\circ$

Figure 19.- Continued.



(e)  $\Lambda = 50^\circ$

Figure 19.- Concluded.

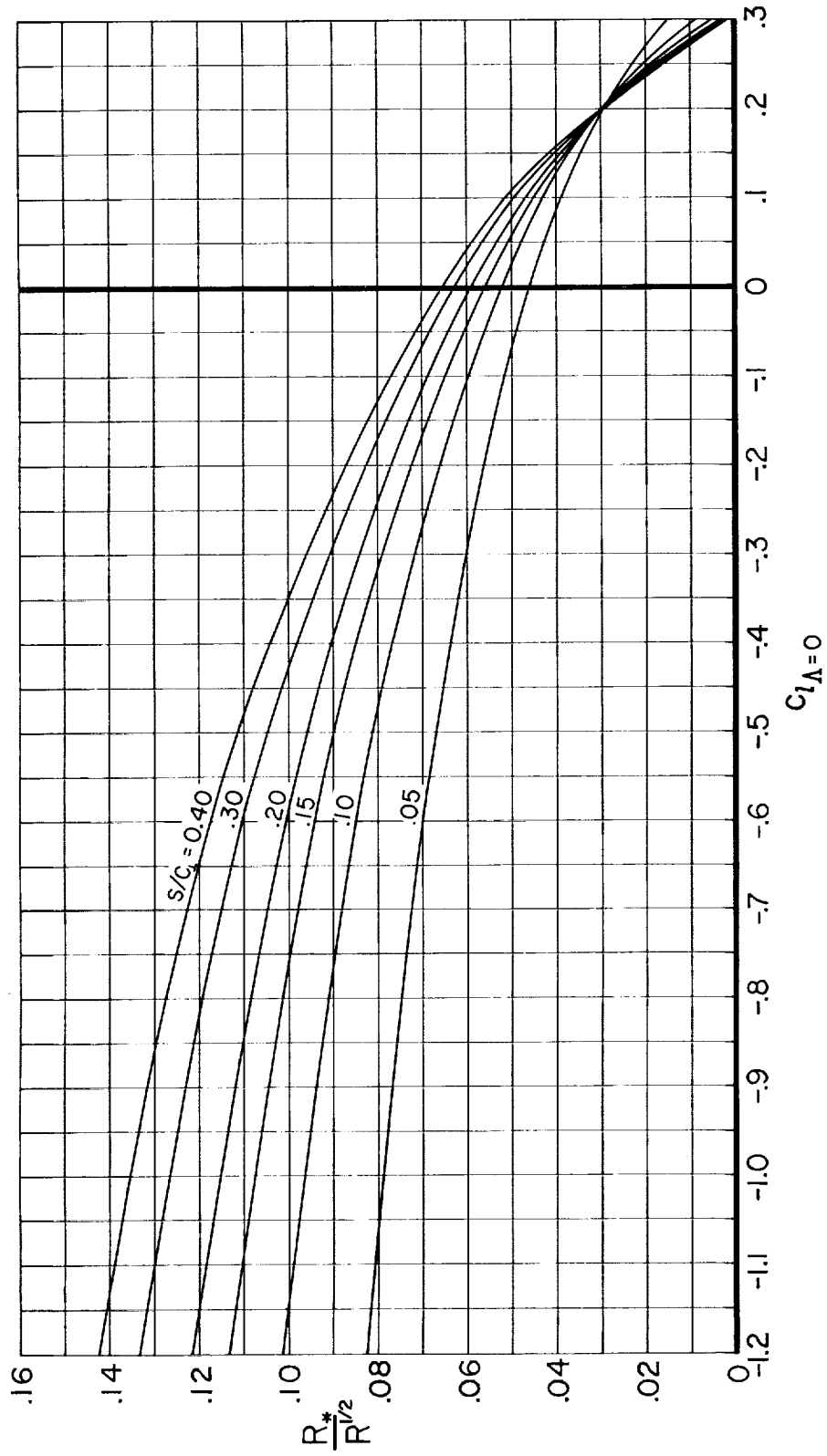


Figure 20.- The variation of  $R^*/R^{1/2}$  with  $c_{l_{\Lambda=0}}$  for several chordwise locations on the wing;  $\Lambda = 30^\circ$ .

